# INSTRUMENTATION FOR MEASUREMENT OF COSMIC NOISE AT 0.75, 1.225 AND 2.0 Mc/s FROM A ROCKET

Technical Report
NASA Grant NASw-54

By:

H. F. Schulte
H. W. Estry
R. L. Miller
J. W. Kuiper

SUBMITTED BY:

Fred T. Haddock
Project Director

THE UNIVERSITY OF MICHIGAN
RADIO ASTRONOMY OBSERVATORY

DEPARTMENT OF ASTRONOMY
DEPARTMENT OF ELECTRICAL ENGINEERING

November 1964

# PREFACE

This is the final technical report concerning the instrumentation for measurement of cosmic noise at 0.75, 1.225, and 2.0 Mc/s from NASA 11.02 launched in September, 1962. The work was supported under NASw-54. The final report on the scientific aspects of this program is to be found in a paper "Cosmic Radio Intensities at 1.225 and 2.0 Mc/s up to an Altitude of 1700 KM," by D. Walsh, F. T. Haddock, and H. F. Schulte, Space Research IV, pp. 935-959, North Holland Publishing Company, Amsterdam, 1964 (Proceedings of the Fourth International Space Symposium held in Warsaw in June, 1963).

TABLE OF CONTENTS

TABLE OF CONTENTS (Concluded)

LIST OF FIGURES

Figure

LIST OF FIGURES (Continued)

Figure

Figure

LIST OF FIGURES (Concluded)

# INTRODUCTION

This report describes design considerations and performance characteristics of a complete rocket-borne instrumentation system for absolute intensity measurements of the radio frequency noise energy which originates primarily in the halo of our galaxy. All portions of the system shown in Figure 1 utilize fail-safe circuits, alternate channel redundancy, and conservative design techniques wherever possible. Simultaneous cosmic noise measurements can be made while in and above portions of the ionosphere at frequencies of 0.75, 1.225 and 2.0 mc. Since the reactive component of the radio astronomy antenna impedance is affected by the ionosphere, it also is measured periodically throughout the flight. The instruments described herein were successfully fired to an altitude of 1691 kilometers on September 22, 1962. The rocket was designated as NASA 11.02UR and the results of the flight are reported separately.*

The radio astronomy antenna diagrammed in Figure 1 consists of a 40-foot tip-to-tip balanced electric dipole deployed from the instrumentation package after last stage rocket burnout and outer nosecone ejection. Three radiometers operating simultaneously from the antenna are alternately switched between the dipole and an electrical equivalent dummy antenna for in-flight noise calibration. During the radiometer calibration interval which is repeated every 12 seconds throughout the flight, the antenna is switched to a bridge circuit which measure the reactive component of the antenna impedance at 1.250 mc. At this frequency, the antenna is electrically very short and thus its terminal impedance appears almost completely capacitive. Since free electrons present in the ionosphere affect the dielectric properties of the medium, the antenna capacitance will vary accordingly. Local electron densities can thus be derived from this measurement. It is also possible with the above data to obtain a correction factor for the radiation resistance of the antenna while it is immersed in the ionosphere. This assists in computing the value of the cosmic noise level, and possibly observing the focussing of incoming noise energy at the radiometer frequencies as the rocket leaves and re-enters the ionosphere.

Figure 2 is a photograph of the prototype and the flight model payload (at the right) after completion of environmental testing. For clarity, a metal

---

*D. Walsh, F. T. Haddock and H. F. Schulte, "Cosmic Radio Intensities at 1.225 and 2.0 Mc measured up to an altitude of 1700 KM," Proc. of the Fourth Int. Space Science Symposium, Warsaw, 1963. North-Holland Publishing Co., Amsterdam, 1964.

cylindrical outer shield normally placed around the instrumentation section is not included. Also in the photograph is a complete telemetering ground station assembled by the project for preflight system checkout, in-flight data acquisition and recording, and post-flight data reduction.

The above system was designed to be carried aboard an Argo D-8 rocket shown in Figure 3. It has a predicted peak altitude of approximately 1800 kilometers for a take-off payload weight of 145 pounds. Of the total weight, 94 pounds is scientific payload. The remaining weight is allocated to the rocket nose-cone, despin system, rocket performance measurement accelerometer, and the other necessary hardware. The total useable measurement interval is approximately 1500 seconds with apogee predicted for 922 seconds after rocket takeoff. The actual flight trajectory for this payload is shown in Figure 4.

## RADIOMETER ANTENNA

An extensive investigation of the antenna problem has been conducted during the course of this research program. It is safe to say that the antenna is the most crucial portion of any rocket or satellite-borne system for absolute intensity measurements at medium or low radio frequencies. This is caused primarily by the physical size, weight, deployment, and environmental limitations imposed by the rocket or satellite vehicle. Pertinent electrical and physical characteristics of air and ferrite cored loop antennas as well as electric dipoles, monopoles and other configurations were all considered for this rocket-borne experiment.

The balanced electric dipole antenna finally chosen for flight use is composed of two DeHavilland Aircraft Company type A2/2 antenna units shown in Figure 5. The antenna element itself consists of a beryllium copper alloy strip, 2 inches wide, 20 feet long and 0.002 inches thick. The strip is tempered by heat-treating in a manner which causes it to spring into a long 0.5 inch diameter thin-walled tube as illustrated by the partially deployed antenna shown in the figure. For storage, the tube is uncurled and wound on a cylinder. The principle is similar to that of the familiar steel-tape carpenter's rule except that in the case of the antenna, the element curls around itself 1-1/2 times. Each unit has a self contained 6 volt DC electric motor and gear train which deploys 20 feet of antenna in approximately 45 seconds. A clutch is also incorporated in the drive system which allows the antenna to be manually rewound on its supply spool.

Also shown in Figure 5 is a spring actuated linear potentiometer for monitoring the antenna position during deployment. The potentiometer shaft is tipped with teflon and bears directly against the antenna supply spool. As the spool diameter changes during deployment, the potentiometer slider picks off the related fraction of the potentiometer supply voltage. When deployment is complete, a limit switch is arranged to cause the potentiometer output voltage to decrease by a factor of two. These signals from both antenna units are telemetered back to the ground so that proper antenna deployment can be confirmed.

Each antenna unit weighs 1.8 pounds exclusive of the external wiring, antenna position indicator, and the mounting brackets which are not supplied by the manufacturer. These items increase the total weight of each antenna unit to 2.25 pounds. The beryllium copper antenna element itself weighs 0.225 ounces per foot for a total of 4.5 ounces per unit. Dimensionally, each antenna unit occupies a volume 4-7/8" wide by 4-1/8" high by 7-1/2" long, exclusive of mounting brackets.

Electrically, each antenna unit can be resolved into either equivalent circuit of Figure 6. The free space radiation resistance is given approxi-

mately by:

$$R_A = \frac{80\pi^2}{\lambda^2} h^2$$

where h is the dipole half length in meters and $R_A$ is in ohms. The effect on $R_A$ of antenna tubing diameter and conductor losses are not considered in this equation. These effects modify $R_A$ less than 10% and will be accounted for during post-flight data reduction and analysis.

The free space reactive component of antenna impedance represented by $C_A$ is given approximately by:

$$C_A = \frac{\pi \epsilon_o h}{\ln(\frac{h}{a})-1}$$

where:

h = dipole half length
a = antenna wire radius

Again, factors such as end and terminal effects are not considered in the equation, but will be measured as discussed below, and considered during data reduction and analysis.

The final element in the equivalent circuit is the stray capacitance $C_B$. This originates from the proximity of grounded conductors and surfaces adjacent to the DeHavilland antenna unit. As installed in the rocket payload with the antenna element fully extended, $C_B$ is 41.5 μμf. It should be noted that $C_B$ forms a capacitive voltage divider with $C_A$ which decreases the output voltage. Because it is undesirable to attempt to tune out $C_B$ at all three frequencies, every effort is made to minimize its magnitude.

Since antenna end and terminal effects cannot be predicted accurately, a full scale model of one half the payload structure was fabricated for antenna impedance measurements. Using the method of ground plane imaging, a conducting ground plane is arranged to bisect the payload longitudinal axis and be perpendicular to the antenna axis as shown in Figure 7. This model was installed at the antenna test range of Jansky and Bailey, Inc., in Alexandria, Virginia, for measurement of antenna characteristics over the frequency range of interest. The final measured value of capacity of the full dipole was:

$$C_A = 32 \pm 0.5 \text{ pf}$$

There was some doubt about whether the conducting plane was large enough and sufficiently well grounded for satisfactory determination of radiation resistance (this does not affect $C_A$ measurement, since $C_A$ depends on near field conditions for which the conducting plane is satisfactory). It was concluded that the radiation resistance was not appreciably different from the theoretical values; these are (for the full dipole):

$$R_A = 0.176 \text{ ohm at } 0.75 \text{ Mc}$$

$$0.466 \text{ ohm at } 1.225 \text{ Mc}$$

$$1.20 \text{ ohm at } 2.0 \text{ Mc}$$

# RADIOMETERS

## 1. PREAMPLIFIER

The block diagram of Figure 1 shows a simplified version of the antenna switching connections. The actual system is more complicated because of the electrically balanced antenna and the need for preventing the 240.2 megacycle 10 watt radiated transmitter power from entering the preamplifier. Figure 8 shows a more complete representation of the input circuitry. The antenna switch is a two-pole, 6 position Ledex rotary solenoid actuated stepping switch which alternately connects the balanced preamplifier input terminals to the antenna or the dummy antenna. During the period when the preamplifier is connected to the dummy antenna, the antenna itself is connected to a circuit for measurement of the capacitive component of the antenna impedance. Additional wafer switch sections are also activated by the Ledex to control timing of the switching intervals and application of supply voltage to the bridge excitation oscillator. Balanced series resonant 240.2 megacycle trap circuits at the antenna output terminals and parallel resonant traps at the preamplifier input terminals effectively prevent transmission of telemetering interference to the antenna capacitance measuring circuit and preamplifier input. The antenna capacitance bridge circuit also shown in Figure 8 will be discussed in a succeeding section of this report.

The preamplifier circuit diagram is shown in Figure 9. It consists of a stable, high input impedance, broadband, low-noise, neutralized cascode amplifier feeding three cathode followers. Each cathode follower has a 50 ohm output impedance and serves to isolate the input of each receiver from the other two. This feature makes it unnecessary to control the receiver input impedance except at its own operating frequency. The receiver input impedance is 50 ohms at band center and decreases sharply outside the operating bandwidth. This decreases the gain of the cathode follower off the band center and thus effectively reduces input signal levels except at the appropriate operating frequency. Spurious receiver responses are thereby minimized.

Physically, the preamplifier is separated into two sections. The first stage shown in Figure 10 is packaged with the antenna switch, dummy antenna and antenna capacitance measurement system. The first stage weighs 1 pound and occupies 38 cubic inches. The second portion of the cascode amplifier and the three output cathode followers shown in Figure 11 weighs 14 ounces and occupies 37 cubic inches.

Of particular interest in the preamplifier is the broadband, balanced input antenna transformer ($T_1$) and neutralized first stage of the cascode amplifier. Considerable effort was allocated to the design and development of this section

of the system. The antenna transformer shown in Figure 12 is wound on a 5.5 inch length of 0.335 inch diameter ferrite rod obtained from a J. W. Miller type 2000 ferrite core loop antenna. The center-tapped transformer primary is a pi-wound coil consisting of 100 turns of 3 x 41 litz wire. The secondary is solenoid wound with 150 turns of 3 x 41 litz wire. Stray capacitance inherent in both the primary and secondary windings of this transformer is carefully controlled so that adequate bandwidth can be achieved.

The overall preamplifier bandpass characteristics are determined by the amount of interstage capacitance, the input transformer coupling coefficient and the amount of feedback from the neutralizing transformer $T_2$. The coupling coefficient of $T_2$ is controlled by sliding the primary winding along the axis of the ferrite rod until the desired point is reached. After the coupling coefficient adjustment is complete, the primary is cemented in place on the two fiberglas traverse rods. The complete assembly is polyisocyanate foam encapsulated in a phenolic tube shown mounted in place at the bottom of Figure 10.

The first stage of the cascode amplifier is a General Electric ceramic-and-metal planar triode type 7462. It is similar to the type 7077, and as used here operates at a plate current of 5.6 milliamperes. This operating point produces a $g_m$ of 9500 micromhos, a plate resistance of 10K ohms, a $\mu$ of 95 and a plate dissipation of 790 milliwatts. Under these conditions the equivalent series noise resistance is approximately 250 ohms. The B+ power required for the complete preamplifier is 33 milliamperes at 200 volts DC.

It will be noted in Figure 9 that all tube filaments are wired in series. Since an open filament in any of the three cathode followers only affects its respective channel, Zener diodes are placed across each of these tubes so that preamplifier operation will be unaffected by one or more cathode follower filament failures. The total filament power required is 400 milliamperes at 25 volts, DC.

Figure 13 illustrates the 2-stage preamplifier frequency response from the input terminals of the dummy antenna to the resistively terminated output with selected values of antenna $C_A$, as a parameter. It should be noted that for the 32 $\mu\mu$f free space value of $C_A$, the capacitive voltage divider action attenuates the input signal by a factor of approximately 0.44. The gain of the preamplifier from the input of the balanced wideband transformer to the second stage output at 1.225 Mc is 31 db. Figure 14 presents measured curves of the preamplifier $R_A T_A$ product in °K-ohms, as $C_A$ in the dummy antenna is varied above and below the antenna free-space capacitance.

The noise performance of the preamplifier with the antenna as a source impedance can also be characterized by a set of noise parameters as discussed by the IRE Subcommittee 7.9 on Noise.[1] These parameters have been measured

[1] "I.R.E. Standards on Methods of Measuring Noise in Linear Twoports, 1959" and "Representation of Noise in Linear Twoports," Proc. I.R.E., vol 48, No. 1, January, 1960.

for a typical preamplifier and are shown in Table I below.

TABLE I

| Freq. (Mc) | $F_o$ | $G_o$ (mhos) | $B_o$ (mhos) | $R_n$ (ohms) |
|---|---|---|---|---|
| 2.00 | 2.47 | $1.8 \times 10^{-4}$ | $+.02 \times 10^{-3}$ | 2310 |
| 1.225 | 2.10 | $3.62 \times 10^{-4}$ | $+.34 \times 10^{-3}$ | 1100 |
| 0.75 | 2.35 | $4.65 \times 10^{-4}$ | $+.49 \times 10^{-3}$ | 1025 |

Using these values, the noise performance can be predicted by using the following equation:

$$R_A T_A \approx R_n T_o X_A^2 \left[ \left( \frac{R_A}{X_A^2} - G_o \right)^2 + \left( \frac{1}{X_A} - B_o \right)^2 \right]$$

The calculated values which show good agreement with the measured performance are also plotted on Figure 14. The minimum detectable antenna temperature capability of the complete system will be discussed in the calibration section of this report.

## 2. RECEIVERS

The three radiometer receivers, each driven from a separate cathode follower in the preamplifier, are conventional superheterodynes. A 2-triode cascode connected R.F. amplifier is followed by a pentode mixer with a separate local oscillator stage. Two pentode intermediate frequency amplifiers with AGC, and operating at 450 kilocycles are followed by a full-wave bridge second detector. The detector drives a transistor audio amplifier and an RC time averaging type integrator with a charge and discharge time constant of 0.1 seconds. This filter is followed by a cathode follower stage which is used to establish the optimum DC level and output impedance for the telemetering system. The audio output is also telemetered so that man-made or atmospheric noise leakage through the ionosphere, or abnormal receiver performance can be monitored. This cannot be done if only a smoothed output channel is available.

Figures 15 and 16 present the receiver details. Except for tuned circuits in the RF amplifier, mixer, local oscillator and a 1.2 Mc series resonant trap circuit in the mixer grid circuit of the 0.75 Mc receiver, all three circuits

are identical. The trap circuit is required because it is necessary to reject a small spurious response produced by the fourth harmonic of the 300 kc local oscillator signal which beats with the incoming frequency to produce a difference frequency at 450 kc.

Figure 17 illustrates the receiver bandwidth characteristic at the second detector output. This response was obtained by varying only the modulation frequency of a sine wave modulated carrier. Other tests showed that the second detector smoothing filter did not affect the low or high frequency bandwidth within the range shown on Figure 17. This response results in an IF amplifier noise bandwidth at the second detector of 7.06 kc.

Power requirements for each receiver are: 130 volts DC at 18.6 milliamperes B+ and 25.6 volts DC at 300 milliamperes filament current.

All components have been carefully selected for stability and ruggedness, and particular attention has been paid to the construction techniques used. After adjustment, each transformer and inductance is potted with a high melting point compound so that the ferrite core materials are not adversely affected by the Test and Enviromental program and the rocket flight itself. The receiver case is fabricated from magnesium, weighs 1 pound 14 ounces when ready for flight and occupies 74 cubic inches.

## ANTENNA CAPACITANCE MEASUREMENT

The antenna capacitance measurement is performed at 1.25 Mc for 2 seconds every 12 seconds throughout the rocket flight. A 25 kc offset from the 1.225 Mc radiometer channel helps reduce the radiometer saturation when the bridge is energized. The capacitance measurement is accomplished by means of the circuits shown in Figures 18 and 19. Strictly speaking, this is not a true electrical bridge, but for convenience the term is used in this report. The "bridge" circuit is in fact a balanced-with-respect-to-ground resistance-capacitance voltage divider. A simplified version of the circuit and its voltage vector relationship is shown in Figure 20. If it is assumed that $R_A \ll X_{C_A}$, that the output detector input impedance is high, and $E'_{in}$ (in Figure 18) is a constant, then the vector relationship of Figure 20 is valid. The locus of the voltage vector $E'_o$ orgin is a semicircle with radius $E'_{in}/2$, and the output detector responds to the magnitude of $E'_{out}$. Note that in Figure 20 $E'_o = E_o + K_1$ and $E'_{in} = K_2 E_{in}$ where $K_1 = B_1 + B_2$ and $K_2 = (R_6 + R_7)/R_7$. For a fixed frequency and any set of $C_B$ plus $C_A$, resistor R can be chosen so that $\theta = 45°$ which is the condition for maximum $\Delta C$ sensitivity. In practice, these assumptions are not always completely met and thus the analysis becomes somewhat more complicated. Two examples of this are of interest. First, the regulation of the balanced-excitation sine wave generator is not perfect, which causes $E_{in}$ to vary slightly with $C_A$ as shown in Figure 35. The system is very stable however and thus subject to calibration. Second, when the antenna is immersed in the ionospheric plasma, the free electrons present modify the dielectric constant of the medium, and $C_A$ and $R_A$ will vary. When $R_A$ is not small with respect to $X_{C_A}$, the bridge output cannot be interpreted as simply a variation in $C_A$.

The bridge shown in Figure 18 is designed to measure the balanced antenna equivalent capacitance $C_A$ from -15 μμf to + 40 μμf when $R_A \ll X_{C_A}$. The $E_{in}$ detector monitors the bridge excitation level so that corrections can be made if necessary. The output detector consists of a full wave voltage doubler rectifier and low pass filter. The series biasing batteries assist in achieving the desired capacitance measurement range and resolution shown in Figure 35. The voltage doubler allows a lower RF voltage level at the antenna terminals and thus reduces antenna sheathing effects in the ionosphere.

The RF excitation voltage is supplied by a Colpitts type crystal controlled oscillator, followed by a buffer amplifier stage shown in Figure 19. The output circuit of the amplifier contains a ferrite, torroidal core transformer which is carefully fabricated and trimmed to produce a phase and amplitude balanced output for the bridge. Figure 21 shows physical details of the oscillator and bridge.

## RANDOM NOISE GENERATOR

The requirement for a reliable and rugged in-flight calibrator for the three radiometers poses a rather difficult design problem because of the 1 x $10^9$°K signal level required. CW, pulse, or amplitude modulated carriers require the generation of constant amplitude signals. If the radiometer center frequency, or bandwidth shifts somewhat during flight, a CW or pulse type calibration will result in a misleading interpretation of the changed response of the radiometer to the actual cosmic noise being measured. The only completely satisfactory solution is the in-flight use of a wide-band random noise generator.

After careful study of various methods for generating wide-band random noise that would have a reasonable chance of surviving the powered portion of the rocket flight, a special, double-diffused silicon junction noise diode* was chosen. The diode is operated reversed biased and well beyond the knee of the Zener region. A good diode does not exhibit the typical spiked or ragged and erratic voltage fluctuations associated with the avalanche conduction mode. When the diode operating current is correctly chosen, the noise output is symmetrical with respect to a zero base-line and appears to have a satisfactory distribution of amplitudes with no frequency coherence when viewed on a high frequency oscilloscope.

The circuit developed here for use with this diode is shown in Figure 22. This circuit with a properly selected noise diode is capable of producing an equivalent noise temperature at the dummy antenna output terminals in excess of 1 x $10^9$°K. A step-down transformer and a high-beta silicon transistor is used as an emitter follower to match the noise diode internal impedance (approximately 300 ohms at 1 Mc) down to 50 ohms for input to the dummy antenna unbalanced-to-balanced input transformer. It has been experimentally verified that the transistor itself contributes a negligible amount of noise to the total output.

At the time the noise diode selection was made, relatively little was known about the long-term characteristics of the device, so an extensive measurement program was undertaken to obtain information on important parameters such as noise output quantity and quality with respect to diode operating current and temperature, spectral distribution of energy, and short and long-term stability. The last item mentioned has been underway for approximately 16 months and the results to date indicate that the stability of the diode as used in the rocket experiment is adequate. Of 11 diodes on continuous life test for 16 months, there has been one unexplained catastrophic failure, and one failure due to

* Solitron Sounvister Diode Type SD2L, Manufactured by Solitron Devices, Norwood, New Jersey.

connecting lead failure. The remainder of the diodes continue to operate satisfactorily. The average noise output change in 16 months is less than 0.4 db. The maximum observed change was +1.3 with a measurement uncertainty of ± 0.25 db. Since these diodes were obtained more than 2 years ago it can probably be assumed now that diodes of recent manufacture will be even better since it is known that the manufacturer is actively engaged in improving the product.

It is important to recognize that the diode as used in this experiment is used only as a comparison device. The laboratory thermionic noise diode calibrations are used as the absolute standard and the in-flight solid-state diode merely serves as a means to determine the magnitude of any change in the radiometer calibrations.

Noise diodes considered suitable for flight must exhibit characteristics at least equal to the following:

1. The spectral distribution of the noise must be constant within ±0.5 db from 0.75 to 2.0 megacycles at constant temperature and diode current.

2. When the noise diode current is varied ± 10% from the optimum value, the output level and spectral distribution of the noise energy must not vary more than ±0.5 db. When the noise signal is viewed on a wideband oscilloscope, there must be no noticeable change in the appearance of the waveform.

3. The noise output must not vary more than ±0.5 db over; the temperature range from 0°F to +140°F.

Figures 23 and 24 show the temperature and spectral performance of the noise diode chosen for flight. Since a measurable temperature coefficient does exist, a small constant temperature oven operating at 90°F ±3°F was designed for the complete noise generator circuit. Construction details are shown in Figures 25 and 26. Both the diode operating current and the oven internal temperature are monitored during flight for reference purposes.

## PHOTOCELL ASPECT SYSTEM

Two self generating silicon solar cells for aspect sensing are mounted on the instrumentation rack as shown in Figure 27. The upper cell for detection of vehicle tumble has a small circular aperture directed upward and parallel to the payload spin axis. The lower photocell for the detection of vehicle spin is mounted to look radially outward in the plane of the spin axis. It is inclined downward at an angle of 45° to a plane perpendicular to the spin axis. At low light levels, the photocell output voltage is proportional to the logarithm of the incident light intensity but when directly viewing the sun, the output is saturated. Each photocell output is sampled for 30 millisecond once each second on the commutated telemetering channel. The azimuth or spin axis cell field of view is shown in Figure 28. It will be recognized that this is a very simple aspect system which cannot provide high accuracy because of the lack of optics and the time-multiplexed data sharing. Spin history of the flight, and detection of payload tumble is possible however, provided that neither the spin or tumble periods are equal to or less than the 1 second telemetering sampling period.

# CALIBRATION

## 1. RADIOMETERS

Calibration of the instrumentation just described divides naturally into two phases: the laboratory pre-flight calibrations, and the in-flight programmed calibration. All laboratory pre-flight radiometer response calibrations are performed with a wide band random noise generator designed and built in this laboratory. The noise generator circuit shown in Figure 30 uses a temperature limited thermionic diode as a noise source followed by a stable wide-band amplifier. Amplifier gain is measured and adjusted if necessary with accurate step attenuators before each calibration is undertaken. This is done at each of the three radiometer operating frequencies. The resultant accurately known noise energy is controlled by cascaded step attenuators which feed the rocket dummy antenna input. This calibration scheme thus requires only a constant output noise generator and stable, accurate step attenuators. Since the diode current can be measured with high precision and and all other measurements require only the use of passive attenuators, it is believed that a minimum amount of systematic calibration uncertainty is introduced.

Correction is made for the dummy antenna unbalanced-to-balanced input transformer insertion loss, and measurement of all capacitors is done with the precision substitution method diagrammed in Figure 29.

In addition to the primary radiometer random noise calibrations through the rocket dummy antenna adjusted to simulate the antenna electrical characteristics in free space, other values of $C_A$ are inserted in the dummy antenna to stimulate the reactance changes which occur when the antenna is immersed in the ionosphere. With a known signal present at the dummy antenna input, it is thus possible to determine the preamplifier voltage transfer function versus $C_A$ and derive correction factors which can be applied to the radiometer results. Curves of these transfer functions are shown in Figure 31.

Correction factors are also determined for ambient temperature effects on the radiometers and antenna capacitance measuring circuitry. The instrument ambient temperature is monitored during flight and thus appropriate corrections can be made if necessary. Experience has shown however, that these factors are usually small.

The complete radiometer calibration curves for 0.75, 1.225 and 2.00 Mc are shown in Figures 32, 33 and 34. Assuming that the smallest resolvable increment of telemetered voltage is 1 part in 100, the minimum detectable

R·T product for each of the three channels is 1 x $10^6$°K·ohms at 0.75 Mc, 6 x $10^5$°K·ohms at 1.225 Mc and 7 x $10^5$°K·ohms at 2.00 Mc. Actually, the telemetering resolution for this system is closer to 1 part in 500. This permits an even lower minimum detectable noise signal level to be attained.

A unique feature of this measurement system is the two-step in-flight radiometer noise calibration. The same switch that connects the antenna to the bridge for antenna capacitance measurement also connects the preamplifier input to the dummy antenna. The first step of the calibration is the zero input signal level thus established. Two seconds later the wide-band random noise generator connected to the dummy antenna is energized, and a known noise level calibration point is obtained. It is not necessary to disconnect the deenergized noise generator from the dummy antenna when the "no-noise" calibration point is obtained. This is because the source impedance at the secondary of the dummy antenna input transformer is very small with respect to the reactance of the antenna capacitance $C_A$ and thus does not affect the input system noise temperature.

## 2. ANTENNA CAPACITANCE

Pre-flight calibration of the antenna bridge involves the precision measurement and pairing of equal capacitors using the test setup shown in Figure 29. These capacitors are then substituted in place of the actual antennas in the rocket payload and the calibration curves shown in Figure 35 are obtained. The phrase "antenna equivalent capacitance", $C_A$ used in the figure refers to the equivalent unbalanced antenna capacitance which is just 1/2 that of each half of the actual balanced antenna as shown in Figure 5. The transfer function shown in Figure 31 aids in data reduction if the excitation level varies or the bridge thermal temperature changes substantially during flight.

Calibration of the negative $C_A$ portion of the total measurement range is accomplished by temporarily reducing the total capacity below that of the stray shunting value ($C_B/2$) only. Since the radiation resistance is so small that it can be neglected, the bridge normally sees the capacitances, $C_A$ and $C_B/2$ in parallel as shown in Figure 6. If the leads to the undeployed antennas are now disconnected, the shunt capacitance is reduced. The bridge cannot distinguish this condition from one where $C_B/2$ is its normal value and $C_A = -C_B/2$. Thus, over the range $0 > C_A > -C_B/2$, the bridge can be calibrated for $-C_A$ by adding known capacitors in place of $C_B/2$. It is necessary, of course, to account properly for all stray capacitance changes that might occur during this substitution procedure.

## COMPLETE PRE-FLIGHT CALIBRATIONS AND MEASUREMENTS

A large number of supporting calibrations and pre-flight measurements is also required. These are intended to aid in monitoring performance and recovering as much usable information as possible if a malfunction occurs in the system during the rocket flight. The following is a typical list of pre-flight calibrations and measurements:

1. Measure insertions loss and input impedance of dummy antenna matching transformer at 0.75, 1.225, and 2.00 Mc.

2. Measure value of flight dummy antenna $C_A$ capacitors.

3. Measure stray (base) capacity to ground of the DeHavilland antennas and associated wiring. Include correction for change in stray capacitance caused by antenna deployment during flight.

4. Measure and adjust dummy antenna shunt capacitors to match item 3 above.

5. Measure dummy antenna-preamplifier voltage transfer function versus antenna $C_A$ at 0.75, 1.225 and 2.00 Mc.

6. Calibrate antenna capacitance measurement circuit from $C_A$ = +40 μμf to -15 μμf.

7. Determine temperature coefficient of item 6 above.

8. Noise calibrate each radiometer through rocket dummy antenna.

9. Determine temperature coefficient of item 8 above.

10. Calibrate each radiometer noise bandwidth at $\int e_o \, dt$ levels of 0, 1.0, 2.0, 3.0 and 4.0 volts.

11. C.W. calibrate each radiometer through rocket dummy antenna.

12. Measure rms output voltage of each radiometer audio output channel for complete range of input noise levels.

13. Repeat item 8 and vary filament voltage by ±5%.

14. Repeat item 8 and vary +200 volt B+ voltage by ±5%.

15. Repeat item 8 and vary +130 volt B+ voltage by ±5%.

16. Calibrate thermistors which monitor receiver base plate, antenna bridge support and noise generator oven temperature.

17. Make a wide-band (100 kc to 7 Mc) true rms voltage measurement of the noise generator output voltage.

18. Optically calibrate the spin and tumble axis aspect photocells.

19. Measure linearity of the five telemetering subcarrier oscillators.

20. Calibrate the antenna right and left-side position monitors.

21. Measure the absolute value of the in-flight telemetering calibrator voltage.

22. Measure the following telemeter-monitored operational voltages:

    a. -32 volt battery

    b. +14 volt battery

    c. +130 volt regulated B+

    d. +200 volt regulated B+

    e. -25 volt regulated filament voltage

    f. +9 volt regulated VCO supply voltage

    g. Noise generator current

    h. nose-cone position monitor

    i. antenna power monitor

    j. receiver audio commutator position monitor

## SWITCHING SEQUENCE TIMER

Because of the involved switching sequence required to perform all of the measurements and calibrations, a rather complicated timer is neccessary. The time relationships can best be illustrated by referring to Figure 39 which illustrates a complete sequence of switching events. Note that 72 seconds are required before the system repeats. In that interval the pre-amplifier and bridge sequence is repeated 6 times, the receiver audio output commutator sequence repeats twice and the telemetering VCO channel calibration occurs once.

Referring to Figure 36, the basic timing interval is generated by the astable multivibrator labeled "Antenna Timer". The output of this timer is a -32 volt pulse with a duration of approximately 50 milliseconds. The pulse is used to drive two power amplifiers, which in turn energize the antenna Ledex and the audio commutator Ledex. The antenna Ledex shown in Figures 8 and 36 drives a twelve-position multi-wafer switch wired as a 6-pole double throw switch. Four of the poles are used to switch the balanced preamp and bridge to the dummy antenna and antenna. One pole is used to furnish -32 volts to the Zener regulator, $D_{10}$. The remaining pole supplies -25 volts to the bridge excitation and noise generator delay circuits. These delay circuits are designed to energize the circuits they control a specified number of seconds after the delay timer is energized.

The audio commutator Ledex shown in Figure 37 is a twelve-position rotary switch with one pole wired as a three-position switch. It thus switches electrically once every two times the Ledex is energized. The second pole is wired to function once for every revolution of the Ledex, and provides power for the VCO calibration timer circuitry for 6 seconds every 72 seconds. The third pole provides an analog switch position voltage to the commutated telemetering channel.

In both the delay circuits and the calibration timer, if the circuits fail in either the energized or de-energized position, they will be switched out within six seconds by the antenna timer. Further, if either or both the antenna Ledex or the video commutator Ledex should malfunction, the antenna timer will continue to energize them in an attempt to restore normal action. Under these circumstances, the audio commutator Ledex may get out of "sync" with the antenna Ledex. This is not serious, however, because the audio commutator and calibration sequence will merely be shifted a multiple of six seconds from the antenna sequence. Also, the position of the audio commutator is telemetered and thus ambiguity is avoided.

Although the above is a brief summary of the switching, a more detailed discussion seems warranted because of the complexity of the system. The basic antenna timer circuit is shown in Figure 38. Applicable waveforms for this and other circuits to be discussed are shown in Figure 39. The first basic circuit is the antenna timer, which is a conventional astable multivibrator with approximately symmetrical 3 second on-off times. The output relay is placed in series with a capacitor from the collector of $TR_8$ to ground. This is done to limit the relay actuation time to 50 milliseconds, while still maintaining a total period of 6 seconds. When $TR_8$ is cut off, $C_4$ charges through $R_4$ and the relay coil. Since the relay is a magnetically biased polarized type, the charging current does not trigger the relay. When $TR_8$ conducts, $C_4$ discharges through the relay coil. The current direction is now correct and the relay operates. The time constant of the relay coil and $C_4$ is adjusted so that the relay remains closed for approximately 50 milliseconds. Diode $D_7$ prevents the relay coil back EMF from damaging capacitor $C_4$.

The second basic circuit is the delay-on timer which is used in the VCO calibration sequencer, the noise generator delay and the bridge excitation delay timer. Referring to the simplified circuit in Figure 40 transistor $TR_3$ is cutoff and $C_6$ initially is not charged. When $-E_{cc}$ is applied, $E_b$ begins falling toward $-E_{cc}$ as the capacitor charges. When $E_b$ reaches about -0.2 volts, the transistor conducts and relay $RLY_2$ functions.

In the circuits for the bridge excitation delay and noise generator delay shown in Figure 36, additional resistors ($R_{13}$ and $R_{17}$) have been provided. They are switched across C when their relays are energized. This is necessary because these circuits must be re-set within 6 seconds after they are de-energized. If this provision is not included, the re-set time is about T = 5 RC where R = 100K which, in the case of the above delay circuits, would require 100 and 75 seconds, respectively. With the re-set provision, the time is shortened to about 1 second, and occurs while the relay is still energized. Thus, if the delay circuit remains on for 1 second or more, the circuit will be fully re-set immediately after de-energization. This provision is not necessary in the VCO sequences because it must function only once in 72 seconds and has a normal re-set time of about 25 seconds.

The delay-off gate shown in Figure 41 and used in the VCO calibration timer is the final type of delay circuit used. In this case, audio commutator Ledex wafer B provides the initiating power, $-E_{cc}$, to the circuit. Relay $RLY_1$ is energized immediately and is de-energized 2 seconds later. This method of terminating the VCO calibration has been chosen because of reliability considerations. If the audio commutator Ledex malfunctions in the VCO calibrate position, for instance, a delay-on timer cannot be wired fail-safe. The delay-off timer will time out and no further VCO calibration can then occur until Ledex wafer $B_1$ completes 12 steps. Circuit operation is basically the same as

that of the delay-on gate previously described except that, instead of using $TR_2$ to energize a relay, the rise in collector voltage when $TR_2$ conducts is used to cut off $TR_1$, which was previously conducting and which has relay $RLY_1$ in its collector circuit.

The audio and antenna commutator Ledex stepping switches each require a 28 volt 35 millisecond 3 ampere pulse for proper actuation. This is accomplished with power transistors $TR_{11}$ and $TR_{12}$ shown in Figure 36. The bases are normally cutoff by the +14 volt supply through relay $RLY_6$ contacts and drive resistors $R_6$ and $R_7$. When $RLY_6$ closes for 50 milliseconds the bases are driven into saturation from the -32 volt supply, the transistors conduct, the Ledexes actuate and step one position. The Ledex coils must not remain energized for extended periods because of their limited duty cycle rating. Also, the large current that flows is a substantial load on the battery. These reasons dictate the choice of a 50 millisecond "on" cycle for relay $RLY_6$.

To eliminate Ledex switching transients from interfering with proper timer performance, it is necessary to operate the collector of $TR_8$ from a separate Zener regulator diode $D_8$. The base drive circuits of $TR_7$ and $TR_8$ are also decoupled with Zener regulator diode $D_{10}$. Precision control of the delay-on circuit timing requires a stable voltage for the base drive circuits. Zener diode $D_9$ provides a regulated source of +10 volts from the unregulated +14 volt battery.

All timing capacitors in the circuits of Figure 36 are hermetically sealed, sintered anode, wet slug tantalum type XT capacitors manufactured by P.R. Mallory. Over all extremes of supply voltage and ambient temperature, antenna switch timing accuracy was maintained within ±5% of nominal. The VCO calibration period varied by ±0.4 second at the extremes. Furthermore, since all circuits varied in approximately the same degree, no timing functions were shortened or lengthened appreciably with respect to the others.

Two additional timer features not used on the flight payload are also shown in Figure 36. The bridge Ledex sequencer (enclosed in the dotted box) is another astable multivibrator similar to the antenna timer for the control of an additional Ledex stepping switch. Antenna Ledex wafer $A_1$ is located in the upper right-hand corner of Figure 36. If the jumper shown across terminals 43 and 44 is removed, the antenna timer astable multivibrator switching intervals will become unequal because timing capacitor $C_{12}$ (and $C_9$ if used) will alternately be switched in and out of the base circuit of $TR_8$. This function is not required however when the bridge Ledex sequence timer is not used.

All timer circuits are mounted together in a subassembly shown in Figure 42. The unit weighs 38 ounces, exclusive of the Ledex actuators and it occupies 81 cubic inches.

## TELEMETERING SYSTEM

The telemetering system adopted for this experiment is a standard FM/FM system which conforms to the IRIG specifications. The FM transmitter-RF power amplifier combination operates at 240.2 Mc with a power output of 10 watts, nominal. Six FM subcarrier channel signals are summed and constitue the transmitter modulation input. True frequency modulation occurs in this transmitter design. The transmitter RF output drives a turnstile antenna designed to have a near optimum radiation pattern for the expected rocket trajectory. Each of the telemetering subsections is described in detail below.

### 1. SUBCARRIER OSCILLATORS

Six voltage controlled subcarrier oscillators (VCO) are used in this system as shown in the upper section of Figure 37. Five are EMR type 184C oscillators and the sixth is a Vector type supplied by NASA Goddard Space Flight Center in the vehicle performance accelerometer package. Each VCO is designed to accept an input voltage range of 0 to +5 volts, DC. The upper modulation frequency limit of each VCO is dependent on its output carrier center frequency. Modulation (i.e., deviation) linearity of the EMR VCO is 0.1% or better, about the best straight line for ±7.5% deviation. Input and output impedance is 500K ohms and 5K ohms respectively. The output carrier level is adjustable to 5 volts rms. Input power required is 4.5 ma at +9 volts regulated. Each VCO is separately fused so that a failure in one VCO will not affect the others.

All VCO outputs are summed in a resistive network shown in Figure 37. Subcarrier preemphasis is used to achieve equal channel signal-to-noise ratio at the telemetering reciever output. Details are shown in Table II.

TABLE II

| IRIG Band No. | Center Frequency, cps | Frequency Deviation, % | Band Width, cps | Output Level, rms v | Data Assignment |
|---|---|---|---|---|---|
| 9 | 3900 | ± 7.5 | 50 | 0.21 | NASA accelerometer |
| 11 | 7350 | ± 7.5 | 110 | 0.20 | 0.75 Mc radiometer $\int e_o \, dt$ |
| 12 | 10500 | ± 7.5 | 160 | 0.23 | 1.225 Mc radiometer $\int e_o \, dt$ |
| 13 | 14500 | ± 7.5 | 220 | 0.30 | 2.00 Mc radiometer $\int e_o \, dt$ |
| 14 | 22000 | ± 7.5 | 330 | 0.35 | 30-channel commutator |
| E | 70000 | ±15.0 | 2100 | 0.62 | Radiometer audio outputs |

## 2. INPUT SIGNAL LIMITING

Since a malfunction of a radiometer or other circuits feeding the VCO's could cause the normal input range of 0 to +5 volts to be exceeded, a signal limiting circuit for each VCO input is required. A series resistor followed by two biased silicon junction diodes shown in Figure 37 is used. This limiter prevents the signal level at the VCO input from exceeding -0.5 v to +5.5 volts. The negative limit diode is biased at zero volts and the positive limit diode is based at +5.0 volts which is derived from the +9 volt regulated supply.

## 3. VCO IN-FLIGHT CALIBRATION

A 0 volt and +4.04 volt two-step in-flight calibration is performed every 72 seconds during flight on all VCO's except the 22 kc commutated channel which uses these same two voltage levels as two of its regular 30 input channels. The +4.04 volt level is obtained from three RM-1 mercury cells. At the beginning of the calibration cycle all limiter inputs except the commutated channel are disconnected, paralleled by relays $RLY_2$ and $RLY_3$ in Figure 37 and connected to the VCO calibration input terminal MB36. This point is first connected to signal ground by relay $RLY_2$ in Figure 36. One second later the signal ground is removed and the +4.04 volt mercury battery is connected to the line. After one additional second, calibration is complete and all VCO's are returned to their normal data inputs. From the two calibration points so obtained, correction factors (if any) can be obtained for all in-flight and ground station telemetering system drifts. The magnitude of the mercury battery voltage is measured to ±.01% before flight and it is assumed that it remains constant throughout the flight. This battery serves no other purpose and is only required to supply $4 \times 10^{-5}$ amperes for approximately 3 seconds every 72 seconds.

## 4. COMMUTATOR

A 30 channel, single pole, 30 sample per second commutator is used to time-multiplex the 22 kc subcarrier VCO. The commutator is a T.I.C. Model R-6-15-30B1 and is connected break-before-make, with a duty cycle of approximately 85%. The increase in channel capacity thus provided permits backup of all continuous channels against VCO failure, transmission of much operational data such as instrument temperature, battery condition, etc., and is also the prime data channel for the antenna capacitance measurement.

The commutator channel assignments are shown in Table III below.

TABLE III

| Commutator Segment No. | Function |
|---|---|
| 1 | Antenna Bridge Input |
| 2 | Antenna Bridge Output |
| 3 | 0 Volt Calibration |
| 4 | +4.04 Volt Calibration |
| 5 | 0.75 Mc Radiometer $\int e_o \, dt$ |
| 6 | 1.225 Mc Radiometer $\int e_o \, dt$ |
| 7 | 2.00 Mc Radiometer $\int e_o \, dt$ |
| 8 | -32 Volt Main Battery |
| 9 | +14 Volt Main Battery |
| 10 | Antenna Bridge Temperature |
| 11 | Antenna Bridge Input (Cross-strap to 1) |
| 12 | Antenna Bridge Output (Cross-strap to 2) |
| 13 | +130 Volt B+ Monitor |
| 14 | +200 Volt B+ Monitor |
| 15 | -25.2 Volt Filament Monitor |
| 16 | Receiver Audio Commutator Position |
| 17 | 0.75 Mc Radiometer Audio Output |
| 18 | 1.225 Mc Radiometer Audio Output |
| 19 | 2.00 Mc Radiometer Audio Output |
| 20 | Nose Cone Position Monitor |
| 21 | Receiver Deck Temperature |
| 22 | Antenna Bridge Output (Cross-strap to 12) |
| 23 | Antenna Right Side Position Monitor |
| 24 | Antenna Left Side Position Monitor |
| 25 | Noise Generator Diode Current |
| 26 | Noise Generator Oven Temperature |
| 27 | Tumble Axis Aspect Photocell |
| 28 | Spin Axis Aspect Photocell |
| 29 | +9 volt VCO Power Monitor |
| 30 | Antenna Power Monitor |

## 5. TRANSMITTER AND RF POWER AMPLIFIER

The decision to fly a transmitter followed by an RF amplifier with an output of 10 watts was arrived at after discussion with the telemetering group at the NASA Goddard Space Flight Center. At the time, there was some question regarding the wisdom of having only 2 watts of radiated power. Furthermore, there was no information what so ever on satisfactory rocket-borne telemetering antennas for the Journeyman D-8 vehicle. This rocket had never been fired from Wallops Island, Virginia. Calculation showed that for a rocket antenna with an isotropic radiation pattern, a ground station antenna with 15 db gain

and a receiver with a noise figure of 4 db, the poorest signal-to-noise ratio would be approximately at apogee where the margin of safety would be 12.6 db for 2 watts of radiated power. Since the rocket antenna could easily have pattern asymmetries of 6 db or more, it was decided to transmit at the 10 watt level. Calculations also indicated that telemetering signals during the last 100 miles of altitude on the down leg of the trajectory would not be received because of horizon cut-off. It was therefore requested that the NASA Bermuda tracking station be operational so that the data obtained during the ionosphere bottom-side breakthrough could be recovered.

The telemetering transmitter selected for this payload is an EMR Model 121C-28-240.2 Quartz-Line-Controlled true FM transmitter, operating at 240.2 Mc. It has a measured output of slightly less than 2 watts into a 50 ohm load and a nominal carrier deviation of ±125 kc. Its spurious output is at least 60 db down with respect to the carrier. It weighs 23 ounces and power requirements are 27.5 volts at 150 ma for filaments and 200 volts at 65 ma for the plate supply. The transmitter output is fed directly into a United Electrodynamics type PA-10 RF power amplifier. This amplifier was chosen in preference to an EMR type because its B+ voltage requirement is the same as the transmitter. The measured power output of this amplifier is a nominal 10 watts into a 50 ohm load when driven by a nominal 2 watt transmitter. The actual pre-takeoff power output was measured as 8.6 watts. Input and output impedance is 50 ohms, bandwidth is 4 Mc and overall efficiency is 25%. The filament power required is 27.5 volts at 200 ma and plate power is 200 volts at 90 ma.

The 200 volt DC to DC converter, its pre-regulator, the transmitter and its power amplifier are all installed in a pressurized container to assist in heat transfer and preclude the possibility of RF voltage breakdown. The complete package weighs 8.21 pounds and is mounted at the top of the payload. It also serves as a support for the telemetering antenna mounted above it. Construction details are shown in Figures 43 and 44.

## 6. TELEMETERING ANTENNA

Ideally, the telemetering antenna radiation pattern should be symmetrical about the payload spin axis, and have its major lobe directed to the rear of the vehicle. Some power should be radiated forward however, so that signal reception will be assured if the payload tumbles after rocket burnout and nose cone ejection. In addition, since the protective fiberglas nose cone is ejected, the antenna must be mounted beneath the nose cone and capable of radiating during the powered portion of the flight. The antenna must be mounted as far away from the radio astronomy antenna as possible to minimize the transfer of telemetering power into the radiometers and antenna bridge. Since the vehicle spin stability is improved if the radio astronomy antenna is mounted at the base of the payload, the telemetering antenna must be located at the top

of the payload where the nose cone diameter is reduced. This in turn requires the use of a deployment scheme for the telemetering antenna and also interposes the radio astronomy antennas between the telemetering antenna and the ground receiving stations.

As a result of the above criteria it was necessary to undertake a development program to select a suitable antenna. Several basically different antenna designs were constructed and radiation patterns were measured on a full size mock-up of the payload with the radio astronomy antennas in place. The design finally chosen is a modified turnstile antenna shown in Figure 45. A normal turnstile is simply a pair of dipoles positioned perpendicular to each other and driven 90° out of phase. The modified turnstile shown here consists of 4 monopoles positioned every 90° around an 8 inch diameter cylinder. Each monopole is phased 90° from the adjoining monopole, with the phase increasing for each element counter-clockwise as viewed from the tail of rocket. This selection of electrical phasing produces right-hand circular polarization. Figures 46 and 47 illustrate details of the phasing network.

Each monopole is approximately $\lambda/4$ long. The length is trimmed until the real part of the monopole impedance equals the 70 ohm impedance of the phasing harness. At the output of the summing junction, a single-stub matching cable is used to transform the impedance to 50 ohms.

The monopoles are fabricated of silver plated 10 mil tempered beryllium copper strips, with a slight upward concavity, perpendicular to the long dimension. This shape is similar to that used in flexible steel tape measuring rules.

Nose cone ejection initiates telemetering antenna deployment by means of the assembly shown in Figure 48. When the nose cone is to be installed on the payload, the monopole tips are folded upward and secured under a phenolic plug. The plug is held in place temporarily by a long threaded rod. The rod projects through the central hole in the nose cone ejection spring assembly as the nose cone is lowered in place over the payload. In this position the monopole tips are pressed against contacts on the inner surface of the plug support. The 4 contacts connect 1500 ohm terminating resistors to the ends of the monopoles so that the RF power amplifier remains terminated with 50 ohms ±20% when the telemetering antenna is undeployed. In this position the radiation pattern is not ideal, but it is adequate for the initial portion of the flight. After the ejection spring assembly is cocked and seated properly on top of the phenolic plug, the long threaded rod can be unscrewed and removed. During nose cone ejection, the spring loaded phenolic plug is released and also ejects. As soon as the nose cone clears the top of the payload, the telemetering monopoles spring into their stable position which is a plane perpendicular to the payload spin axis. Release of the phenolic plug also actuates a switch which signals nose cone ejection via the telemetering system.

Measured radiation patterns obtained from a full-scale model of the payload with radio astronomy antennas deployed are shown in Figures 49, 50 and 51.

Since the antenna test range used was less than ideal, the patterns and magnitudes shown are probably not precisely correct. Enough work was done with various antennas however to provide reasonable confidence in the results. On each polar pattern, the 0 db point corresponds to the signal received from a $\lambda/2$ dipole antenna transmitting an equal amount of power. On these plots, 180° corresponds to reception of the signal by a ground station looking up at the tail of the rocket. As viewed from the ground, the transmitted signal is right-hand circularly polarized which complies with the standard polarization of most ground station helical antennas. It is of interest to note that many of the nulls, particularly in the forward direction of the right circular polarized pattern, are filled in when viewed with a left-hand polarized ground station helix. Because of this fact, a left-hand helix is used to feed a separate telemetering receiver. This precludes data loss in case the rocket tumbles and presents low signal levels to the right-hand helix.

# POWER SUPPLIES

## 1. BATTERIES

The primary power for all portions of this experiment is supplied by 33 type HR-5 Yardney Silvercels. Ten of the cells are connected in series to form a +14 volt battery and the remaining 23 are connected in series to form a -32 volt battery. The +14 volt battery is also tapped at approximately +7 volts. Each cell is rated at 5 ampere hours at 75°F which allows a minimum safety factor of 2 for the period of a normal rocket flight of approximately 30 minutes. The choice of these voltages and capacities is dictated by the need for high reliability in the power supplies. At least one cell in each battery can be completely discharged, forced to reverse its polarity, and begin charging in the opposite direction without affecting normal payload operation. The +14 volt battery has a somewhat greater safety factor because it is impossible to exactly balance the total load between each battery.

These cells are freely vented to their surroundings and thus not protected from the vacuum which exists during flight in the unpressurized nose-cone. Experiments have shown that although the battery electrolyte does boil during simulated space flight, the electrolyte loss in 30 minutes is not excessive. The payload test and environmental program (T. and E.) however often requires a number of hours in a hard vacuum. For this reason, it is necessary to enclose the batteries in the pressurized container shown in Figure 52. This adds 7 pounds to the total battery and hold-down hardware weight of 18 pounds.

One further consideration involved in the use of silver-zinc cells is the variation in terminal voltage during battery charge and discharge. The trickle charge terminal voltage of a fully charged cell is 2.0 volts at 75°F. This voltage increases somewhat if the cell is cold and decreases when the cell is hot. When a cell is discharging at the 1 hour rate (i.e., 5 amperes), the terminal voltage at the 50% discharge point is 1.4 volts. If the cell is cold, the voltage is even lower and vice versa. This means that the negative battery can vary from -32 volts to -46 volts at room temperature. If the battery is cold, the voltage range will be even greater. The positive battery varies from +20 volts to +14 volts. This variation of more than 40% in terminal voltage must be well tolerated by all circuits supplied directly or indirectly by the primary batteries.

## 2. DC TO DC CONVERTERS

Two DC to DC transistorized converters are used in this experiment. One, a 200 volt, 200 milliampere converter, shown in Figure 57 supplies B+ power to

the telemetering transmitter and the telemetering RF power amplifier. The second converter, a 235 volt, 200 milliampere unit shown in Figure 53 supplies power to the +130 volt and the +200 volt regulators for receiver and preamplifier B+, respectively. Both converters are conventional common emitter saturating core type power multivibrators. The switching rate for both units is approximately 3.5 kilocycles. Input currents for the transmitter and receiver converter are 1.4 and 1.3 amperes respectively.

It was known that this type of converter is capable of generating a considerable amount of pulse type RF noise so careful attention was paid to the converter input filtering. In addition to the converter pre-regulators discussed below, additional filtering was also required in two -32 volt supply lines before the interference in the radiometer output became undetectable. Proper methods of grounding to avoid ground loops and inductive paths also proved to be important.

Construction details of the +235 volt radiometer converter are shown in Figure 54. The +200 volt transmitter converter is mounted in the pressurized telemetering transmitter container shown in Figure 55.

## 3. REGULATORS

The eight power supply regulators used fall into 3 categories. One simple uncompensated Zener diode is used for regulation of the supply to the bridge oscillator. Three Zener diode biased emitter follower preregulators are used for the transmitter DC to DC converter, the transmitter filaments and the radiometer DC to DC converter. And finally, there are four highly compensated series pass transistor regulators for the radiometer filaments, preamplifier B+, receiver B+ and the +9 volt VCO power.

The pre-regulators shown in Figures 56, 57 and 58 are used to reduce the battery supply voltage variations and decouple the converter noise from the main battery lines. The Zener diodes used in these regulators are selected to achieve the desired input voltage to their respective loads. The transmitter preregulator is located inside the telemetering transmitter container to minimize the radiation of converter noise pulses and take advantage of the convective cooling afforded by the air inside the pressurized container.

Filament and plate power for the three radiometers must be well regulated if stable operation is to be achieved. With a possible variation of 40% in the battery supply voltage, the use of regulators with high internal loop gain is required. Figure 59 shows the -25 volt, 1.5 ampere radiometer filament regulator. Transistors $T_1$ and $T_2$ are paralleled series passing elements used to drop the input voltage the required amount. Resistors $R_1$ and $R_2$ also assist in dropping a portion of the input voltage. $T_3$ and $T_4$ are cascaded emitter followers providing sufficient current gain to drive the bases of $T_1$ and $T_2$. The error

amplifier, $T_5$ compares a fraction of the output voltage with the reference Zener diode $D_2$ voltage, and amplifies this difference. Resistor $R_{12}$ applies an error signal directly from the input to improve the compensation of input voltage variations. Temperature compensation is effected by adding a sufficient amount of positive temperature coefficient resistance to $R_9$. Typical performance of this regulator is as follows:

1. The output voltage is reduced by 1 mv for each 20 ma increase in current. This is an equivalent output impedance of 0.05 ohm. Full load current is 1.5 amperes.

2. The output voltage changes less than 6 mv for each 1 volt change in the input voltage.

3. For a constant input voltage, the output voltage changes less than 10 mv between 40°F and 120°F ambient temperature. Construction details of this regulator are shown in Figure 60.

Both B+ regulators are very similar in design as shown in Figure 61. Both receive their input power from the +235 volt radiometer converter which has a fairly constant output voltage because of its preregulator input. Transistor $T_1$ is the series passing element driven by the emitter follower connected transistor $T_2$. The error amplifier, $T_4$, compares a fraction of the output voltage with the reference Zener diode $D_6$ voltage and amplifies the difference. Additional voltage amplification is obtained from $T_3$. Diode $D_2$ protects $T_1$ from accidental overvoltage. One difference is the use of a power Zener diode $D_1$ used to drop 70 volts at the input of the +130 volt regulator only.

The amplifiers in each B+ regulator have the same operating voltages when referred to the positive polarity side of the regulator output. The error divider ratio and dropping resistors $R_5$ and $R_6$ for the Zener diodes have the values as indicated for the +130 and +200 volt operation. Each regulator will supply at least a 70 ma load. Temperature compensation is done with $R_8$ in the manner described for the -25 volt filament regulator.

Typical performance of this regulator type is as follows:

1. Less than 10 mv change in output occurs from no load to full load of 70 ma. This is an output impedance of 0.14 ohm.

2. The output voltage changes less than 0.5 mv per volt of input change.

3. For a constant input voltage, the output changes less than 50 mv between 40°F and 120°F.

Figure 62 is a photograph of the B+ regulator.

The +9 volt regulator shown in Figure 63 is a low voltage version of the B+ regulators and its electronic performance is similar. Its characteristics are as follows:

1. The output voltage varies less than 10 mv from no load to full load of 100 ma. Its output impedance is less than 0.1 ohm.

2. The output changes less than 1 mv per volt of input change.

3. For a constant input voltage, the output varies less than 10 mv between 40°F and 120°F.

This circuit board is shown in Figure 64.

## NASA ACCELEROMETER PACKAGE

As a result of prior vehicle in-flight performance malfunctions, the Vehicles Section of NASA Goddard Space Flight Center required that an accelerometer oriented to measure acceleration along the thrust axis be incorporated in the payload. The accelerometer package including a voltage regulator and a VCO was supplied by GSFC. The unit weighed 1.3 pounds and was furnished fused power from the +9 volt regulator. The VCO was also in-flight calibrated and input signal limited along with the other VCO's.

# INSTRUMENTATION SYSTEM

## 1. REMOTE CONTROL AND INTERCONNECTIONS

Remote control of the complete system is accomplished with a nine wire pull-off plug cable between the payload and a remote control box which can be located more than 300 feet away. Batteries can be monitored and charged, all equipment can be turned on and off and checked for proper operation without access to the payload. This is a great convenience during the firing count-down because any operational delays can be managed without difficulty. Normally, the total payload power requirements are supplied externally until just before rocket firing, at which time the system is switched to internal battery power and the pull-off plug is removed.

Three Ledex stepping switches designated "Receiver", "Transmitter" and "Monitor" in Figure 37 execute all remote control and monitor functions. They can be energized only by switched external power from the remote control box shown in Figure 66. The control box is connected via the pull-off plug cable and the payload interconnections shown on Figure 65. Both receiver and transmitter control Ledexes are wired as 6-position switches. The monitor Ledex is wired as a 12-position switch. The functions performed by these switches are summarized in Table IV.

The monitor Ledex output is connected to voltmeter M1 in the control box. The meter reading for normal operation is known by the remote control operator and thus any possible malfunctions can be noted and diagnosed. The monitor Ledex has a separate meter M2 that indicates which monitor Ledex position has been selected.

The other two meters M3 and M4 indicate the -32 volt and +14 volt external supply current to the payload at all times. This current is furnished by independently controllable power supplies external to the control box. Merely by adjusting these supplies, all or any intermediate level of external power can be metered to the payload.

Provision is also made to continuously monitor the receiver deck temperature so that during long operational holds in the rocket firing count-down, it is possible to monitor the payload temperature rise. The temperature rise is caused by the dissipation of approximately 230 watts in the payload when the batteries are fully charged and all power is supplied externally. During flight the dissipation drops to approximately 160 watts. The payload normally has enough thermal capacity to limit the temperature rise to a satisfactory degree. The fiberglas nose cone is an excellent thermal insulator however so that full power operation prior to take off cannot be maintained indefinitely. The

TABLE IV

| Switch Position | Function |
|---|---|
| | A. Receiver Control Ledex Functions |
| 1 | OFF |
| 2 | All radiometer filaments ON<br>Noise generator oven ON<br>+9 volt regulator ON |
| 3 | Receiver +130 volt B+ ON |
| 4 | Preamplifier +200 volt B+ ON |
| 5 | Sequence timer ON<br>Bridge power ON |
| 6 | Noise generator oven OFF<br>Fly position |
| | B. Transmitter Control Ledex Functions |
| 1 | OFF |
| 2 | Transmitter and RF amplifier filaments ON |
| 3 | Transmitter B+ ON |
| 4 | VCO power ON<br>Regulated +9 volt switched ON |
| 5 | Commutator motor ON |
| 6 | Fly position |
| | C. Monitor Ledex Functions |
| 1 | -32 volt battery monitor |
| 2 | Transmitter control Ledex position |
| 3 | 0.75 Mc receiver No. 1 $\int e_o \, dt$ |
| 4 | 1.225 Mc receiver No. 2 $\int e_o \, dt$ |
| 5 | 2.00 Mc receiver No. 3 $\int e_o \, dt$ |
| 6 | Regulated +200 volt monitor |
| 7 | Regulated +130 volt monitor |
| 8 | Regulated +9 volt monitor |
| 9 | Antenna bridge output |
| 10 | +14 volt battery monitor |
| 11 | Receiver control Ledex position |
| 12 | Master ON (fly) position |

normal procedure is to return to position No. 2 on the control Ledexes until the firing count-down is resumed. This condition can be maintained as long as is necessary.

Prior to removal of the pull-off plug before take off, it is mandatory that all control circuits be set up properly. The receiver and transmitter Ledexes must be in position 6 and the monitor Ledex must be in positon 12. Since it is possible to accidentally position these Ledexes in the wrong position a safety provision has been incorporated in the Ledex circuit wiring. One switch section on each Ledex closes only when the Ledex is in the "fly" position. All circuits are wired in series with a supply voltage to the monitor Ledex position 12. If the operator observes an up-scale reading on the monitor output meter $M_1$, in position 12, he can be assured that all control Ledexes are properly set.

Because it has been reported that pull-off plugs are occasionally damaged during pull-off just prior to vehicle lift-off, this possibility must be guarded against. In this design, the pull-off plug can suffer any combination of short circuits between pins or to ground, without affecting any portion of the system. This is accomplished by placing diodes in series with the two battery charging lines. Placing a ground on either line at the pull-off plug merely reverse biases the diode and no current can flow. The other lines with voltage present are the monitor Ledex position and output circuits. In each case, a large series resistor in the lines prevents excessive current flow.

Location and interconnections of all subsections of the payload are shown in Figures 65 and 67. The "A" deck shown at the top of Figure 65 is the base of the instrumentation rack. It is mounted on top of the drum-shaped nose-cone extension tube shown at the bottom of Figure 67. The extension section in turn is bolted to the thrust face of the fourth stage rocket motor. The extension section contains batteries and timers used to actuate the nose cone release and vehicle despin mechanisms. A plan view of the location of all major assemblies is shown to the left of the interconnections for each deck. Each terminal shown in a box is accessible for disconnect or check. The number on each line to each terminal refers to the origin or destination of that line. There are two main vertical cable runs (I and II) with branches at each deck. All branches shown enclosed by ovals are laced together. Coaxial cables are shown only at their termination points. Extensive use is made of barrier strip type terminals. Although this adds slightly to the overall payload weight, the problems of testing, interference tracing, calibration and trouble shooting are greatly minimized. Wiring used throughout is silver plated, high strand count, with spiral wrapped teflon insulation.

## 2. MECHANICAL DETAILS

Figure 68 is a scale drawing of the instrumentation rack structure. It is fabricated of magnesium plates and hollow tube vertical members, most of

which are heliarc welded in place. One post between the B and C deck is removable and the D deck is completely bolted in place. This construction technique requires that all mounting holes in decks A and B be completed before welding. Additions or modifications are difficult, but not impossible, because the space between plates A,B, and C does permit the entry and use of hand tools.

A 0.042 inch thick aluminum outer skin is bolted to each deck with 24 flat-head screws. This forms a stressed skin construction which is very stiff. Early tests with a payload rack which used smaller diameter solid vertical members which were bolted in place in a staggered pattern and which did not use the stressed outer skin, exhibited some very undesirable modes of vibration. The present structure weighs 5 pounds more than the early model, but no vibrational problems appear to exist.

Placement of subassemblies is determined by consideration of electrical, mechanical, accessibility, thermal and vehicle spin and balance requirements. With the configuration finally arrived at, only 0.8 pounds had to be added to comply with the 1 ounce static and 20 ounce inch-squared dynamic balance limits for the Argo D-8 vehicle.

Table V is a compilation of payload subassembly and nose cone hardware weights.

TABLE V

| Item | Weight | |
|---|---|---|
| | Pounds | Ounces |
| Instrumentation rack including skin (skin only: 2 lb, 6 oz) | 29 | 8 |
| Telemetering transmitter including container (pressurized container only: 2 lb, 6 oz) | 8 | 11 |
| Telemetering antenna and phasing cables | 3 | 11 |
| 3 radiometer receivers | 5 | 1 |
| Remote control and VCO assembly | 5 | 7 |
| Sequence timer | 2 | 6 |
| Radiometer DC-DC converter | 2 | 9 |
| -25 v filament regulator | 0 | 15 |
| +200 v B+ preamplifier regulator | 0 | 13 |
| +130 v B+ receiver regulator | 0 | 13 |
| Telemetering filament preregulator | 0 | 3 |
| VCO calibration batteries | 0 | 5 |
| Radiometer DC-DC converter preregulator | 0 | 3 |
| Silvercell batteries and container (pressurized container only: 7 lb, 0 oz) | 18 | 3 |
| 2 radio astronomy antennas and mounts | 4 | 9 |
| Random noise generator, oven, and transformer | 1 | 6 |
| Preamplifier first stage, antenna switch, and bridge | 2 | 8 |
| Preamplifier second stage | 0 | 15 |
| Plugs, cable harness, filters, etc. | 6 | 4 |
| Balance weight | 0 | 13 |
| NASA accelerometer | 1 | 5 |
| Outer nose cone with thermo lag coating | 31 | 5 |
| Nose cone locking ring and despin weights | 7 | 10 |
| Extension section including wiring | 9 | 10 |
| Total payload at takeoff | 145 lb | 1 oz |

## ROCKET DESCRIPTION AND PREDICTED PERFORMANCE

The Argo D-8 vehicle shown in Figure 69 is a four-stage solid propellant sounding rocket designed to be fired from a zero length launcher. The first three stages are fin stabilized and the fourth stage is spin stabilized. The maximum spin rate is 7.5 revolutions per second. With a total payload weight of 145 pounds, the predicted peak altitude is approximately 1300 miles for an 83° launch angle. The vehicle staging consists of a first stage Sergeant TX 20-6 with two Recruit XM-19 booster rockets attached to the sides. The booster rockets give a high initial acceleration to build up the velocity immediately after release from the launcher. Each recruit burns for 1.8 seconds and has a thrust of 38,000 pounds. The second stage is a Lance XM45 which ignites after a 10 second first stage coast interval. The third stage is another Lance XM45 rocket. Its fins are canted so that at burnout, the vehicle spin rate is increased to approximately 7 rps for fourth stage spin stabilization. The fourth stage is an Altair X248-A6 which ignites after a 13 second third stage coast interval. The X-248 remains attached to the payload throughout the flight. At 180 seconds the nose cone is spring ejected and a "yo-yo" despin mechanism is deployed. The vehicle spin rate is reduced by a factor of about 10 with this despin technique.

Table VI presents a summary of the rocket predicted performance, and sequence of events.

TABLE VI

| EVENT | TIME (sec) | ALTITUDE (feet) | VELOCITY (ft/sec) | THRUST (pounds) | WEIGHT (pounds) | ACCELERATION (G) |
|---|---|---|---|---|---|---|
| 1st Stage Ignition | 0 | 0 | 0 | 132,200 | 13,964 | 9.5 |
| Booster Burnout | 1.8 | - | - | 56,200 | 13,428 | 4.2 |
| 1st Stage Burnout | 27.5 | 42,242 | 2,822 | 56,200 | 6,402 | 8.8 |
| 1st Stage Detaches | 35.0 | ~60,000 | ~2,450 | 0 | 4,306 | ~-1.0 |
| 2nd Stage Ignition | 37.5 | 66,576 | 2,284 | 44,000 | 4,306 | 10.2 |
| 2nd Stage Burnout | 43.9 | 87,337 | 4,603 | 44,000 | 3,106 | 14.2 |
| 3rd Stage Ignition (2nd Stage Blast Separates) | 43.9 | 87,337 | 4,603 | 44,000 | 2,497 | 17.6 |
| 3rd Stage Burnout | 50.3 | 128,755 | 9,197 | 44,000 | 1,298 | 34.0 |
| 4th Stage Ignition (3rd Stage Blast Separates) | 63.0 | 237,227 | 8,772 | 3,040 | 702 | 4.3 |
| 4th Stage Burnout | 101.8 | 676,557 | 17,596 | 3,040 | 198 | 15.4 |
| Nose Cone Separation and Despin | 180.0 | 1,750,149 | ~14,300 | 0 | 166.5 | 0 |
| Apogee - for 83° Launch Angle | 922.0 | 6,965,563<br>1,319 mi<br>2,123 km | 5,198<br>(Horizontal) | 0 | 166.5 | 0 |

# PAYLOAD EVIRONMENTAL TEST REQUIREMENTS

It is standard practice to subject rocket payloads to a series of rigorous tests to determine functional reliability of all components and construction techniques. The first payload constructed is designated as the prototype. It is subjected to environmental rigors more stringent than those expected for transportation, handling, prelaunch tests, launch, boost phase and coasting flight. A second model designated the flight unit is subjected to tests which demonstrate the ability of the design to meet all performance requirements without harmful degradation at the expected flight levels.

The required test facilities available at GSFC and the tests prescribed by NASA for The University of Michigan Radio Astronomy Observatory Cosmic Noise Rocket Payload designated NASA 11.02 UR are itemized in the Appendix.

## TELEMETERING GROUND STATION

A complete telemetering ground station has been assembled for this experiment. It provides a means to perform pre-flight system checks, in-flight data recording, real time readout and post-flight data reduction. A photograph of the telemetering ground station set up in the Wallops Island Block House is shown in Figure 70. The tape recorder rack contains the main items of the FM/FM telemetering station. Below the Ampex Model CP-100 tape recorder is a Nems-Clarke Model 1432 phase lock FM receiver. Below it is a bank of six EMR Model 167-01 phase lock subcarrier discriminators. An interconnect and control panel is below the discriminators, followed by a Nems-Clarke Model 200-3 spectrum display unit for the FM receiver. The bottom panel is an EMR Model 101-A crystal reference oscillator and mixer amplifiers for the tape recorded subcarrier oscillator tape speed compensation system. The right hand rack contains another FM receiver, a CMC Model 727A counter, a H-P Model 200CD audio oscillator, a special 70 watt 135 cycle power amplifier, a NLS Model 484 digital voltmeter, a Boonton Model 202 FM/FM signal generator and a H-P Model 100D precision frequency standard. Except for the counter and digital voltmeter, all equipment in the right hand rack plus an antenna preamplifier not shown was borrowed from other NASA supported groups at The University of Michigan. To the left of the two racks is a CEC Model 5-124 direct recording oscillograph with seven active galvanometers for quick readout information. A Tektronix Model 533 oscilloscope for waveform monitoring completes the telemetering ground station. To the right on the table is the rocket remote control box and the two power supplies for payload battery charging.

For telemetering reception and recording during rocket flight, the ground station is arranged as shown in Figure 71. In general, this is typical of a high precision system with extra features added to optimize its performance for this application. Following signal capture by the right-hand helical antenna with a gain of 20 db, the signal is amplified by a 33 db gain, 5 db noise figure preamplifier at the antenna site. The amplified signal enters receiver No. 1 and is demodulated. The resulting composite subcarrier signal is fed to a mixer amplifier where a precision 100 kc sine wave is added to the subcarriers. Introduction of the 100 kc signal provides a reference frequency for the tape speed compensation channel which is used during tape playback. The mixer output goes to two direct channels on the one inch 7 channel tape recorder. The direct channels have a frequency response from 200 cps to 100 kc at a tape speed of 30 inches per second. This speed allows approximately 34 minutes of uninterrupted recording time. Two channels are used to preclude the loss of data if one channel fails during recording. From Receiver No. 1, the signal also goes to the subcarrier discriminators via the receiver selector switch. Each discriminator has an input band-pass filter to select the appropriate channel as shown. The

discriminator output is a replica of the corresponding payload telemetering input voltage and is recorded on the direct readout recording oscillograph. Provisions are also made to record the discriminated output on the FM channels of the tape recorder which have a frequency response from 0 to 10,000 cycles per second.

The receiver signal strength information is displayed on a meter at the antenna location so that the operator can manually track the antenna by positioning for maximum signal strength. Signal strength from both receivers is also time multiplexed with a 60 cycle chopper and recorded on a FM tape channel.

Take-off time is recorded both on tape and the oscillograph. At take-off, a microswitch on the rocket launcher rail actuates. Relay circuits shown in Figure 72 in the ground station lock on, and key a 10 kc signal to the tape recorder and 1 cycle per second pulses to the time line generator in the oscillograph. The 10 kc timing channel also accepts audio signals from a microphone and amplifier shown in Figure 73 for voice recording before and during the rocket flight. During playback, a filter separates the two signals.

Signals from the left-hand helix are handled in much the same fashion. The receiver selector switch allows transfer of either receiver composite signal to the discriminator inputs. Only one tape channel for direct recording is provided for this signal because it is not expected to be as good as that from the right hand helix.

The overall circuit for the telemetering ground station is shown in Figure 74. Not shown are the circuits used for recording take-off time and automatic three-step calibration of the direct (FM) channels of the tape recorder. The take-off circuit shown in Figure 74 is actuated from a normally closed microswitch on the rocket launcher rail. At lift-off, this switch opens and $RY_1$, is deenergized. It cannot be energized again until the "arm" switch is depressed. Requiring the take-off switch to open on lift-off and arranging to lock out the relay provides a measure of fail safe protection. Because of the location of the take-off switch, the wires are likely to burn off at rocket ignition and thus cannot be depended on for continuity.

Automatic three-step calibration of the tape recorder FM channels is desirable because these channels do not have playback tape speed compensation. Any drift caused by speed variation cannot be separated from a signal level change without resort to a calibration procedure such as this. Since the discriminators are arranged to vary from -2.5 volts to +2.5 volts for 0 to +5 volt variations in the rocket payload, -2.5, 0 and +2.5 volt calibration setups are programmed automatically for two seconds once every two minutes by the ground station calibrator circuit shown in Figure 75. In addition to the automatic calibration sequence, a manual switch allows additional calibrations to be made at any other time. This switch does not disturb the regular two minute calibration cycle.

The tape recorder and discriminators are also used for tape playback. As Figure 74 indicates the cable patch panel is arranged to transfer the played-back composite signal from the signal delay line into the discriminators for demodulation. In this mode, the 70 kc tuning units for Channel No. 6 discriminator are removed and 100 kc units are substituted. If the tape recorded signals contain any speed variations, they appear as steady-state offsets or fluctuations in the 100 kc discriminator output. This error signal is inserted at the proper point in each of the other discriminators. Cancellation of output variations due to tape speed changes is thus accomplished. The composite signal to the 100 kc channel does not pass through the signal delay unit. In this way, the proper time delay between the tape speed error signal and the other discriminator outputs is maintained. When properly adjusted, this technique produces an improvement of at least 100:1 in tape recorder flutter and wow compared to an uncompensated system.

The 10 kc timing signal which is keyed "on" at take-off provides a time base for all events that occur during flight. The filtered 10 kc waveform drives a digital counter. Every 10,000 counts is one second of flight. In effect, an accumulating counter can thus be used to assign a serial number to each event which then can be uniquely related to the instant of take-off within $\pm 2 \times 10^{-4}$ seconds. The oscillograph time lines perform the same function although the absolute magnitude of the uncertainty is somewhat larger.

Figure 76 shows a section of a typical telemetering record. All data is encoded in the form of oscillograph trace deflections from the reference traces at the record top and bottom. The in-flight calibration sequence provides a means to determine the trace "zero level" and the trace deflection factor for the 4.04 volt calibration level. One second time lines and digital time trace derived from the National Bureau of Standards WWV time signal allows precise time resolution of all events.

## TELEMETERING DATA REDUCTION

Manual data reduction from records such as shown in Figure 78 is very tedious. Each second of flight, the trace deflection for each channel must be scaled, corrected for zero level and then converted to a true voltage. In many cases, this procedure must be done as often as ten times a second where fine detail in the record is important. On the commutated channel, this procedure must be repeated thirty times a second if a complete readout is required.

The true voltage readings and their associated times from take-off are next used to enter appropriate calibration tables or curves for each channel. If necessary, corrections for factors such as ambient temperature, base-line shift and gain variations must also be introduced. The final result is a tabulation of the measured parameters with respect to time from rocket take off. These data can then be related to altitude with the altitude versus time trajectory data.

The above procedure can be automated to a considerable extent with a consequent reduction in time and cost of data reduction, and an increase in accuracy. Figure 77 illustrates an analog to digital data conversion and oscillograph recording system used to assist in reduction of data from the rocket flight. This data logging section and the LGP-30 computer were loaned by other groups at The University of Michigan. The A to D system is limited to a single channel of data input at a rate of 10 samples per second. Each sample consists of sign, 4 binary coded decimal digits, and the LGP-30 computer stop code. The maximum data rate is limited by the output paper tape punch which has a maximum rate of 15 samples per second. This rate precludes automatic reduction of the commutated channel. Fortunately, it is not necessary to readout all 30 segments each second, since many have a very slow rate of change.

If the system shown in Figure 77 is arranged to reduce a radiometer output channel, it is very important to be able to assign a time from takeoff to each sample. The data logging system itself has no provision for including this information, so indirect means must be used. This is done by using the 10 kc precision timing signal (on the tape) which is keyed "on" at take off. The 10 kc signal is filtered from the voice channel and routed to the counter. The counting mode is set for total counts and in effect functions as a frequency divider, in this case, by 1000. The resultant 10 pulses per second are used to control the digitization sample rate of the A to D converter. Time from takeoff is thus uniquely associated with each sample point throughout the flight.

The first step in the data reduction is to take the digitized raw data and enter the LGP-30 computer. A program is written to "serialize" the data.

This consists of adding a sequential serial number at the beginning of each 20 data samples which will hereafter be called words. The computer also adds typewriter carriage return and spacing commands to automate the readout, and prints out a new punched paper tape. This tape is called the serialized raw data tape and now is printed out or "listed" by a paper tape controlled typewriter called a Flexowriter. Over 16,000 four digit numbers plus sign are printed out for each channel for a 1525 second flight.

The next step is the reduction of the serialized raw data to true volts. It will be recalled from an earlier section that the ground station VCO discriminator outputs are arranged to have symmetrical plus and minus voltage variations as the VCO input voltage varies from 0 to +5 volts. Level shift and multiplying factors must be derived and applied to convert the data to the original VCO input voltages. This is done by manually referring to the raw data during the VCO in-flight calibration sequences. A table of factors and the serialized intervals over which they apply is prepared along with the necessary programming and the computer is again reentered. The computer output is now a serialized true voltage punched tape which again is listed. This listing is done to check the accuracy of the computer results by observing whether the true voltages during VCO calibration are as expected. Spot checks can also be made against the oscillograph recordings. Gross errors can readily be seen, but little else, because the digital system has an inherent accuracy of at least 10 times that of the analog records. Experience has shown that as confidence is gained in the automatic data reduction program, less intermediate data listing is required. With the relatively low listing rate of the Flexowriter, less listing materially decreases the time required to process the data.

One further step in data reduction can now be done. The radiometer preflight noise calibration data in the form of tabulated values of $T_A R_A$ input versus $\int e_o \, dt$ radiometer output can now be stored in the computer. A program for conversion from true volts to uncorrected $T_A R_A$ can be formulated and a final computer run will produce an output tape of serialized uncorrected $T_A R_A$. Although even further computer reduction is possible, it was not carried out in this program. Corrections for radiometer no-noise and noise calibrations were performed manually.

# APPENDIX

## ENVIRONMENTAL TESTS

The following is a description of the environmental test program required by NASA for the prototype and the flight model instruments described above.

### General Instructions

### TEST FACILITIES

#### General

The apparatus used in conducting tests shall be capable of producing and maintaining the test conditions required, with the equipment under test installed in/on the apparatus and operating or non-operating as required. Changes in test apparatus conditions may be the maximum permitted by the test apparatus, but shall not exceed the applicable equipment specification requirements.

#### Volume

The volume of the test facilities shall be such that the bulk of the equipment under test shall not interfere with the generation and maintenance of test.

#### Heat Source

The heat source of the test facilities shall be so located that radiant heat shall not fall directly on the equipment under test, except where application of radiant heat is one of the test conditions.

#### Standard Conditions for Test Area

Normally checkout will be conducted at room-ambient conditions. Reversion to "standard" conditions will be required only in the case of equipment malfunction or unresolved questionable operation. For this condition, standard conditions are defined as follows:

a. Temperature: 25 ± 3°C (77° ± 5°F).
b. Relative humidity: 55 percent or less.
c. Barometric pressure: Local ambient.

## MEASUREMENTS

All measurements shall be made with instruments whose accuracy conforms to acceptable laboratory standards, and which are appropriate for measurement of the environmental condition concerned. If tests are conducted outside of GSFC facilities, the accuracy of the instruments and test equipment shall be verified before test, after test, and periodically as required by GSFC.

### Tolerances

The maximum allowable tolerances on test conditions shall be as follows:

a. Temperature: Plus or minus 2°C (3.6°F).
(Exclusive of accuracy of instruments.)
b. Relative humidity: Plus 3 percent minus 2 percent R.H.
c. Vibration amplitude: Plus or minus 10 percent.
d. Vibration frequency: Plus or minus 2 percent.
e. Additional tolerances: Additional tolerance shall be as specified.

### Vacuum Gages

The vacuum shall be indicated by a vacuum gage the sensing element of which is located within the chamber test space. The gage shall measure the vaccum as it exists at the payload.

## TEST SEQUENCE

| Prototype | Flight Unit |
|---|---|
| Dynamic Balance | Dynamic Balance |
| Spin | Spin |
| Acceleration | Vibration |
| Temperature | Thermal Vacuum |
| Humidity | |
| Vibration | |
| Thermal Vacuum | |

## DYNAMIC BALANCE

Although not an environmental test, balancing is necessary for a spin stabilized payload and shall be performed prior to exposure to environmental tests. Balancing is chosen as the first operation so that the adhesion and effect of the balance weights on payload operation may be evaluated during the course of the tests.

The payload, while non-operative, shall be balanced about the thrust axis in accordance with the following:

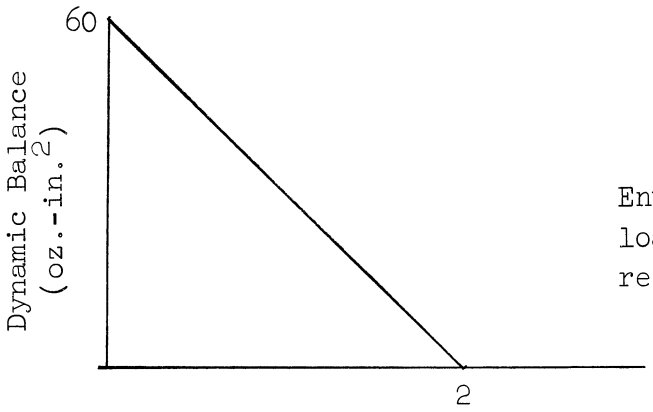


Envelope of acceptable payload balance restraints in relation to C.G. of payload.

The payload and the fourth-stage (X-248) shall be balanced as a composite unit upon completion of all environmental tests.

## SPIN TEST

This test will demonstrate the ability of the electronics and payload structure to withstand the spin forces experienced during flight.

### Pre-exposure Examination and Test

Before exposure to spin, the payload shall be visually examined and functionally tested to assure correct performance.

### Prototype Test

The payload, while in an operational condition normal to powered flight, shall be spun about the thrust axis at 625 RPM for a period of 5 minutes.

Flight Unit Test

The payload, while in an operational condition normal to powered flight, shall be spun about the thrust axis at 500 RPM for a period of 5 minutes.

Post-exposure Examination and Test

After exposure to spin, the payload shall be visually examined and functionally tested to assure correct performance.

ACCELERATION TEST

This test will demonstrate the ability of the electronics and payload structure to withstand acceleration forces experience during flight.

Pre-exposure Examination and Test

Before exposure to acceleration, the payload shall be visually examined and functionally tested to assure correct performance.

Prototype Test

The payload, while in an operational condition normal to powered flight, shall be exposed to the following acceleration levels:

| Direction (Axis) | Acceleration (g's) | Duration (Minutes) |
|---|---|---|
| Thrust (+Z) | 50 | 5 |
| Transverse (+X) | 3 | 3 |
| Transverse (+Y) | 3 | 3 |

Post-exposure Examination and Test

After exposure to acceleration, the payload shall be visually examined and functionally tested to assure correct performance.

TEMPERATURE TEST

The temperature test is designed to demonstrate the ability of the payload to withstand the environment of temperature which could be encountered in shipment and storage of the payload if no attempt is made to control the ambient conditions. The operational tests under temperature are conducted before attemping thermal-vacuum testing of the prototype. They serve to indicate the resistance of the design to extremes of expected in-flight temperatures plus a safety factor, and to give some assurance that it is worthwhile to attempt to conduct the more complicated and expensive thermal-vacuum test procedure.

Pre-exposure Examination and Test

Before exposure to temperature, the payload shall be visually examined and functionally tested to assure correct performance.

Prototype Test

While non-operative the payload shall be subjected to a test chamber temperature of -30°C ± 2°C (-22°F) for a period of 6 hours followed by a temperature of +60°C ±2°C (138°F) for a period of 6 hours. The payload shall be functionally tested at 25°C ± 5°C between and after the storage temperature exposures to assure correct performance.

The chamber temperature shall then be lowered to a temperature of -25°C ± 2°C (-13°F) and the temperature of the payload stabilized. The payload shall be functionally tested to assure correct performance. The chamber temperature shall be raised to +34°C ± 2°C (93°F), and the temperature of the payload stabilized. The payload shall be functionally tested to assure correct performance.

HUMIDITY TEST

The humidity test is designed to demonstrate the ability of the payload to withstand the environment of humidity which could be encountered in shipment and storage of the payload if no attempt is made to control the ambient conditions.

Pre-exposure Examination and Test

Before exposure to humidity, the payload shall be visually examined and functionally tested to assure correct performance.

Prototype Test

The payload, while non-operative shall be exposed to a chamber temperature of +30°C ± 2°C (86°F) with a relative humidity of 95% +3 -2% for a period of 6 hours.

Post-exposure Examination and Test

After exposure to humidity, the payload shall be visually examined and functionally tested to assure correct performance.

VIBRATION TESTS

The vibration tests given herein are intended to provide assurance that the payload will survive the expected flight environments and are applicable to the complete payload in its powered flight configuration. The prototype test levels are increased by 50% above the anticipated flight levels to provide a factor of safety in design. The vibration tests are based principally on the excitations generated by use of the ABL-X-248 rocket motor. The vibration excitation shall be applied at the interstage connection between the final stage and the payload. In establishing the test levels some allowance has been made for excitation generated by earlier stages, aerodynamic disturbances and handling and transportation effects. The resonance test is required because of unique resonant burning observed in the X-248 rocket motor.

Pre-exposure Examination and Test

Before exposure to vibration, the payload shall be visually examined and functionally tested to assure correct performance.

Prototype Test

The payload, while in an operational condition normal to powered flight shall be exposed to the following vibration levels:

Sinusoidal Swept Frequency

| Direction | Frequency Range cps | Test Duration ≃ Min. | Acceleration g. 0-to-peak | |
|---|---|---|---|---|
| Thrust (Z-Z axis) | 5-50 | 1.6 | 2.3 | (a) |
| | 50-500 | 1.6 | 10.7 | |
| | 500-2000 | 1.0 | 21.0 | |
| | 2000-3000 | 0.26 | 54.0 | |
| | 3000-5000 | 0.34 | 21.0 | (b) |
| | Total | ≃ 5.0 Min. | | |
| Lateral A (X-X axis) | 5-50 | 1.6 | 0.9 | (a) |
| | 50-500 | 1.6 | 2.1 | |
| | 500-2000 | 1.0 | 4.2 | |
| | 2000-5000 | 0.6 | 17 | (b) |
| | Total | ≃ 5.0 Min. | | |
| Lateral B (Y-Y axis) | 5-50 | 1.6 | 0.9 | |
| | 50-500 | 1.6 | 2.1 | |
| | 500-2000 | 1.0 | 4.2 | |
| | 2000-5000 | 0.6 | 17 | (b) |
| | Total | ≃ 5.0 Min. | | |

Sweep Rate: 2 octaves/minute

(a) Amplitude limited to 0.5 peak to peak.

(b) Within frequency limitation of vibration generator.

Random Motion Vibration

| Direction | Frequency Band cps | Spectral Density $g^2$/cps | g-rms |
|---|---|---|---|
| Thrust axis | 20-2000 | 0.07 | 11.5 |
| Transverse axes | 20-2000 | 0.07 | 11.5 |

Duration: 4 minutes each direction

Total time: 12 minutes

Control accelerometer response shall be equalized with peak-notch filterization such that the specified PSD values are within ± 3 db everywhere in the frequency band. The filter roll-off characteristic above 2000 cps shall be at a rate of 40 db/octave or greater.

Combustion Resonance

Apparent Weight. The apparent weight of the prototype may be measured at 600 cps. The amplitude values given below are based on an apparent weight of 7 lb at this frequency. Correction of the amplitude in inverse proportion to the actual apparent weight should be made, but in no case shall the amplitudes be greater than those given. An alternate method may be substituted wherein vibration force is programmed into payload between 550 and 650 cps at ± 600 lb force thrust direction and ± 100 lb force transverse direction if a suitable force control is employed.

Combustion Resonance Vibration

| Direction | Frequency cps | Acceleration 0-to-peak | Test Duration Sec. |
|---|---|---|---|
| Thrust axis | 550-650 | 86 | 30 |
| Transverse axes | 550-650 | 15 | 30* |

*30 seconds each axis.

Flight Unit Test

The payload, while in operational condition normal to powered flight shall be exposed to the following vibration levels:

Sinusoidal Swept Frequency

| Direction | Frequency Range cps | Test Duration ≃ Min. | Acceleration g, o-to-peak |
|---|---|---|---|
| Thrust (Z-Z axis) | 5-50 | 0.8 | 1.5 (a) |
| | 50-500 | 0.8 | 7.1 |
| | 500-2000 | 0.5 | 14 |
| | 2000-3000 | 0.13 | 36 |
| | 3000-5000 | 0.17 | 14 (b) |
| | Total | ≃ 2.5 Min. | |
| Lateral A (X-X axis) | 5-50 | 0.8 | 0.6 (a) |
| | 50-500 | 0.8 | 1.4 |
| | 500-2000 | 0.5 | 2.8 |
| | 2000-5000 | 0.3 | 11.3 (b) |
| | Total | ≃ 2.5 Min. | |
| Lateral B (Y-Y axis) | 5-50 | 0.8 | 0.6 (a) |
| | 50-500 | 0.8 | 1.4 |
| | 500-2000 | 0.5 | 2.8 |
| | 2000-5000 | 0.3 | 11.3 (b) |
| | Total | ≃ 2.5 Min. | |

Sweep Rate: 4 octaves/minute

(a) Amplitude limited to 0.5 peak to peak.

(b) Within frequency limitation of vibration generator.

Random Motion Vibration

| Direction | Frequency Band cps | Spectral Density $g^2$/cps | g-rms |
|---|---|---|---|
| Thrust axis | 20-2000 | .03 | 7.8 |
| Transverse axes | 20-2000 | .03 | 7.8 |

Duration: 2 minutes each direction
Total Time: 6 minutes

Control accelerometer response shall be equalized with peak-notch filterization such that the specified PSD values are within ± 3 db everywhere in the frequency band. The filter roll-off characteristic above 2000 cps shall be at a rate of 40 db/octave or greater.

Combustion Resonance

Apparent Weight. The apparent weight of the flight payload may be measured at 600 cps. The amplitude values given below are based on an apparent weight of 7 lb at this frequency. Correction of the amplitude in inverse proportion to the actual apparent weight should be made, but in no case shall the amplitudes be greater than those given. An alternate method may be substituted wherein vibration force is programmed into payload between 550 and 650 cps at ± 400 lb force thrust direction and ± 67 lb force transverse direction if a suitable force control is employed.

Combustion Resonance Vibration

| Direction | Frequency cps | Acceleration, g 0-to-peak | Test Duration Sec. |
|---|---|---|---|
| Thrust axis | 550-650 | 56 | 15 |
| Transverse axes | 550-650 | 8 | 15* |

*15 seconds each axis.

Post-exposure Examination and Test

After exposure to vibration, the payload shall be visually examined and functionally tested to assure correct performance.

Thermal Vacuum Test

This test will demonstrate the ability of the electronics and payload structure to withstand both flight temperatures and pressure.

Pre-exposure Examination and Test

Before exposure to thermal vacuum, the payload shall be visually examined and functionally tested to assure correct performance.

Prototype Test

Low Temperature Vacuum

With the payload in the non-operative condition, the temperature of the chamber shall be reduced to -30°C ± 2°C (-22°F). Upon reaching temperature stabilization, the payload shall be turned on and the chamber shall be evacuated to a pressure of 1 x $10^{-5}$ mm of Hg or less.

After a pressure of 1 x $10^{-4}$ mm Hg has been reached, the payload may be turned off and the chamber shall remain stabilized at -30°C ± 2°C for a period of 6 hours. At the end of this 6-hour period, the payload shall be functionally tested to assure correct performance. At the end of this performance check, the payload may be turned off.

High Temperature Vacuum

At the conclusion of the low temperature vacuum exposure, the chamber temperature shall be raised to +35°C ± 2°C (95°F), allowed to stabilize at this temperature, and held there for 6 hours. At the end of this 6-hour period, the payload shall be functionally tested to assure correct performance. The chamber temperature and pressure shall then be returned to normal room conditions.

Flight Unit Test

Low Temperature Vacuum

With the payload in the non-operative condition, the temperature of the chamber shall be reduced to -20°C ± 2°C (4°F). Upon reaching temperature stabilization, the payload shall be turned on and the chamber shall be evacuated to a pressure of 1 x $10^{-5}$ mm of Hg or less.

After a pressure of 1 x $10^{-4}$ mm Hg has been reached, the payload may be turned off and the chamber shall remain stabilized at -20°C ± 2°C for a period of 6 hours. At the end of this 6-hour period, the payload shall be functionally tested to assure correct performance. At the end of this performance check, the payload may be turned off.

High Temperature Vacuum

At the conclusion of the low temperature vacuum exposure, the chamber temperature shall be raised to +25°C ± 2°C (77°F), allowed to stabilize at this temperature, and held there for 6 hours. At the end of this 6-hour period, the payload shall be functionally tested to assure correct performance. The chamber temperature and pressure shall then be returned to normal room conditions.

Post-exposure Examination and Test

After exposure to thermal vacuum, the payload shall be visually examined and functionally tested to assure correct performance.

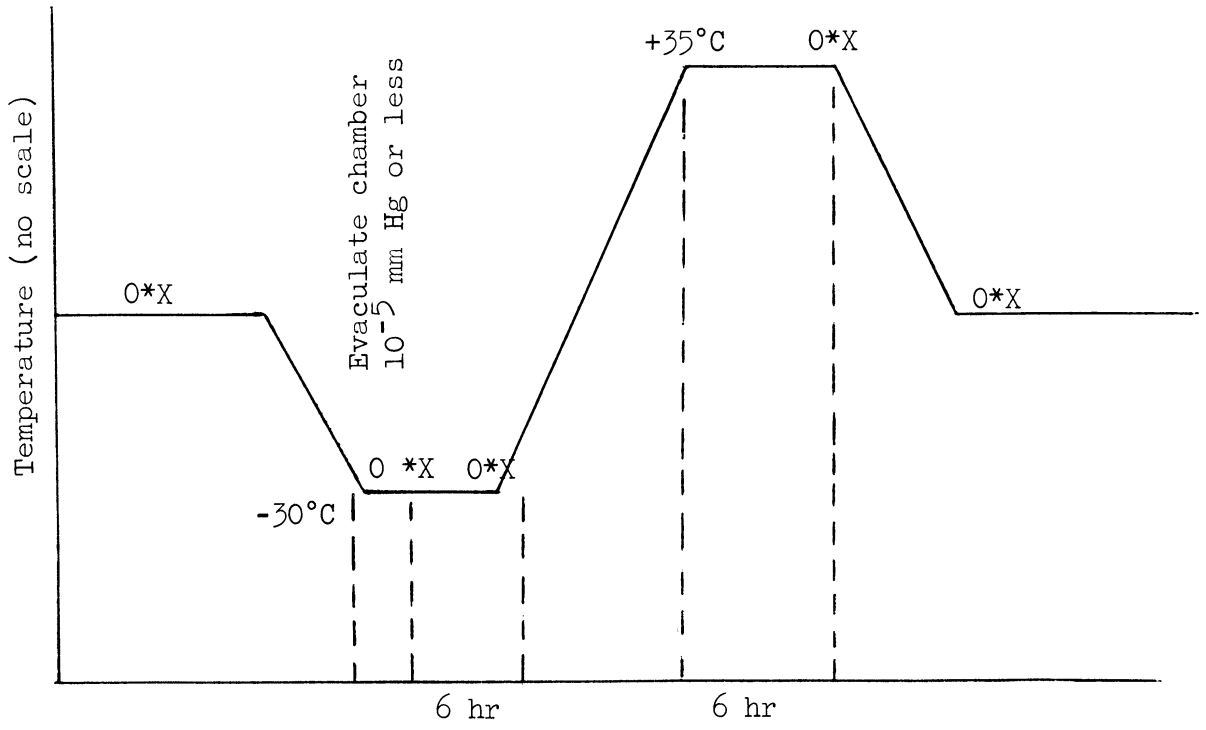


0 - Payload On
X - Payload Off
* - Payload Checkout

TIME (no scale)

FIGURES

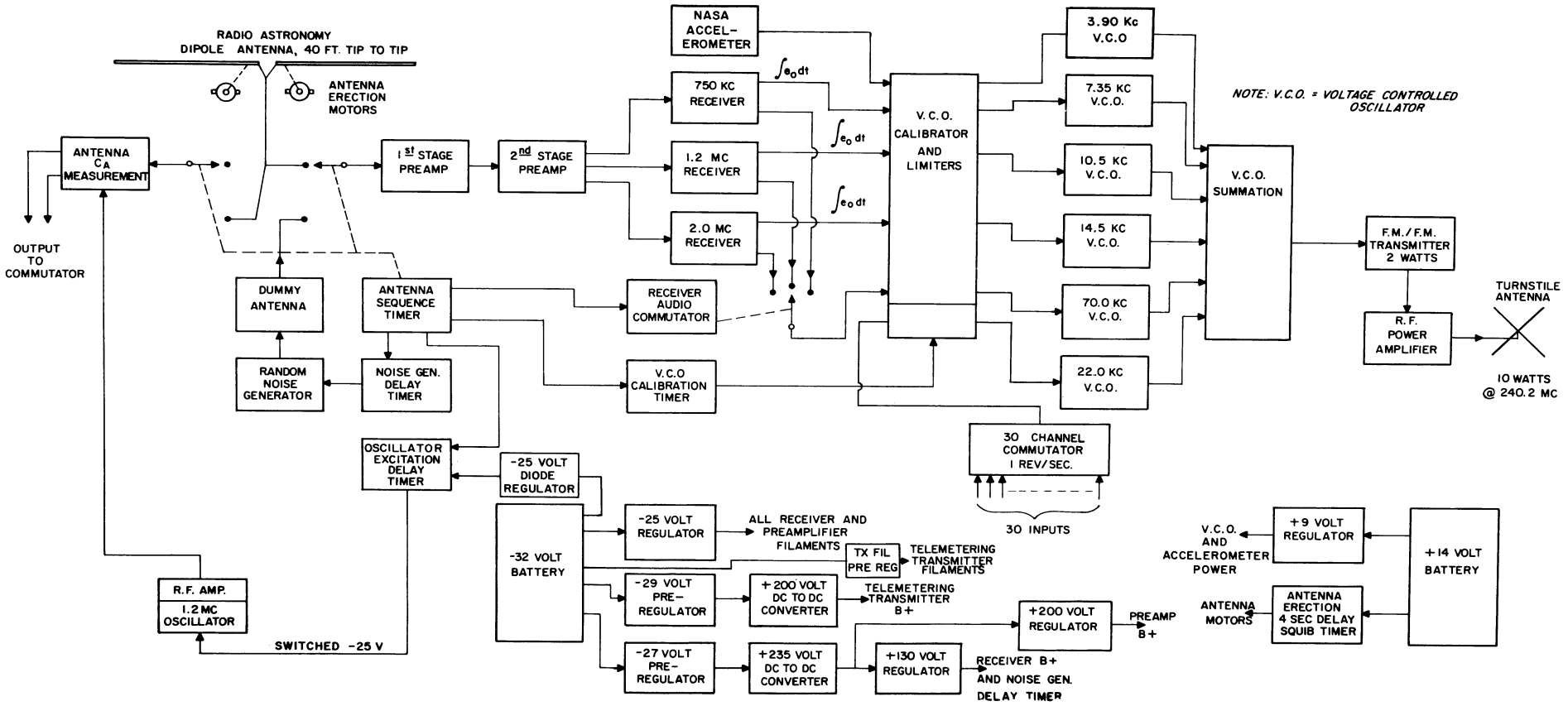


Figure 1. Rocket-borne cosmic noise measurement system.

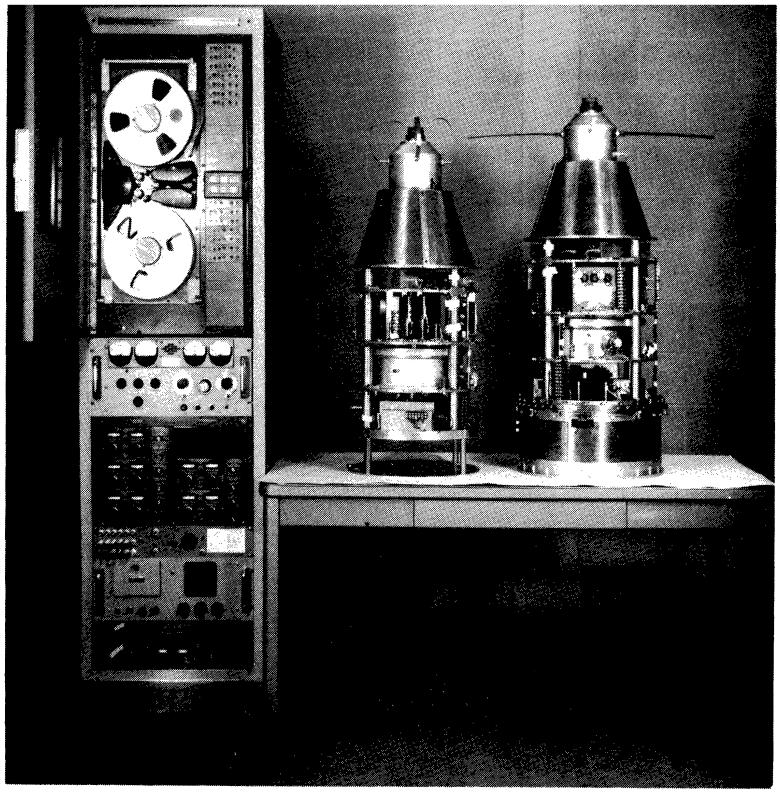

Figure 2. Prototype, flight model, and telemetering ground station.

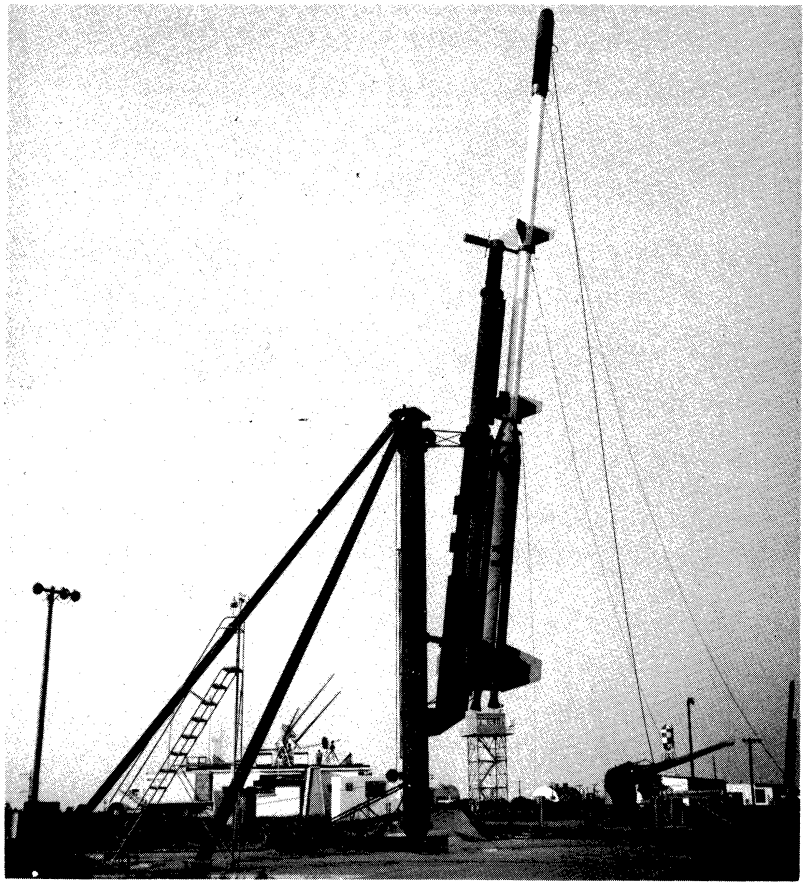

Figure 3. Journeyman D-8 rocket.

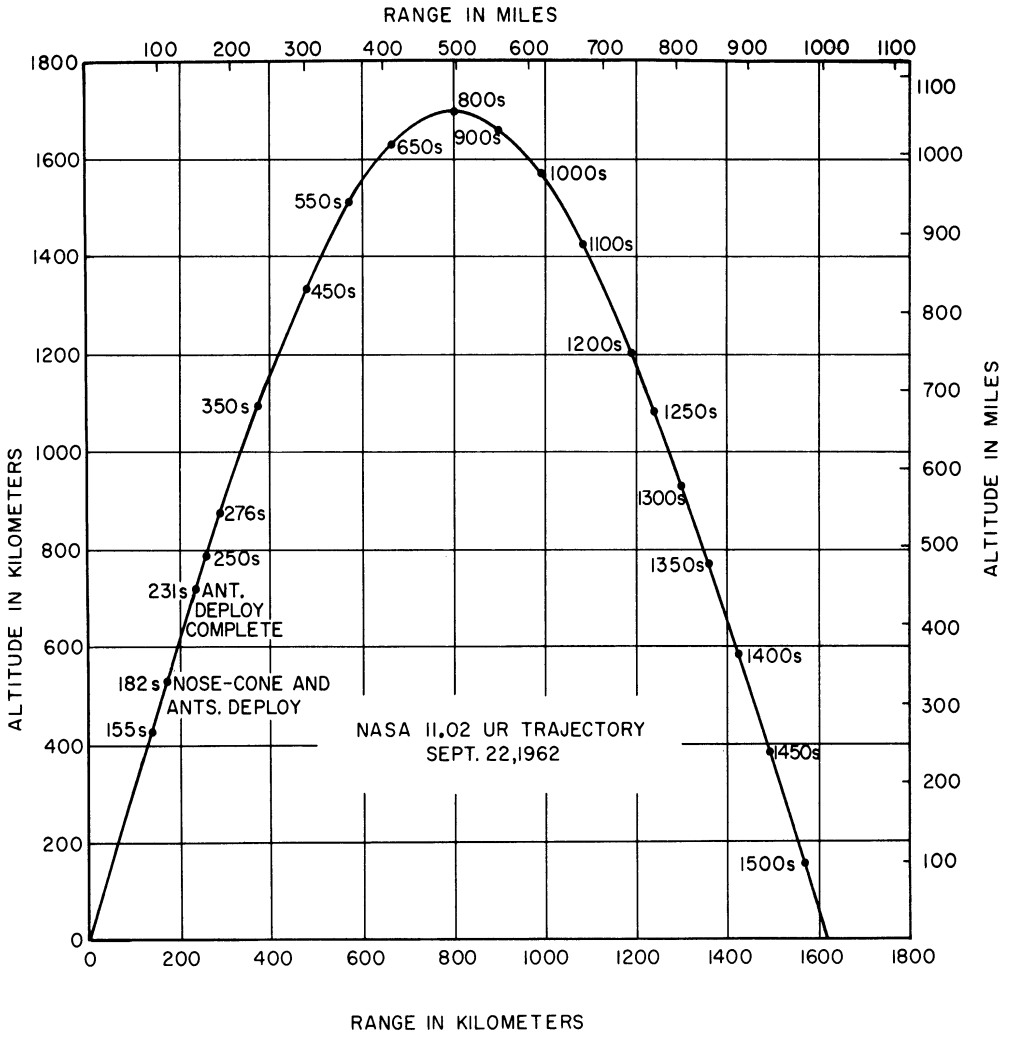


Figure 4. Rocket flight trajectory.

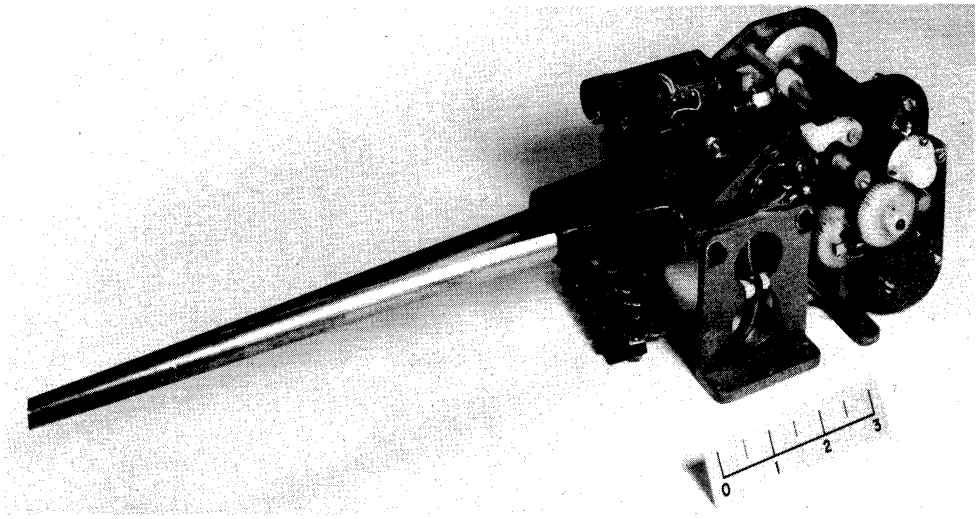


Figure 5. DeHavilland A2/2 antenna.

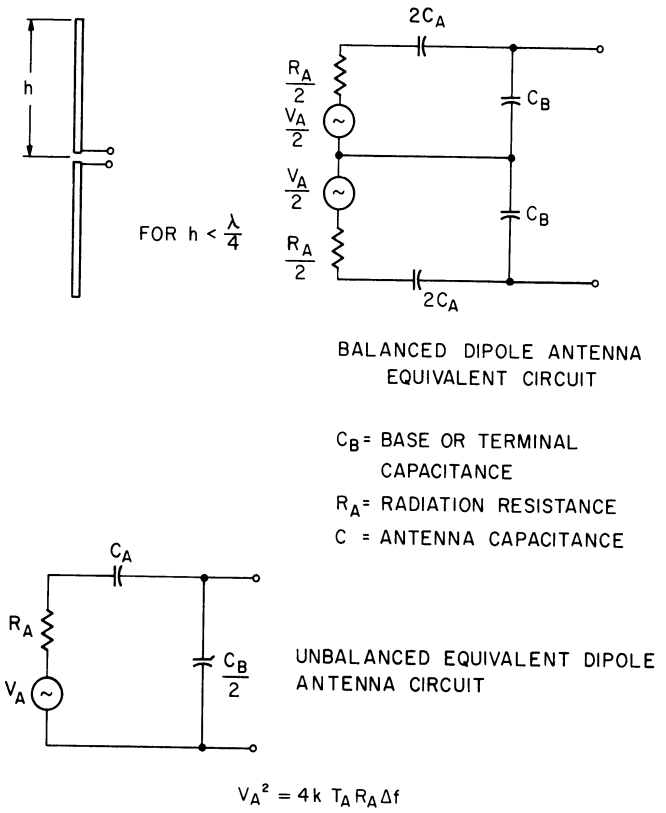


Figure 6. Equivalent circuit of radio astronomy antenna.

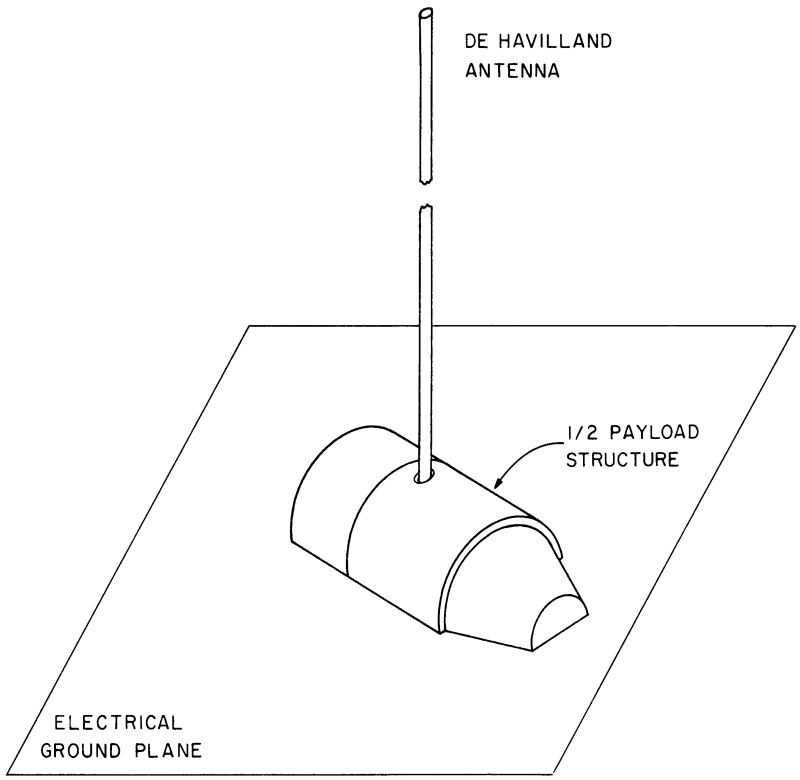


Figure 7. Mockup for Jansky and Bailey antenna tests.

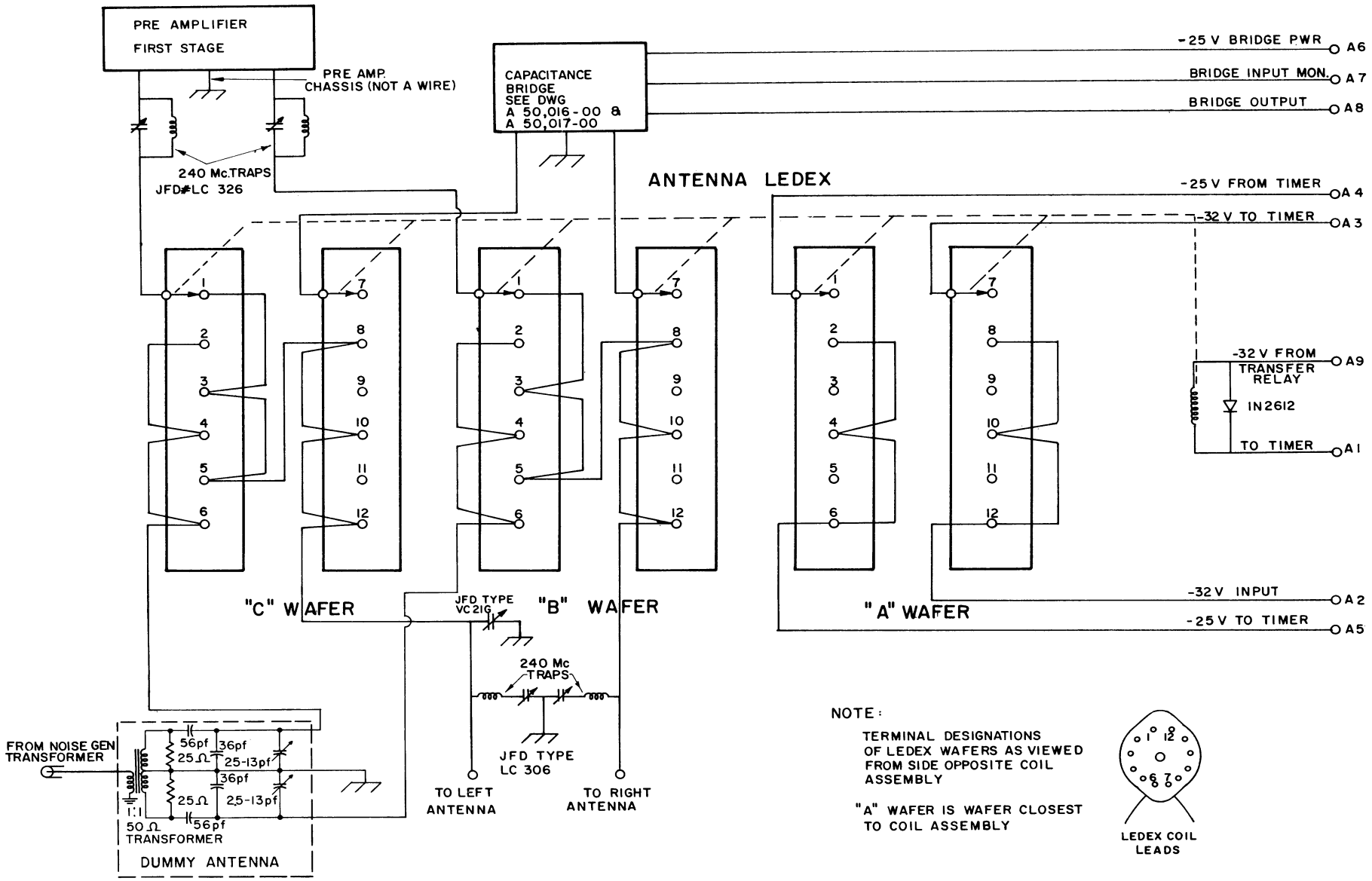


Figure 8. Antenna switching circuit.

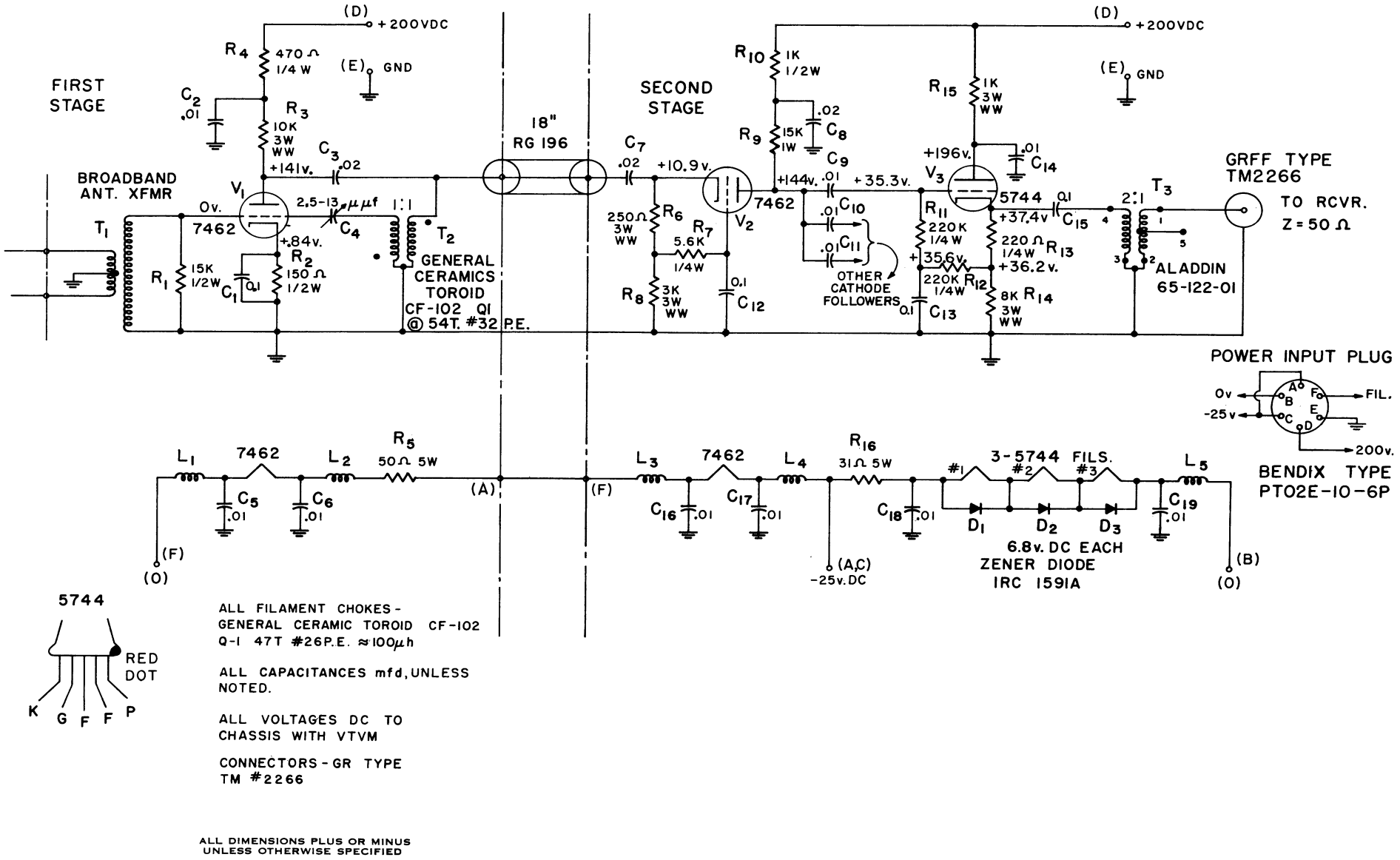


Figure 9. Radiometer preamplifier circuit.

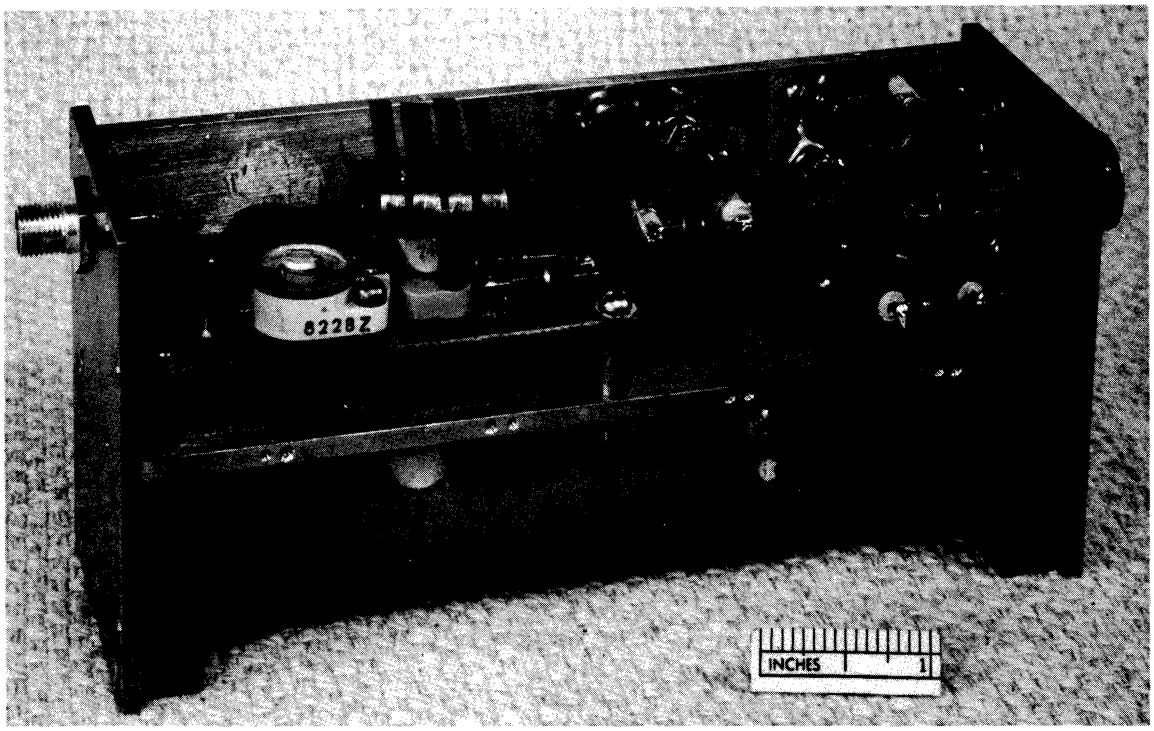


Figure 10. Preamplifier first stage.

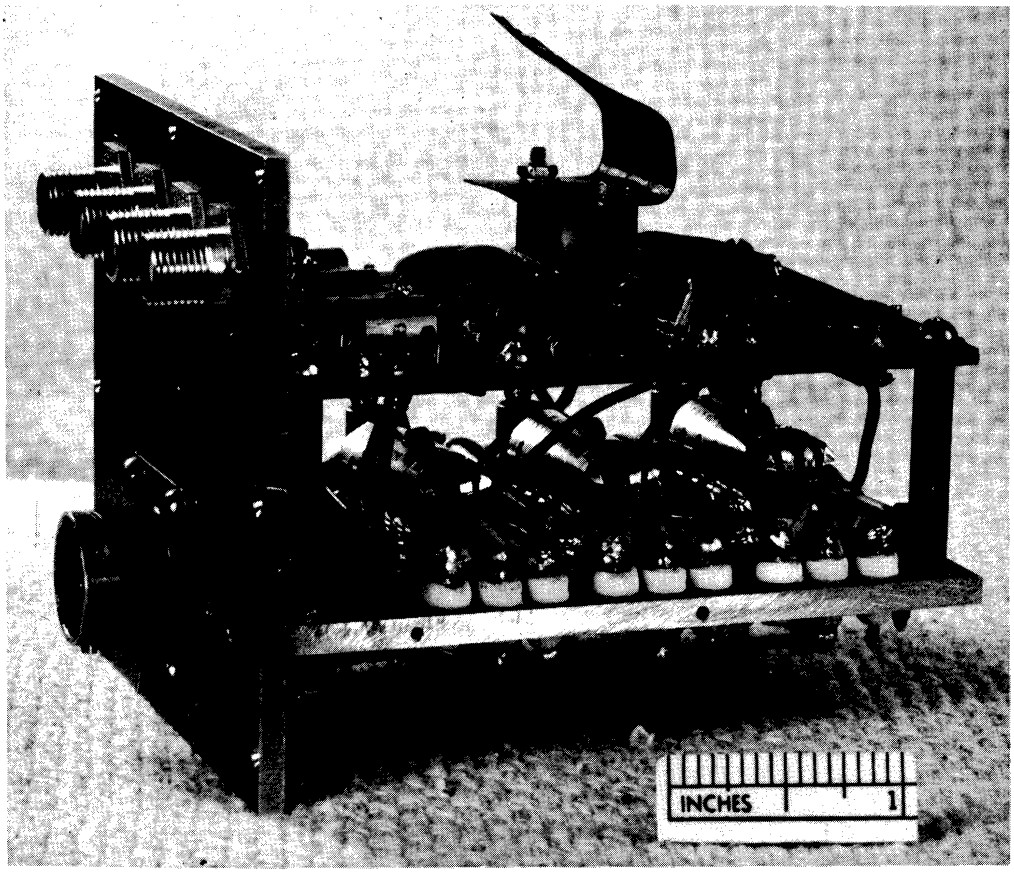


Figure 11. Preamplifier second stage.

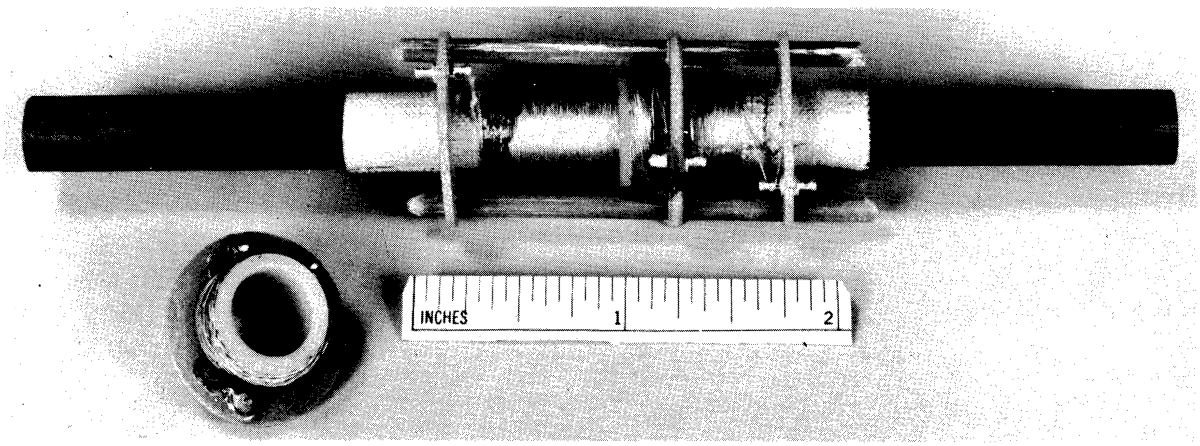


Figure 12. Preamplifier input transformer.

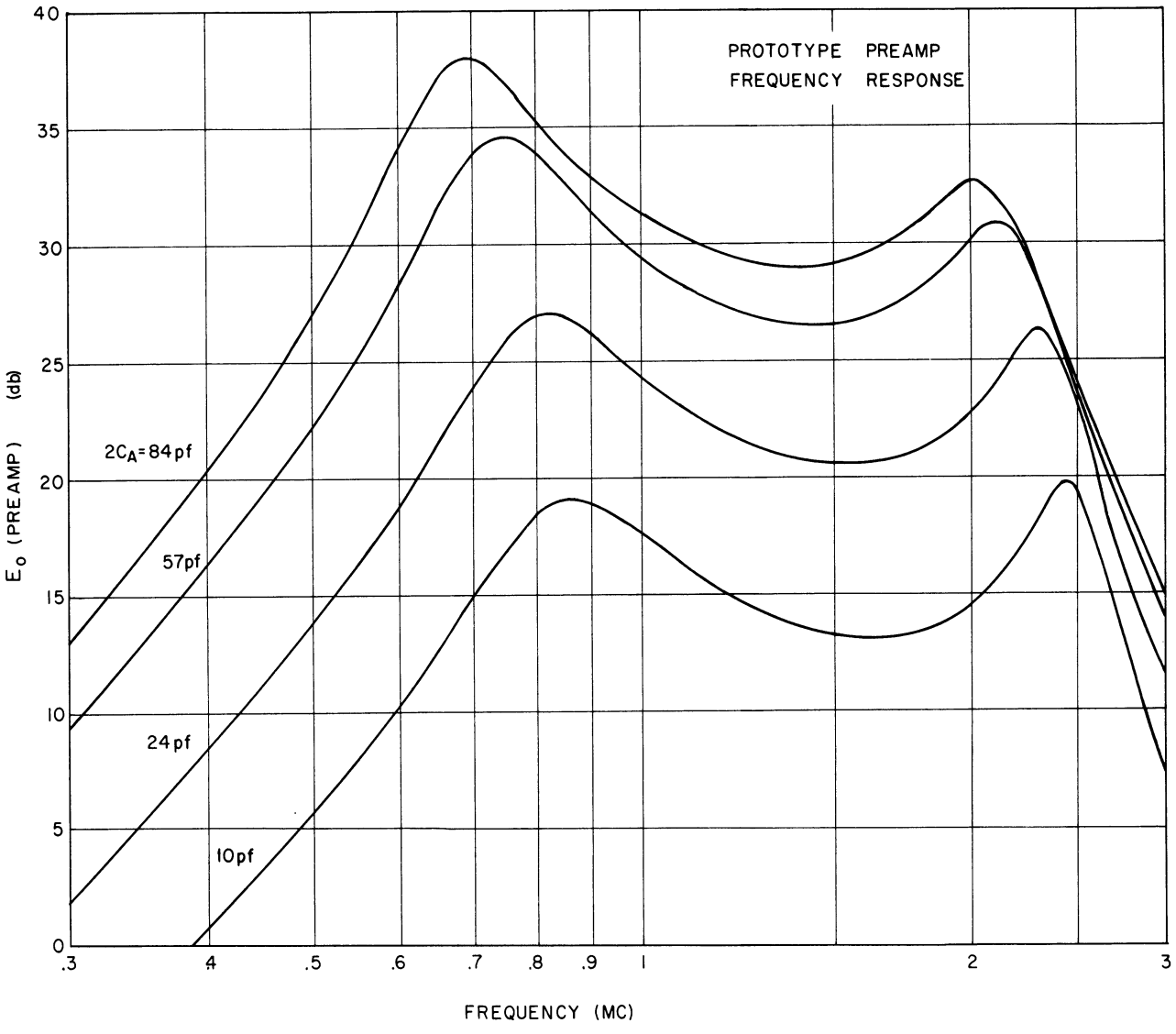


Figure 13. Preamplifier frequency response curves.

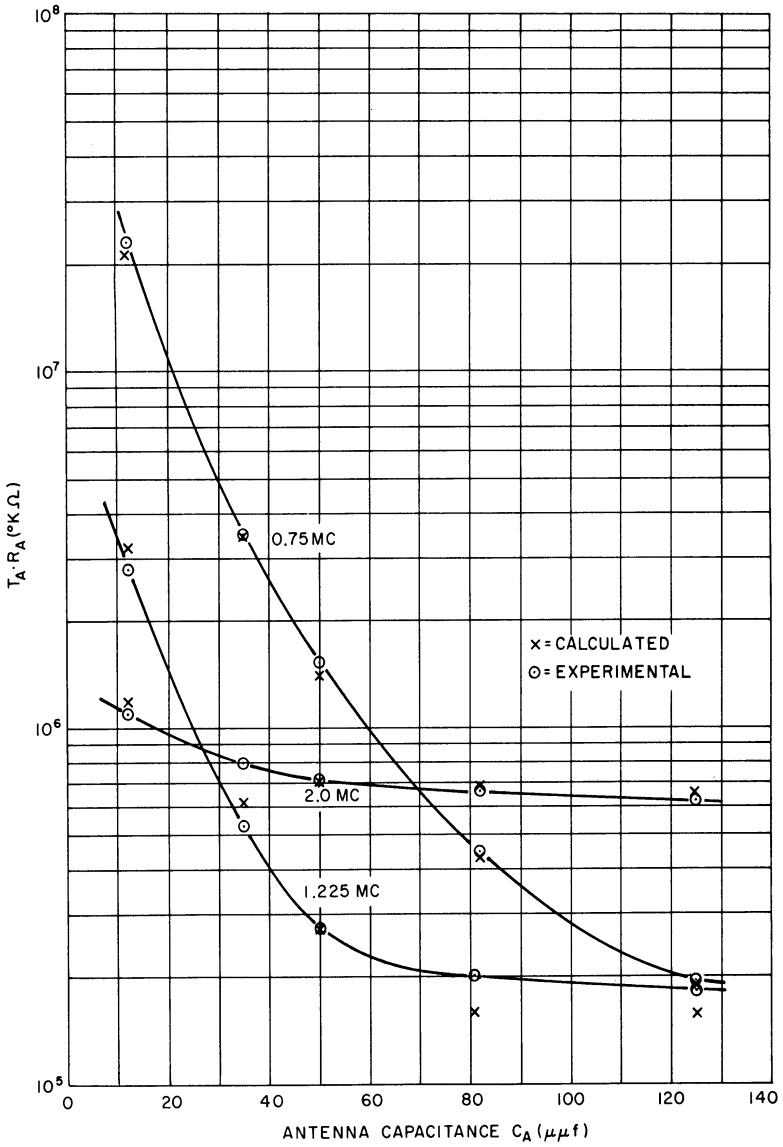


Figure 14. Preamplifier RT product curves.

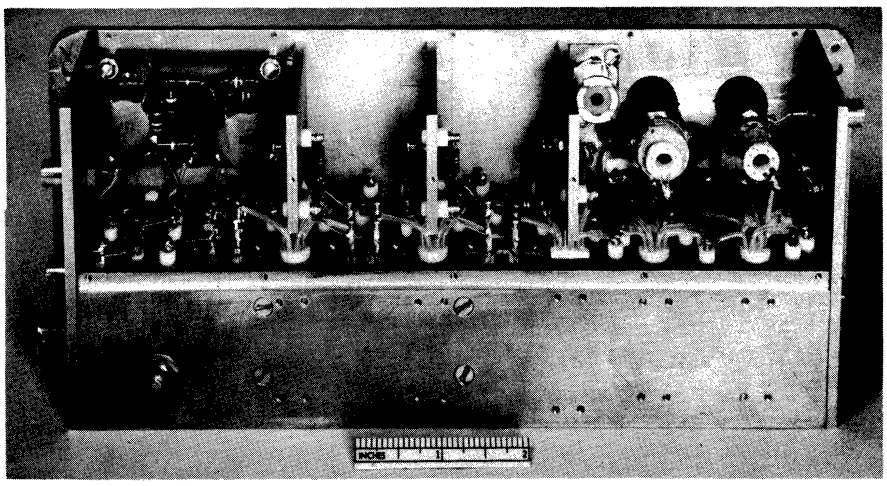

Figure 15. Typical receiver construction.

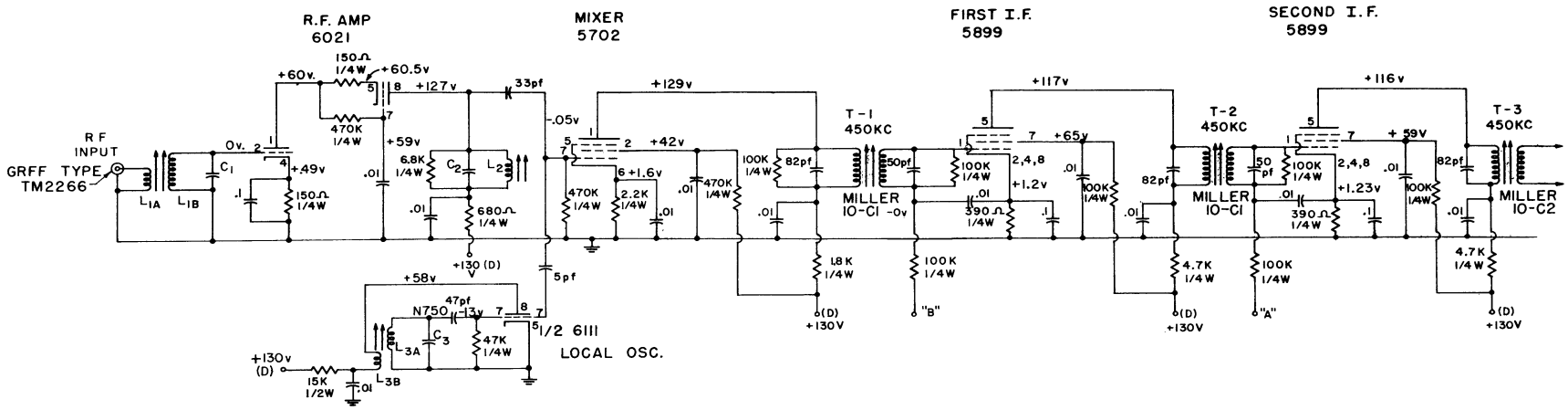


NOTES

| Part | 750 kc | 1225 kc | 2000 kc |
|---|---|---|---|
| $L_{1A}$* | 9-1/2T #33P. E. | 4-1/2T #33P. E. | 4-1/2T #33P. E. |
| $L_{1B}$ | 41A154CB1 (Miller) 30T removed | 41A104CB1 (Miller) 40T removed | 41A335CB1 (Miller) 15T removed |
| $C_1$ | 620 pf | 500 pf | 500 pf |
| $C_2$ | 75 pf | 33 pf | 33 pf |
| $L_2$ | 41A474CB1 | 41A334CB1 | 41A154CB1 |
| $C_3$ | 300 pf Parallel {100 pf S-M, 25 pf N750} | | {50 pf S-M, 20 pf N750} |
| $L_{3A}$ | 41A103CB1 | 41A334CB1 | 41A334CB1 25T removed |
| $L_{3B}$* | 30T #33P. E. | 20T #33P. E. | 20T #33P. E. |

* -Link wound at bottom end of secondary of $L_1$ and $L_3$.

-All capacitances in mfd, unless noted.

-Voltages dc to chassis with no signal applied (ant. open). Measured on 2000 kc prototype 7 Nov. 1961 with HP412A VTVM.

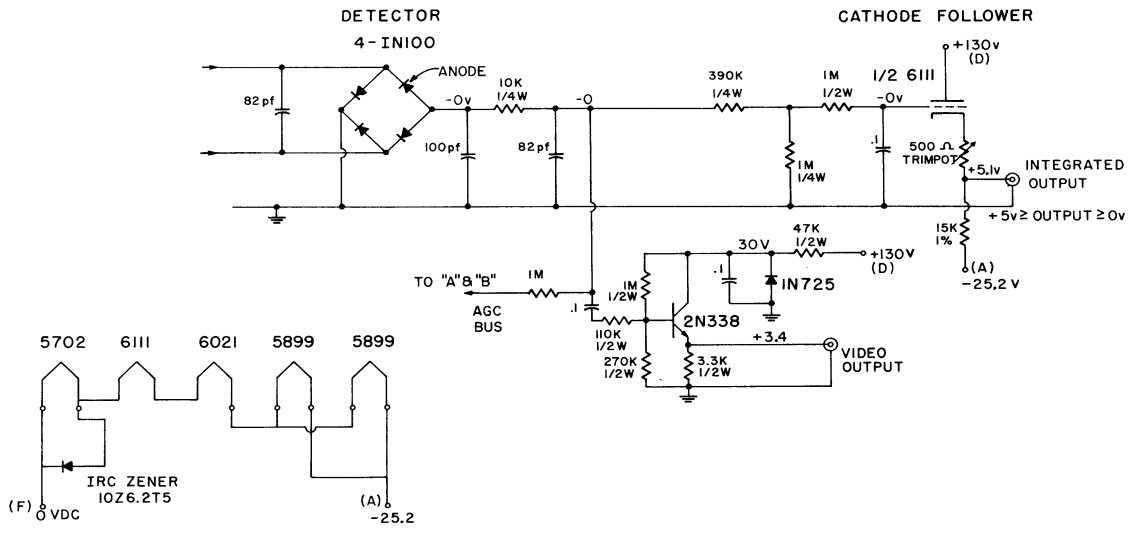


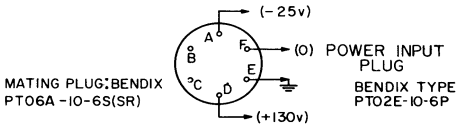


Figure 16. Receiver circuit.

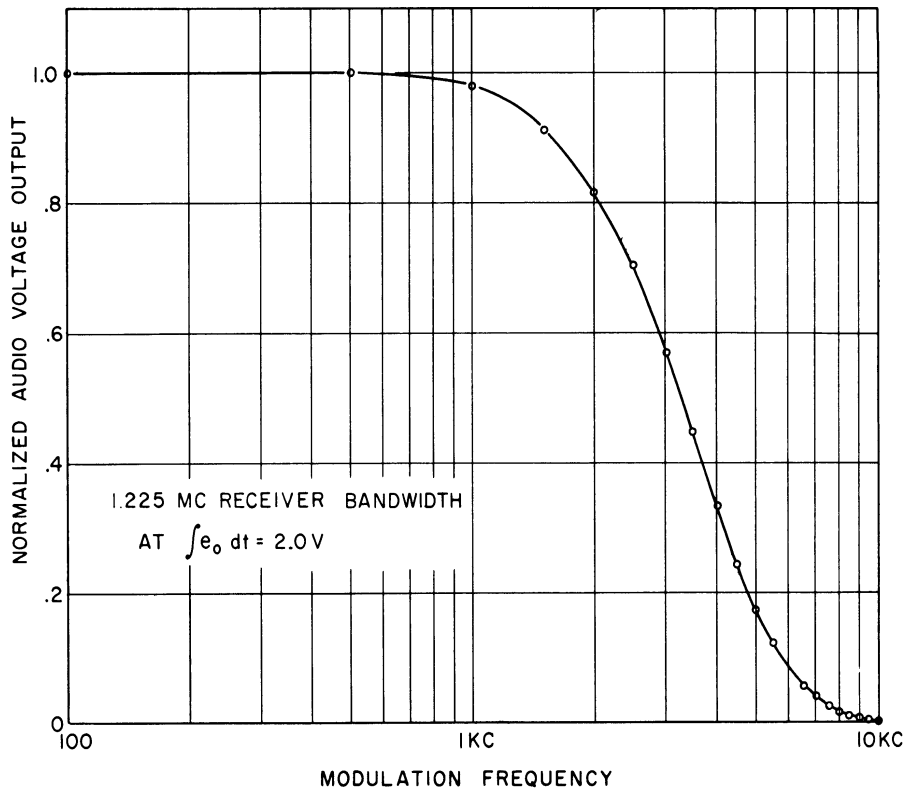


Figure 17. Receiver bandwidth curve.

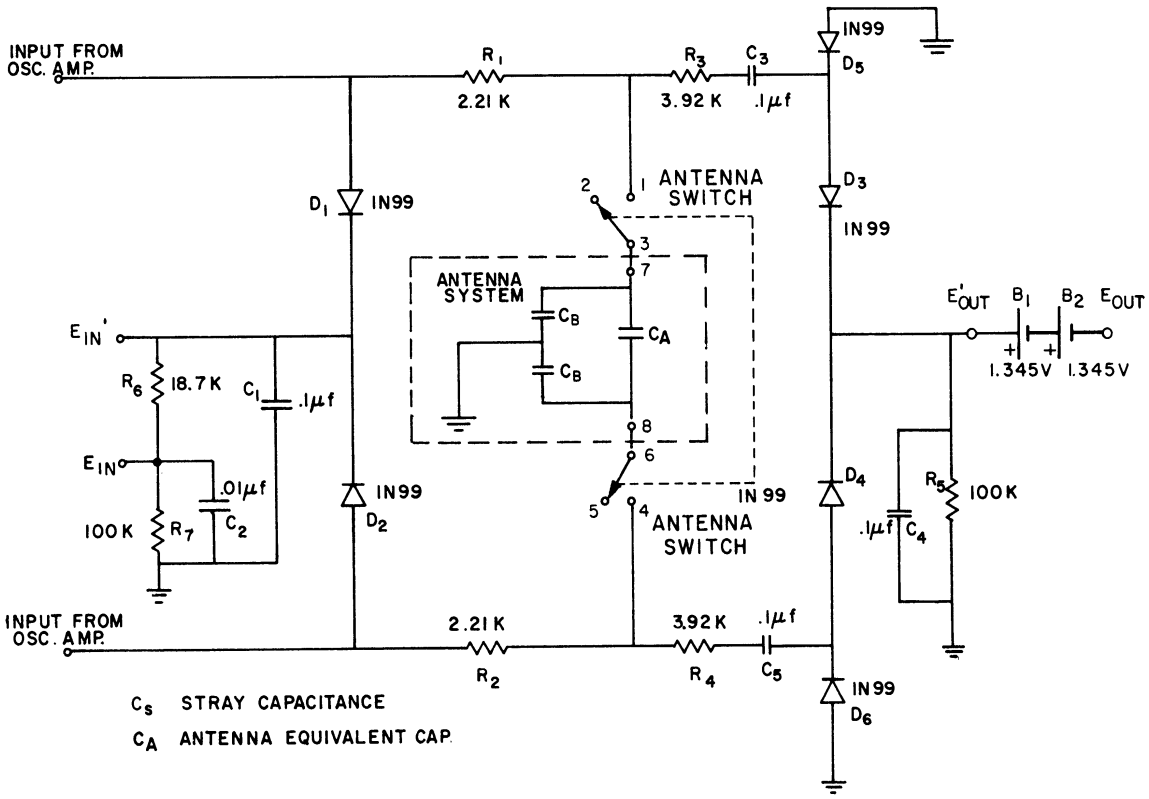


Figure 18. Antenna bridge circuit.

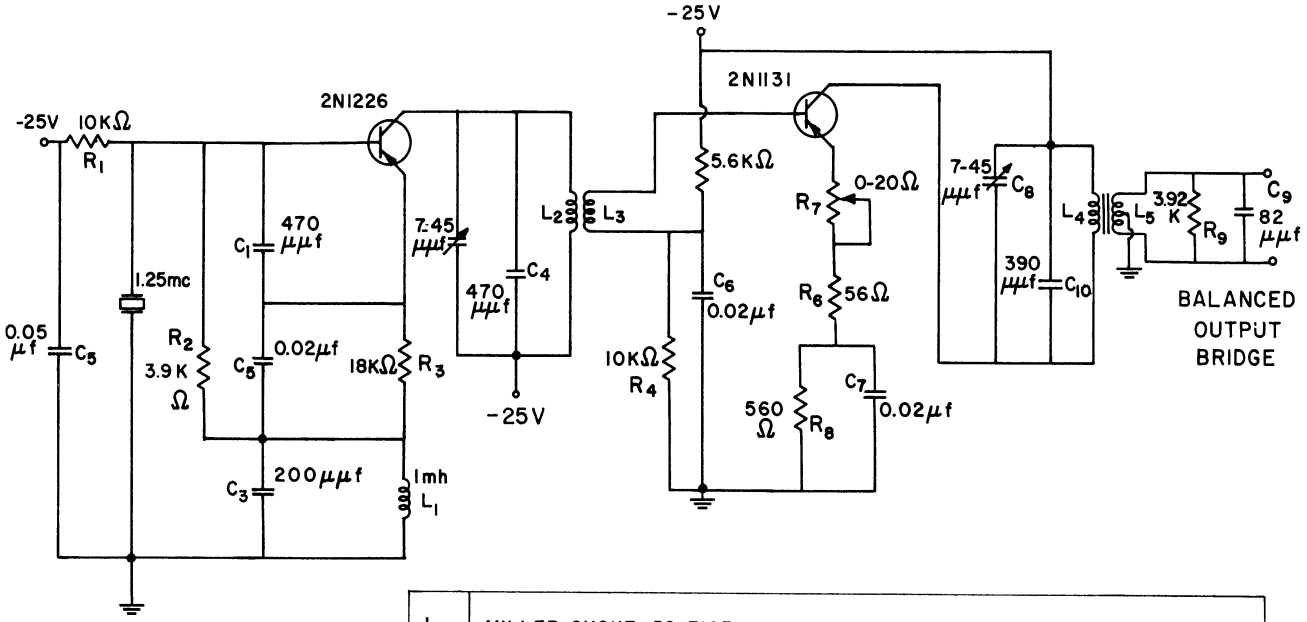


| | |
|---|---|
| $L_1$ | MILLER CHOKE 70 F103A1 |
| $L_2$ | MILLER 41 A104 CB1, 40 TURNS REMOVED. |
| $L_3$ | 11 TURNS #32, WOUND ON PORCELAIN BODY OF $L_2$ |
| $L_4$ | TOROID 24 TURNS # 32, DISTRIBUTIVELY WOUND ON GENERAL CERAMIC CF 102 Q1 CORE |
| $L_5$ | TOROID 48 TURNS CENTER TAPPED DISTRIBUTIVELY WOUND ON CORE OF $L_4$ |

Figure 19. Antenna bridge oscillator circuit.

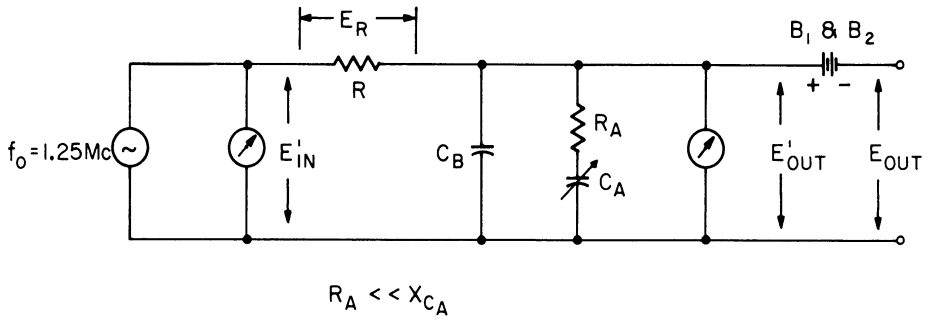


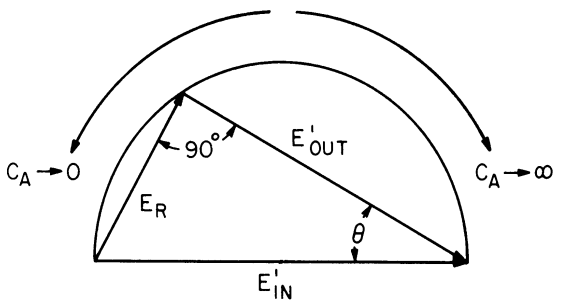


Figure 20. Bridge vector relationship.

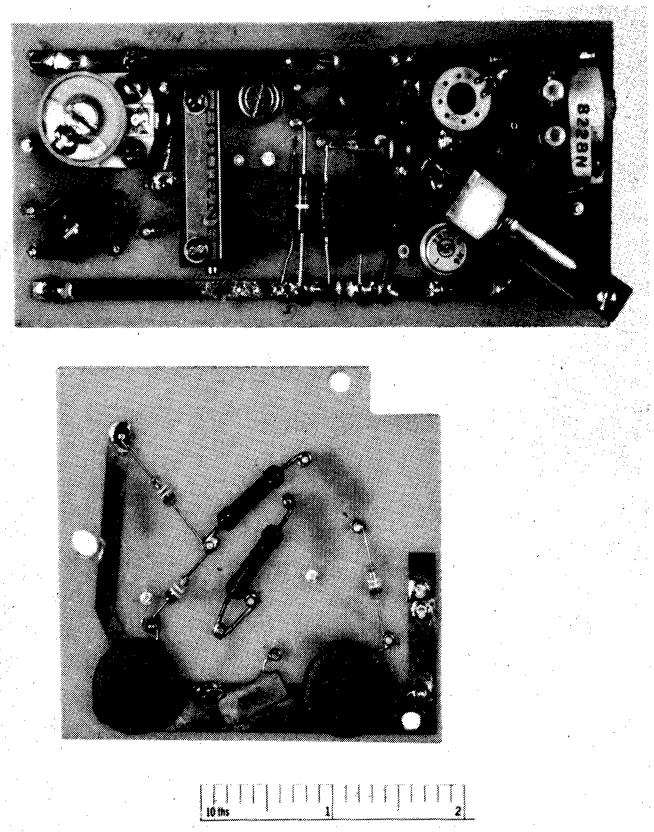

Figure 21. Bridge and oscillator.

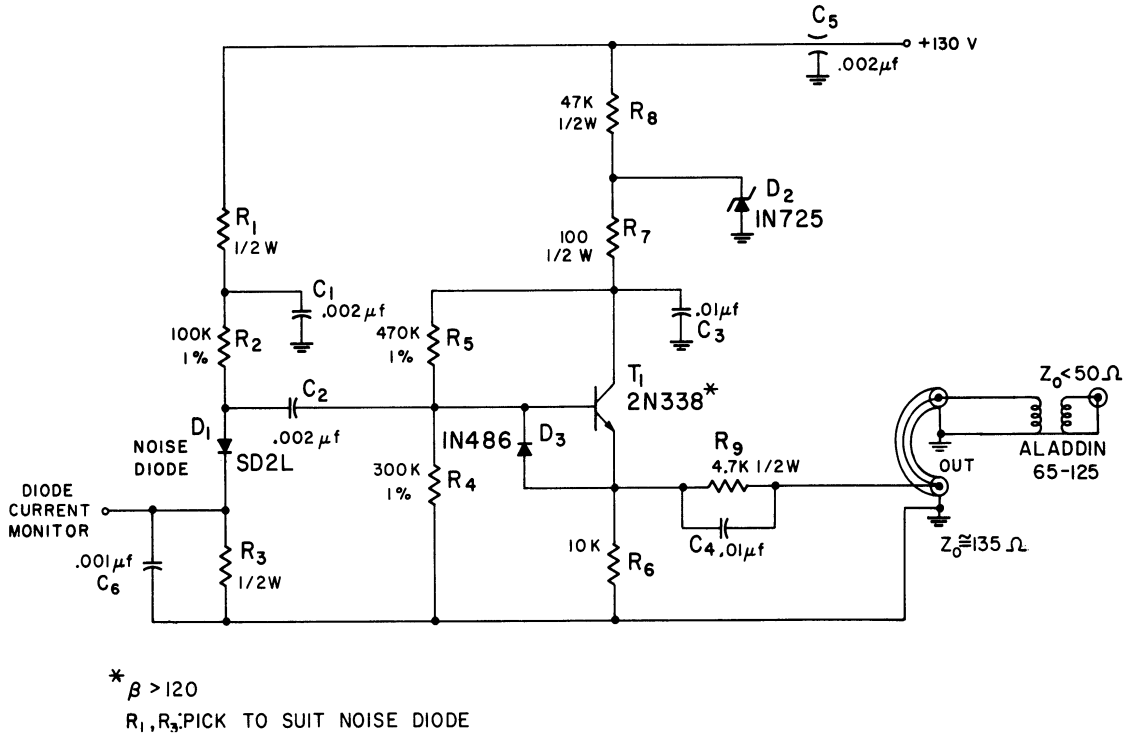


*β >120

R1, R3: PICK TO SUIT NOISE DIODE

Figure 22. Noise generator circuit.

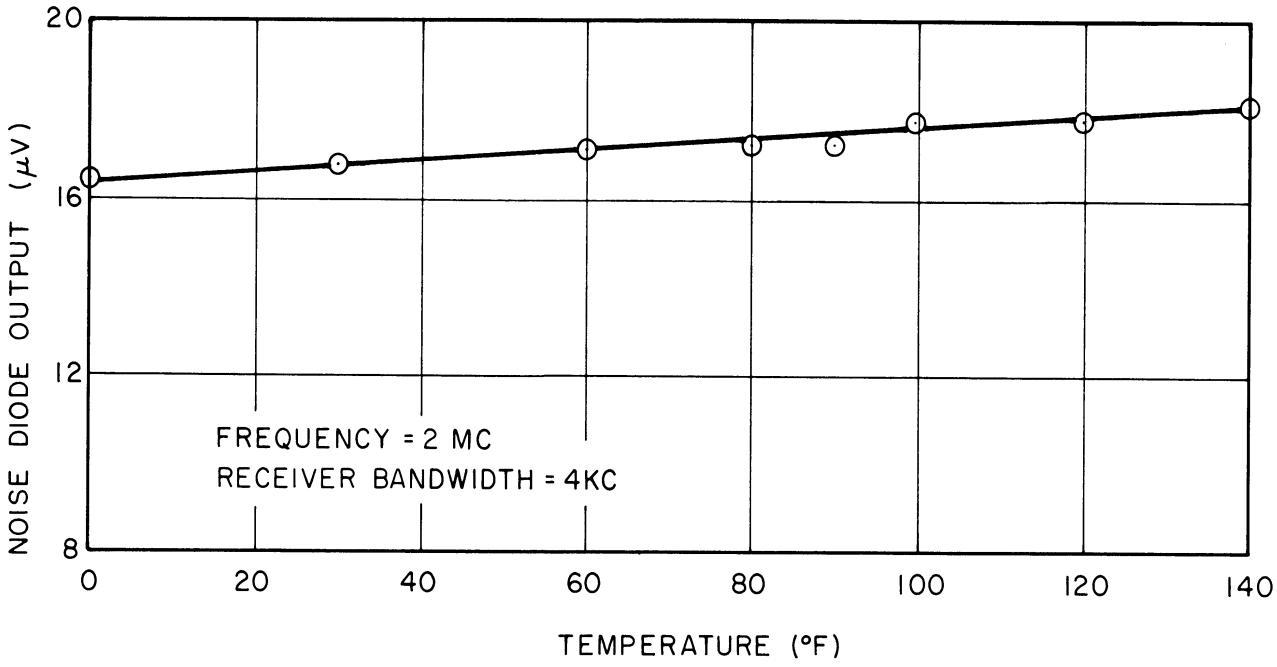


Figure 23. Noise generator temperature sensitivity.

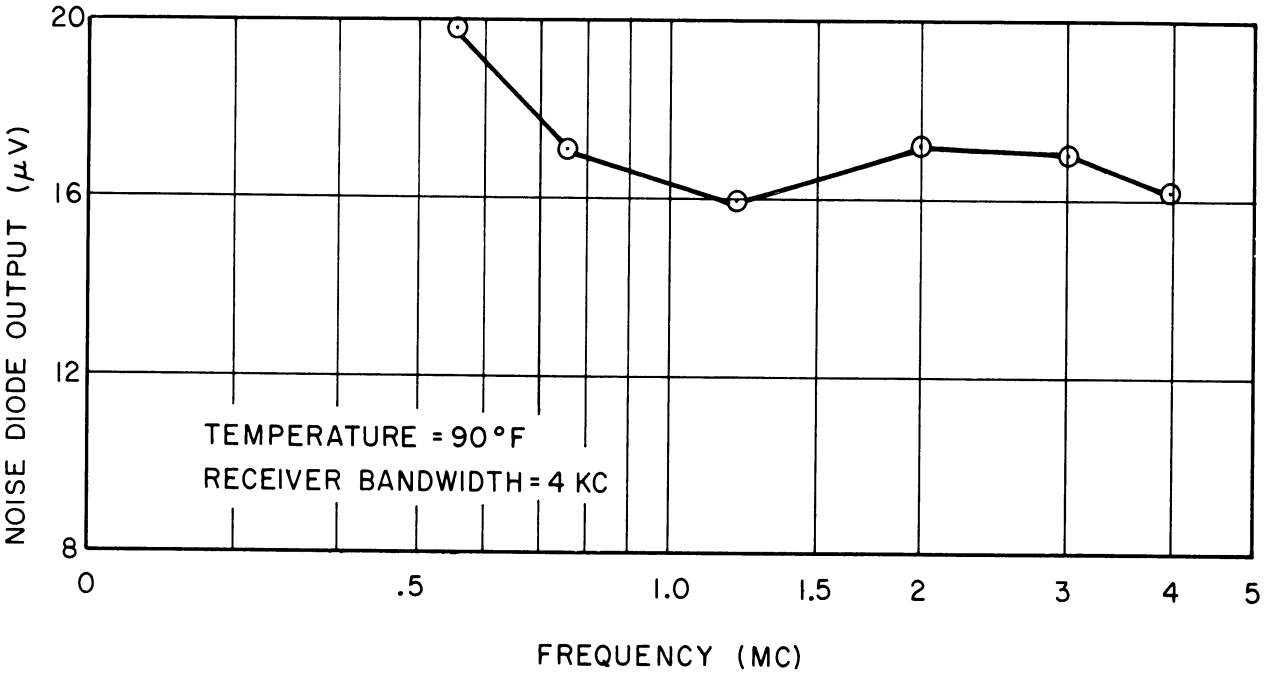


Figure 24. Noise generator spectral output.


Figure 25. Noise generator disassembled.

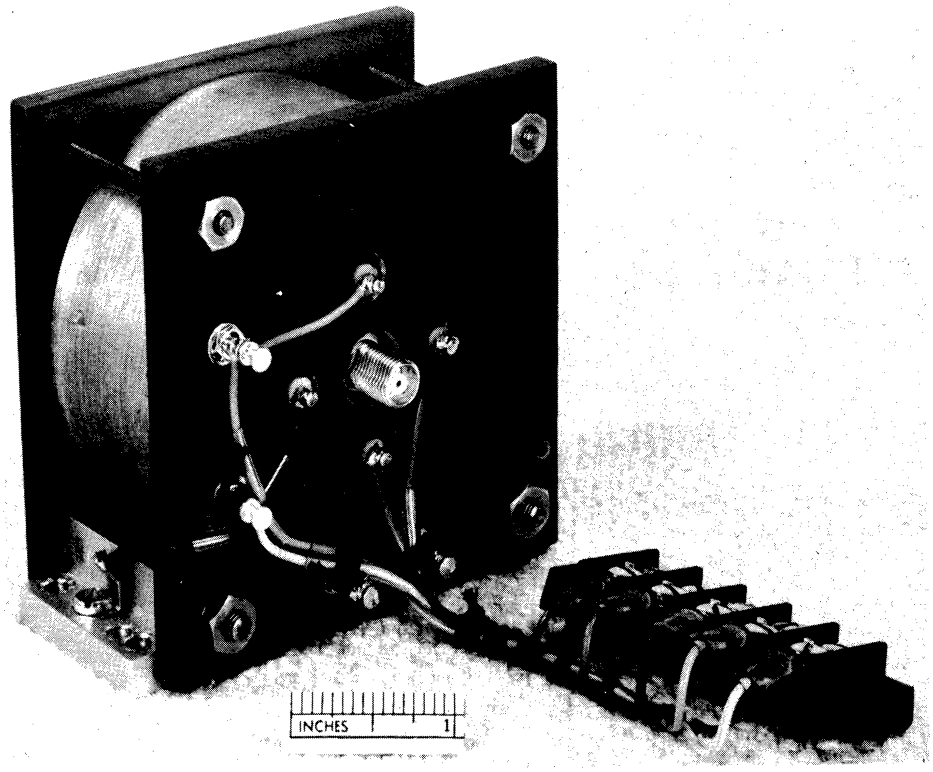


Figure 26. Noise generator assembled.

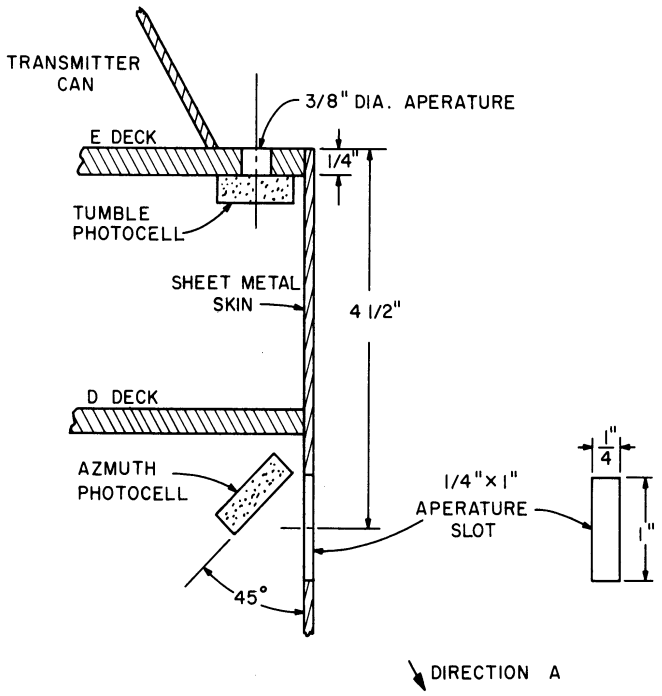


Figure 27. Photocell mounting detail.

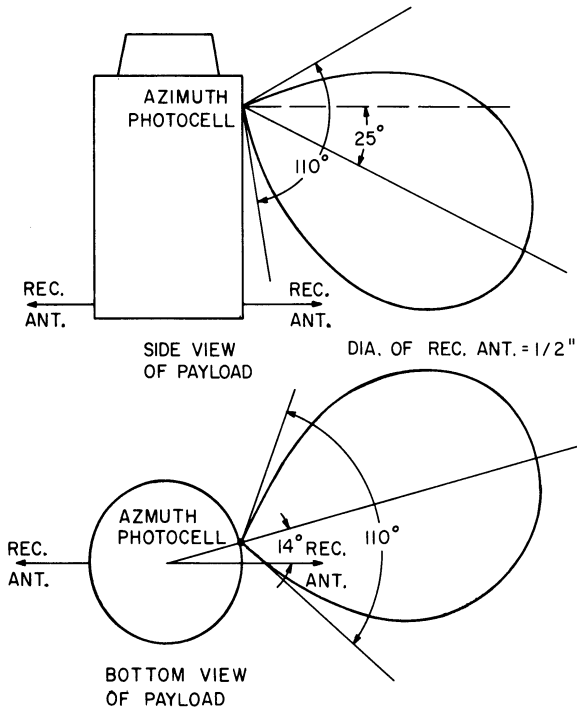


Figure 28. Spin axis photocell field of view.

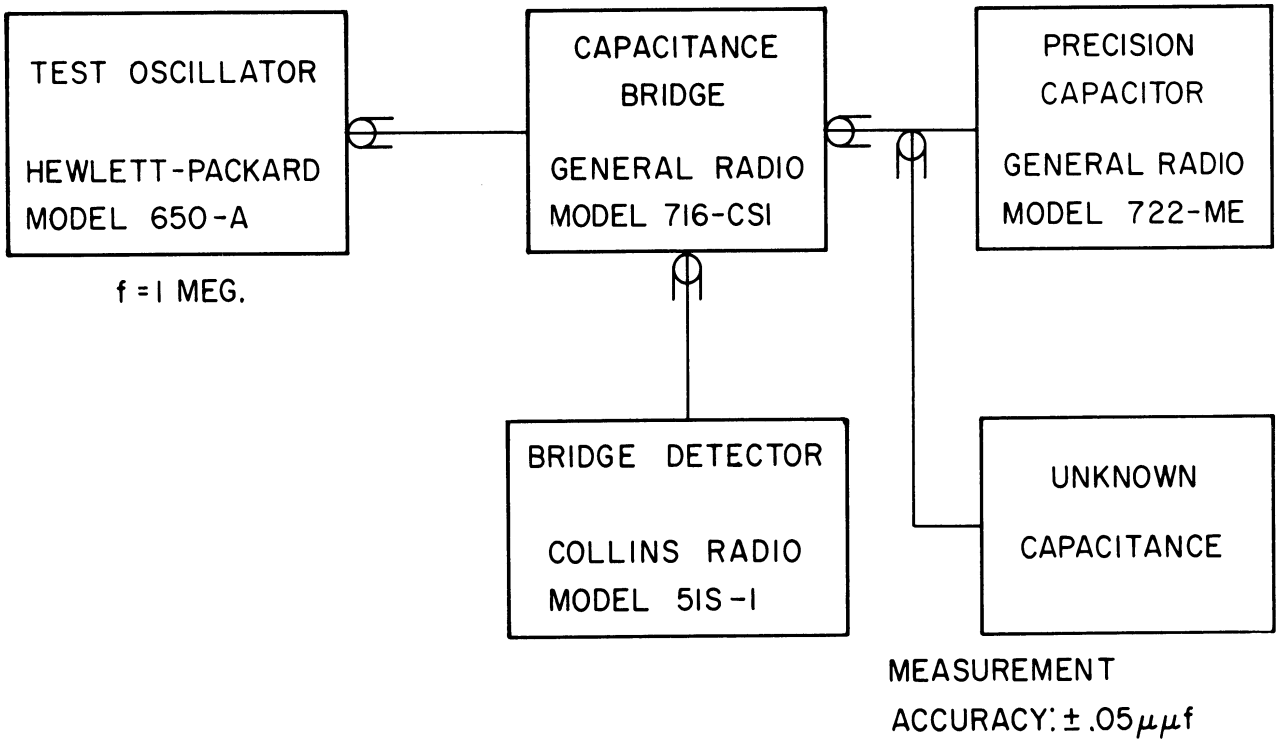


Figure 29. Laboratory capacitance measuring setup.

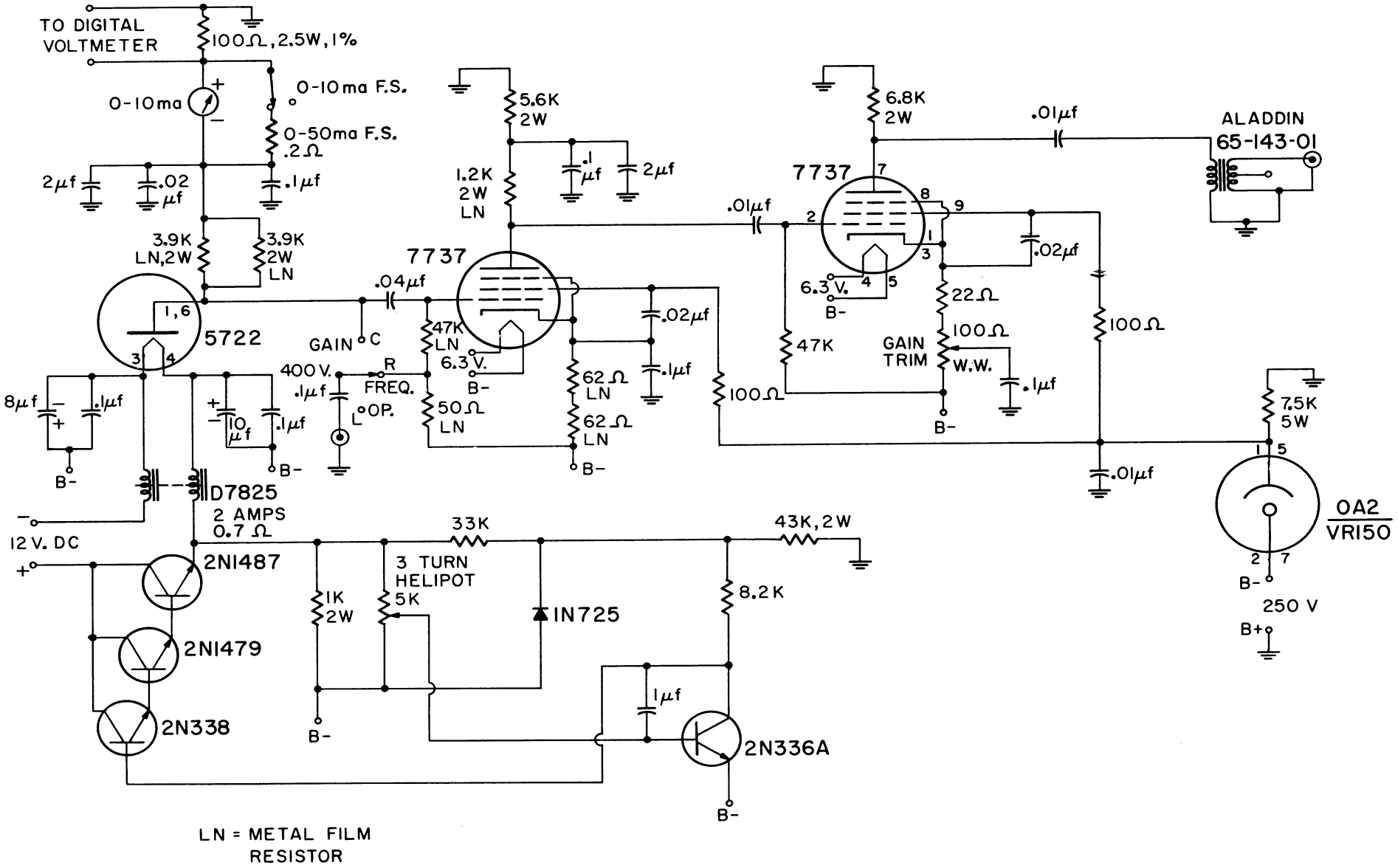


Figure 30. Laboratory noise generator.

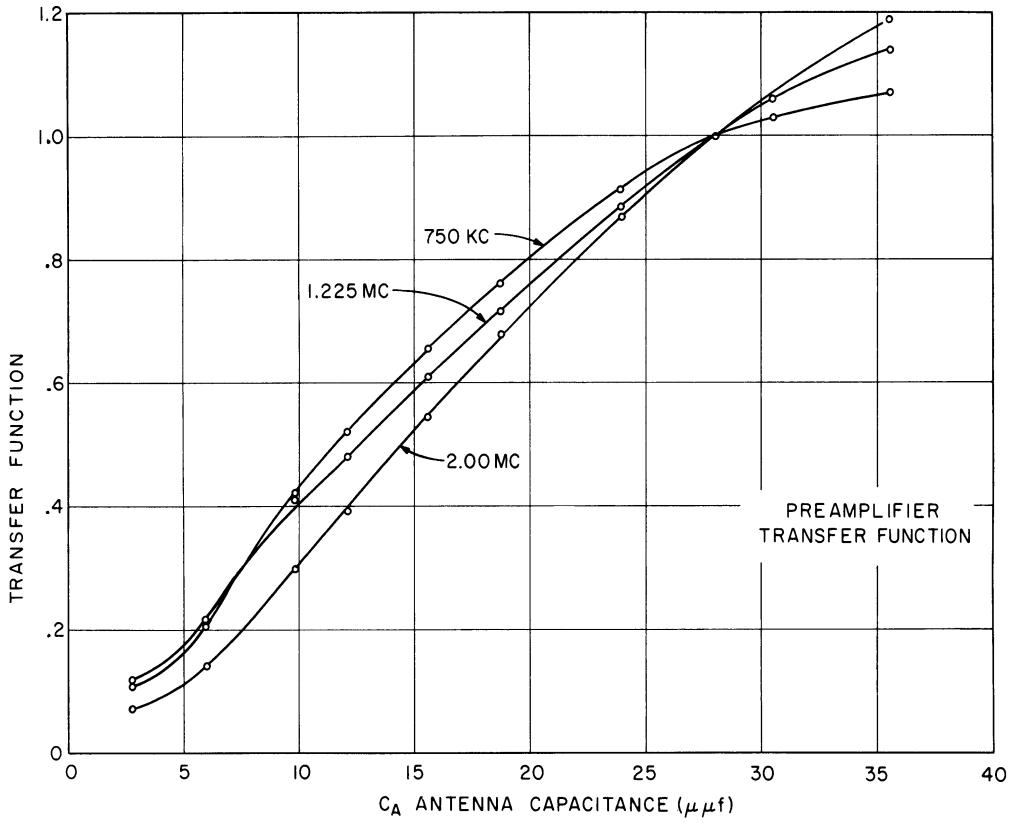


Figure 31. Preamplifier transfer function curves.

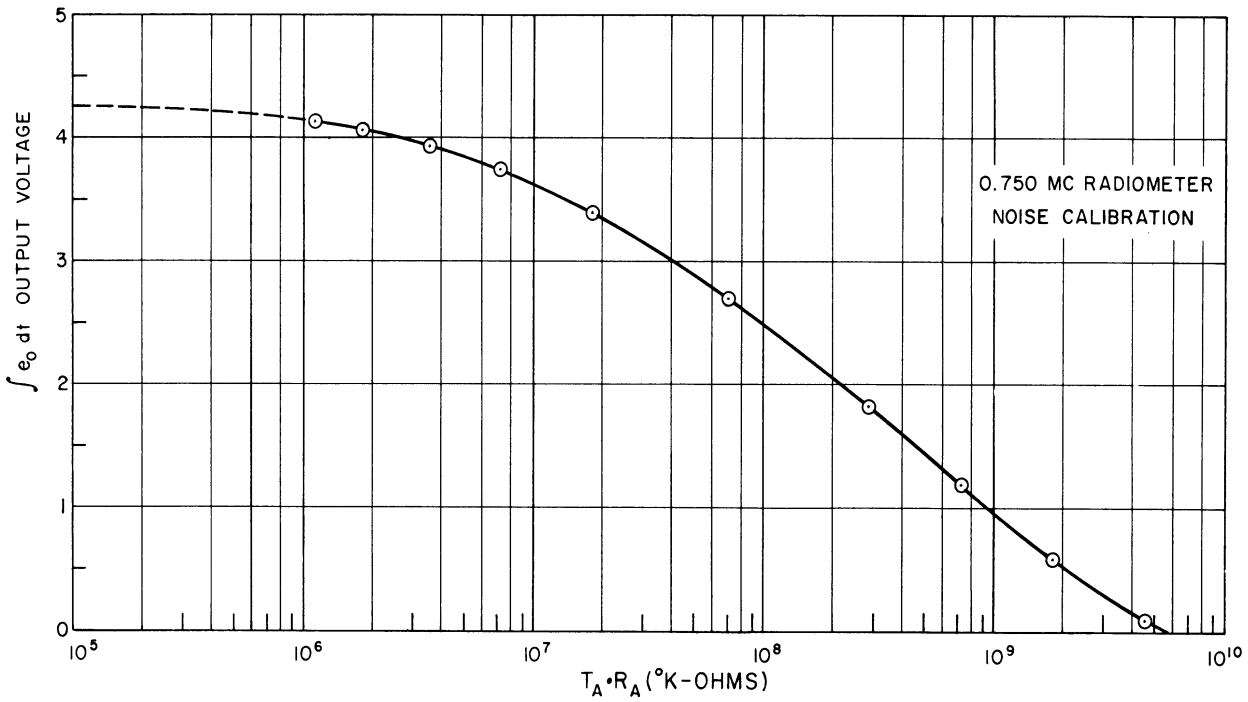


Figure 32. 0.75 Mc radiometer calibration curve.

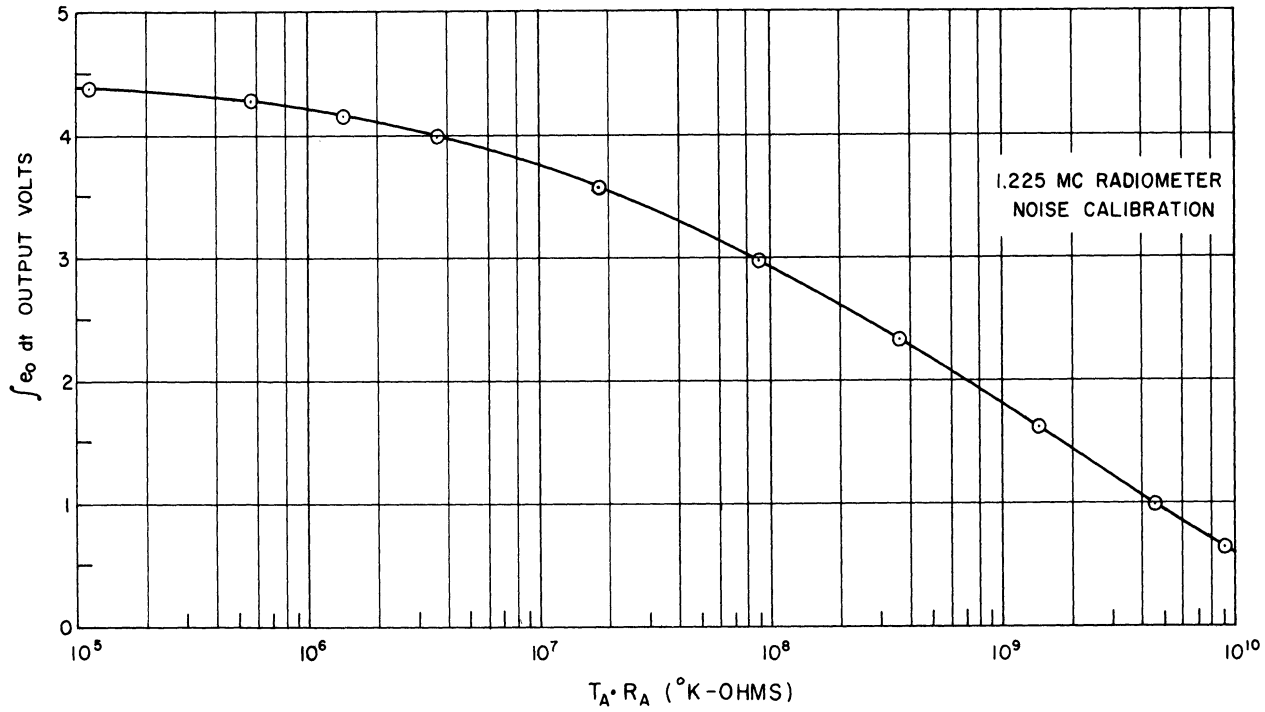


Figure 33. 1.225 Mc radiometer calibration curve.

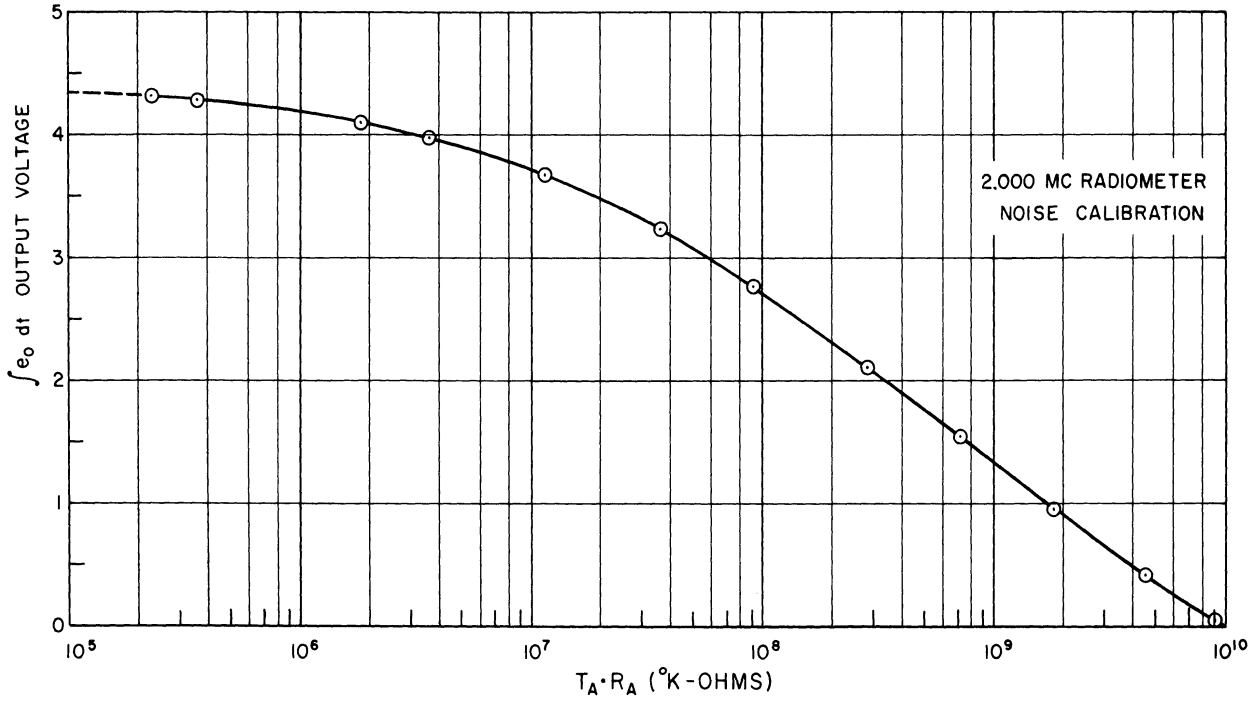


Figure 34. 2.00 Mc radiometer calibration curve.

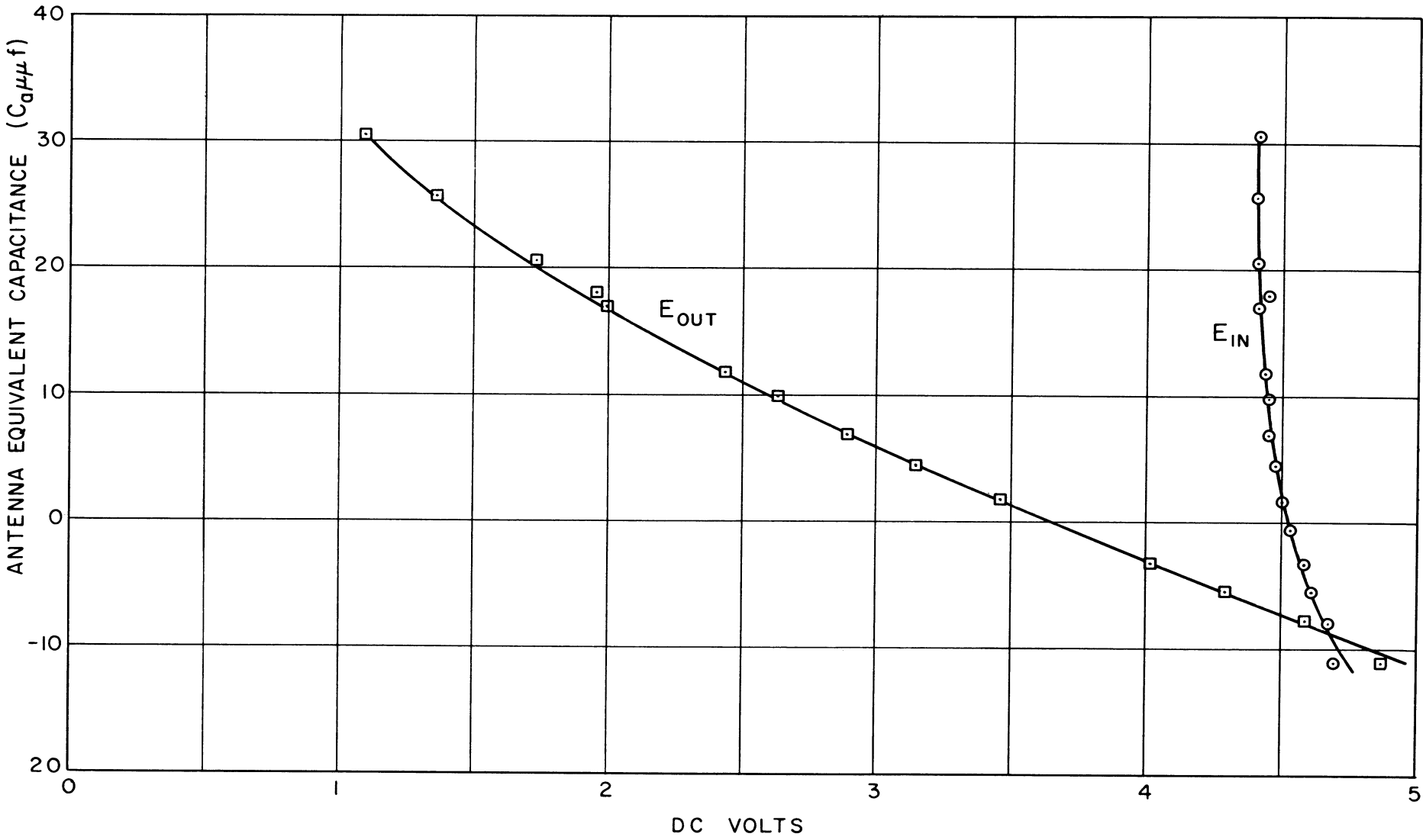


Figure 35. Antenna bridge calibration curves.

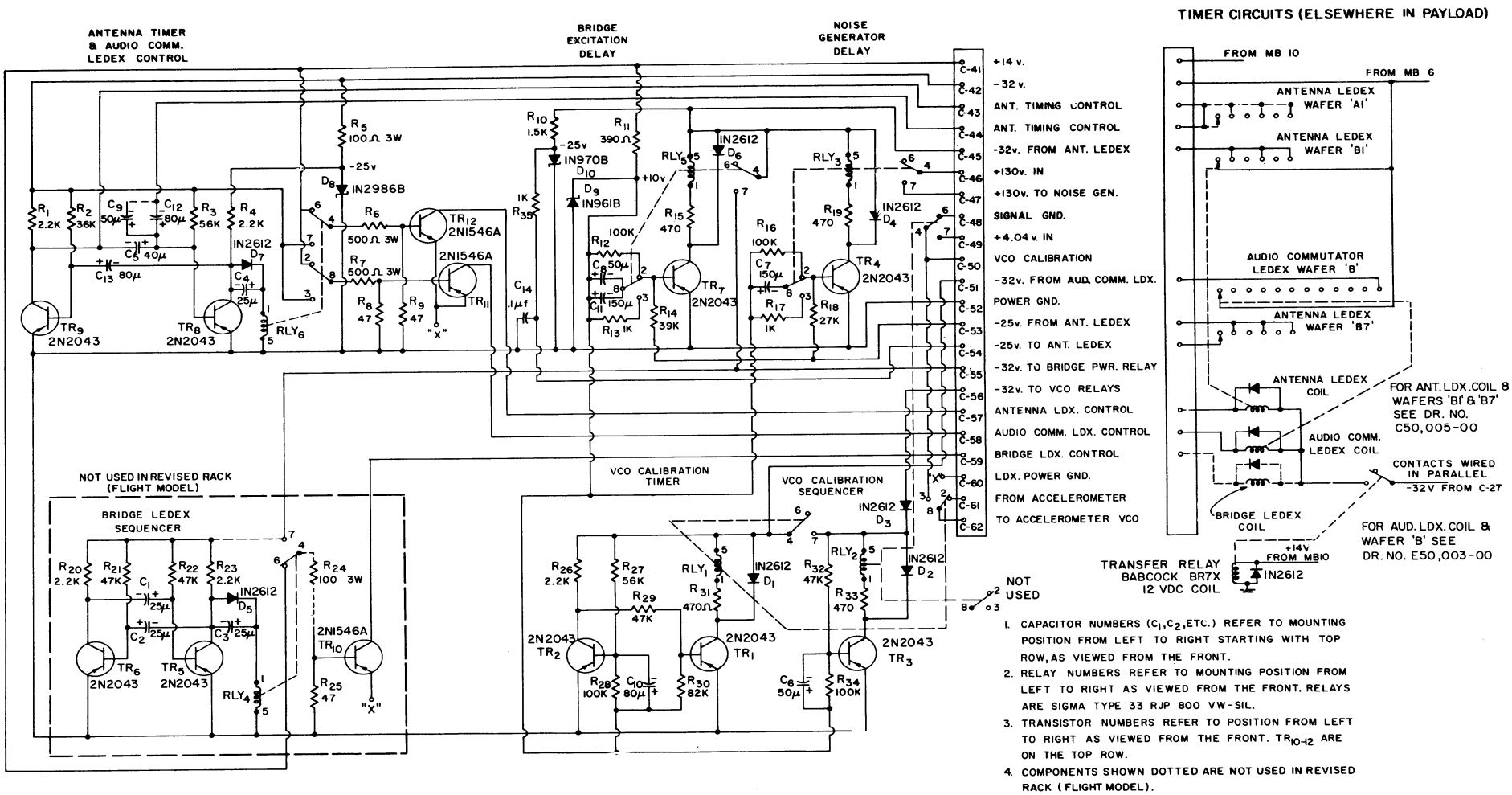


Figure 36. Complete timer circuit.

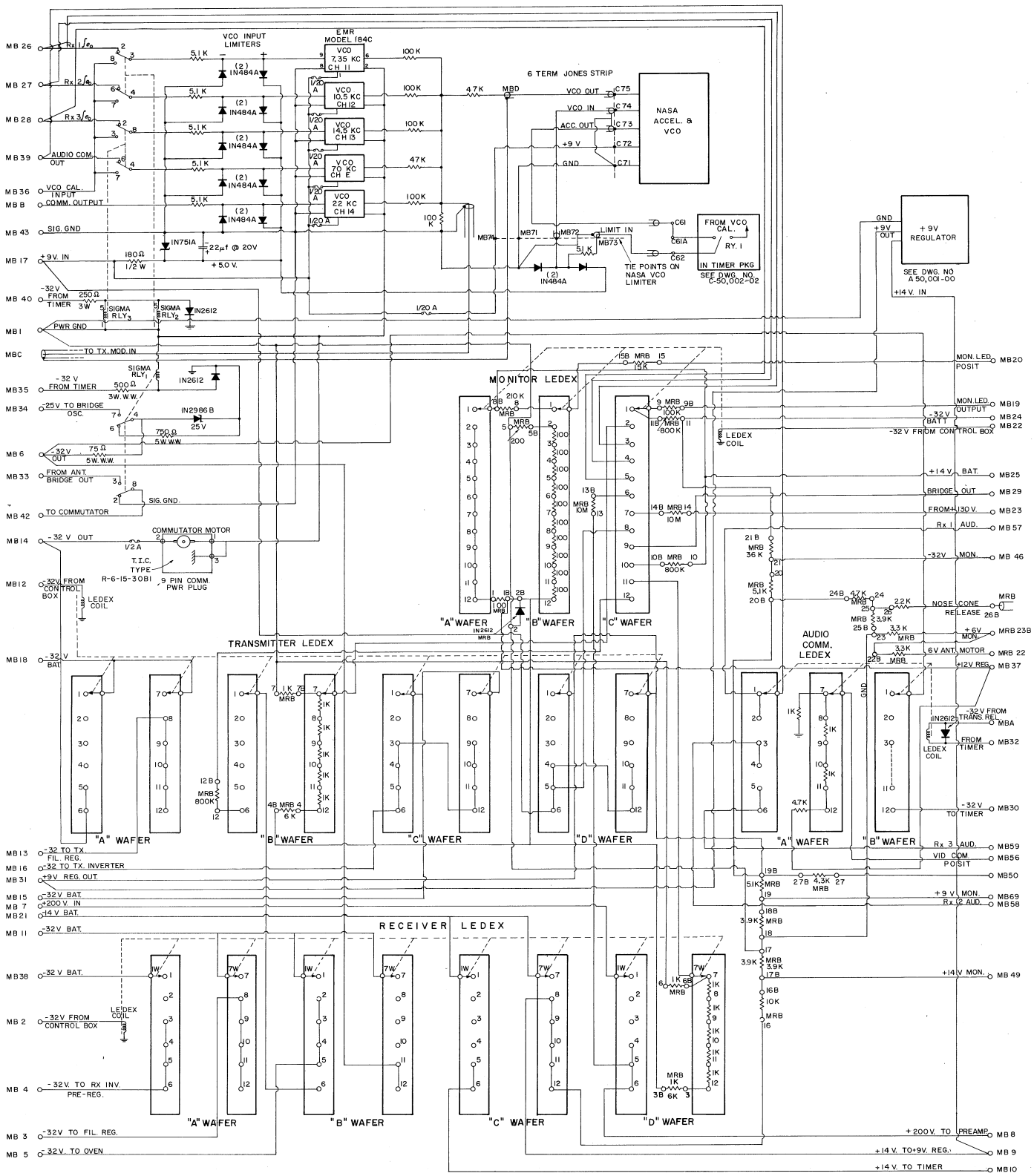


NOTES:

1. LEDEX WAFER WIRING - TERMINAL DESIGNATIONS OF LEDEX WAFERS AS VIEWED FROM SIDE OPPOSITE COIL ASSEMBLY.

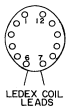


2. FOR EXACT LEAD PLACEMENT OF COMPONENT INTERCONNECTS REFER TO MONITOR RESISTOR BOARD DWG. # A 50,012-00 AND VCO RESISTOR BOARD DWG # A 50013-00

3. ALL COMPONENTS ON SCHEMATIC DESIGNATED MRB PLUS TYPE NUMBER OR VALUE AND TWO TERMINAL NUMBERS, AS - 12○-MRB-○12B 10K ARE COMPONENTS LOCATED ON MONITOR RESISTOR BOARD AT THE POSITIONS DESIGNATED BY THE TERMINAL NUMBERS.

4. MB TERMINALS 41 THRU 70 & M8B ARE OCCUPIED, IN ADDITION TO THOSE CONNECTIONS SHOWN ON THIS DWG, BY THE SEGMENTS & WIPER, RESPECTIVELY, OF THE 30 SEGMENT COMMUTATOR WHOSE DRIVE MOTOR IS SHOWN IN THE LEFT CENTER OF THIS DWG.

5. ALL SIGMA RELAYS SHOWN IN THIS DWG ARE TYPE RJP-800 VW-SIL.

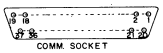


Figure 37. Main board control circuit.

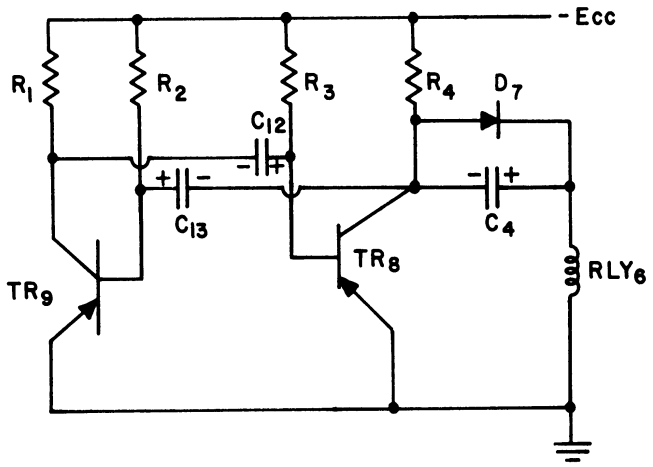


Figure 38. Simplified antenna timer circuit.

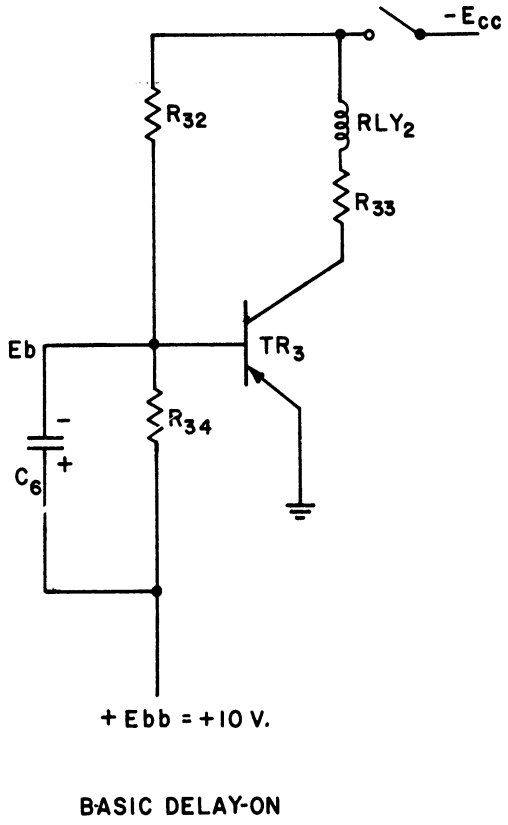


Figure 40. Delay-on timing circuit.

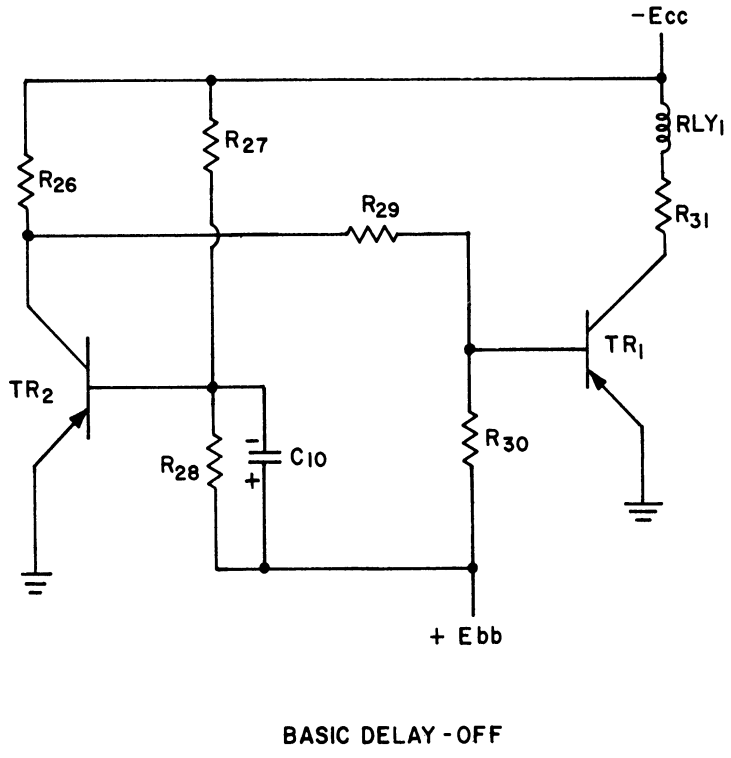


Figure 41. Delay-off timing circuit.

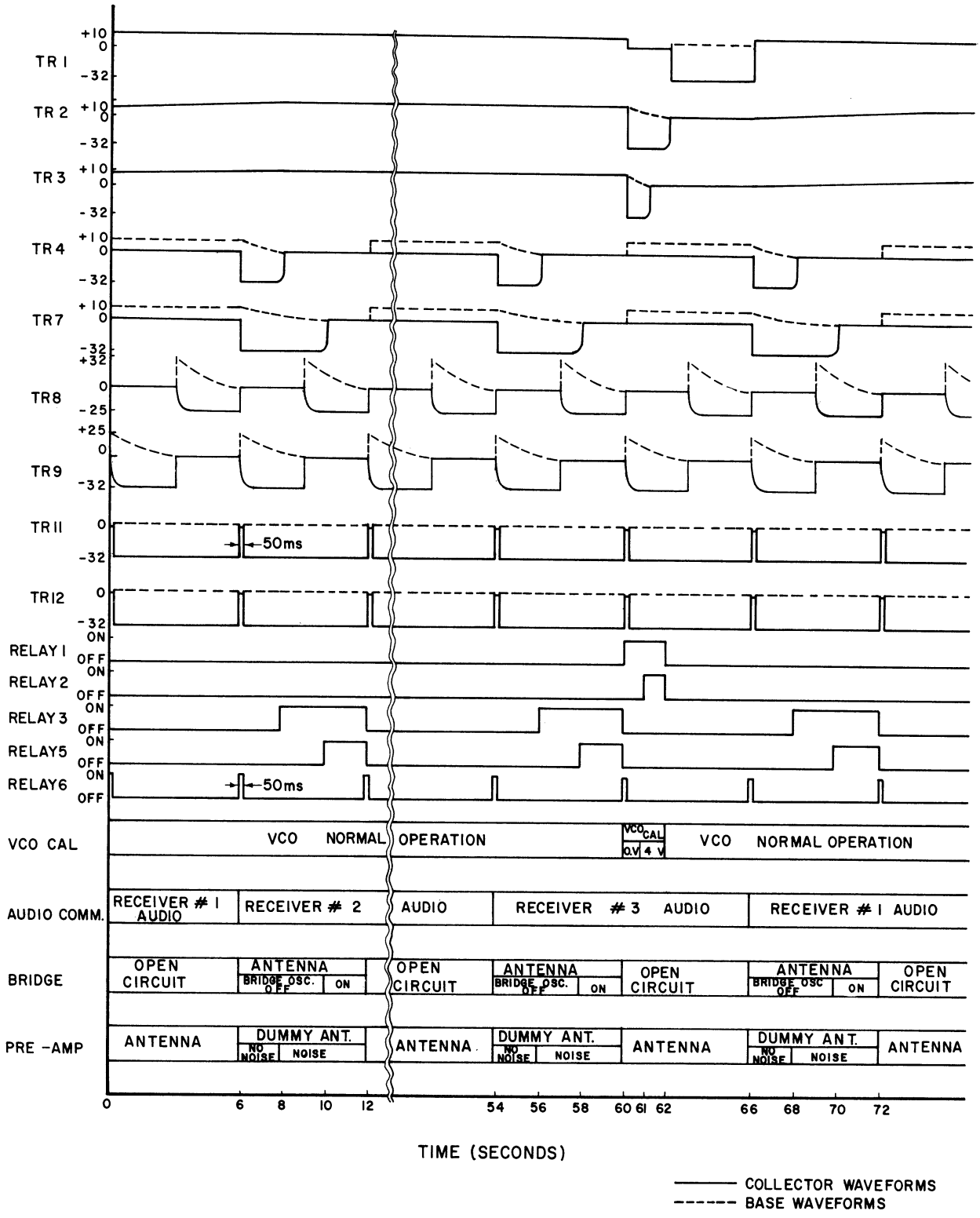


Figure 39. Timing circuit waveforms.

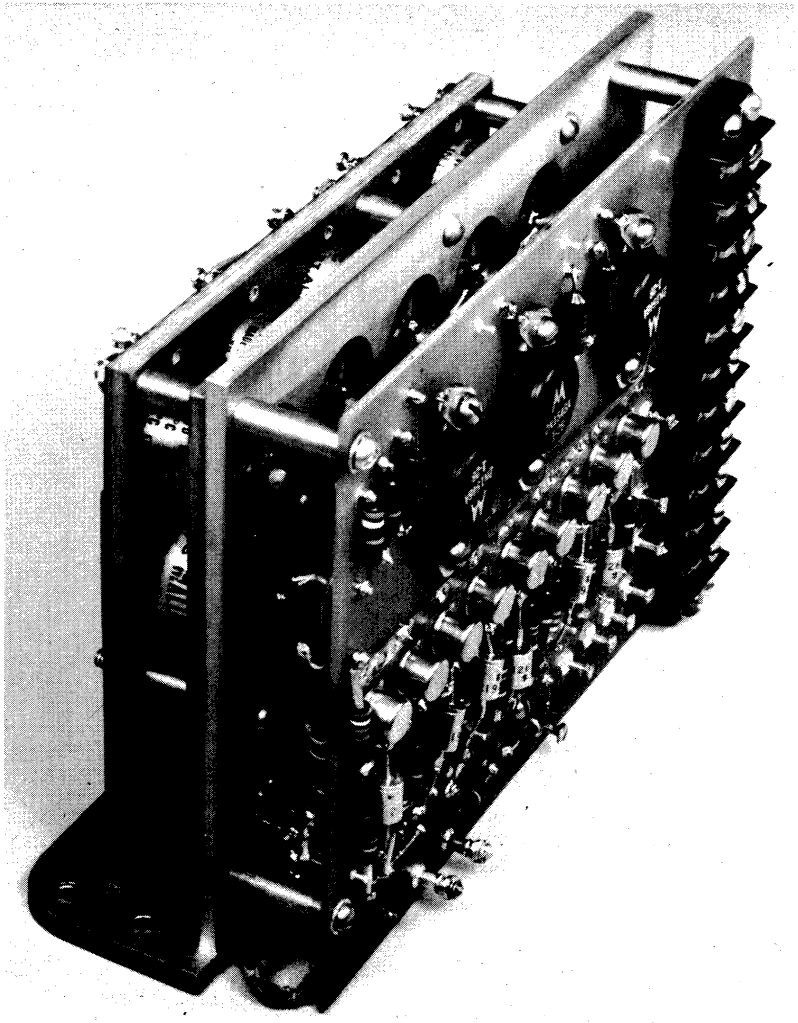

Figure 42. Timer subassembly.

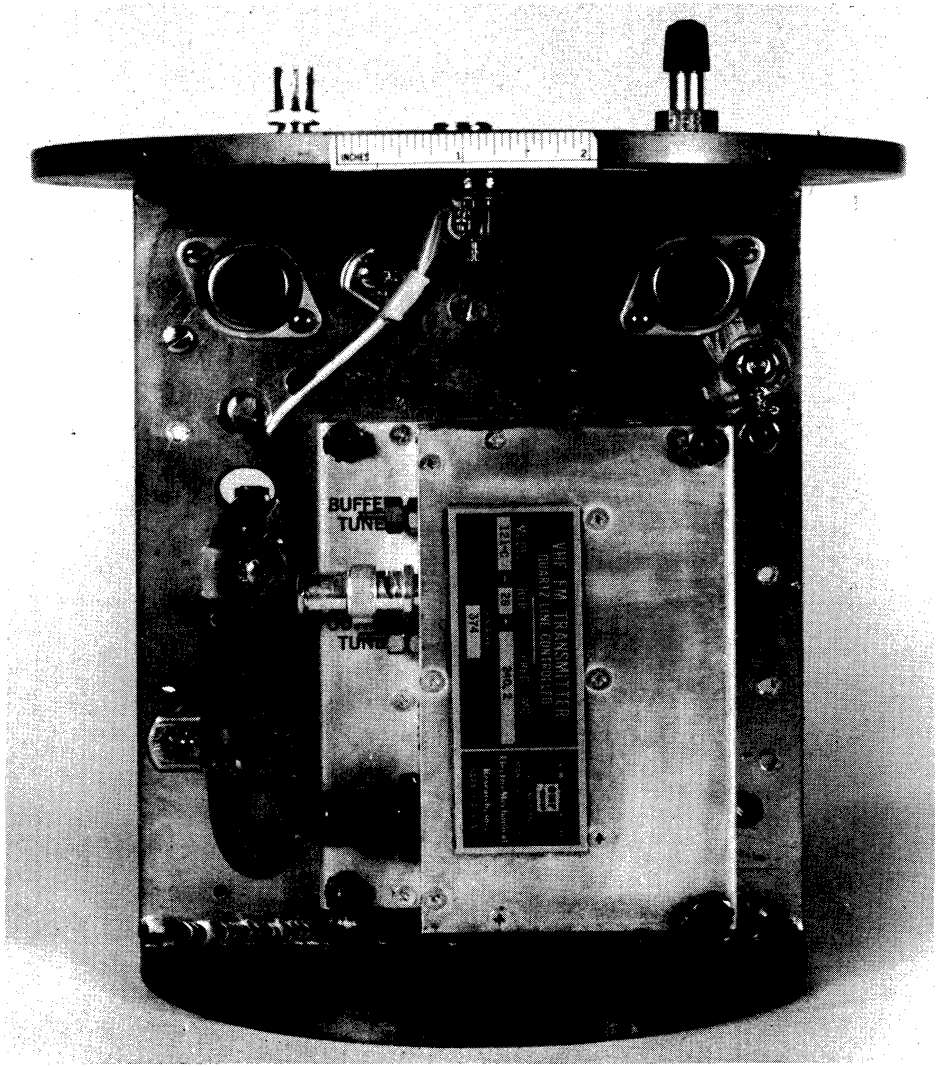


Figure 43. Transmitter.

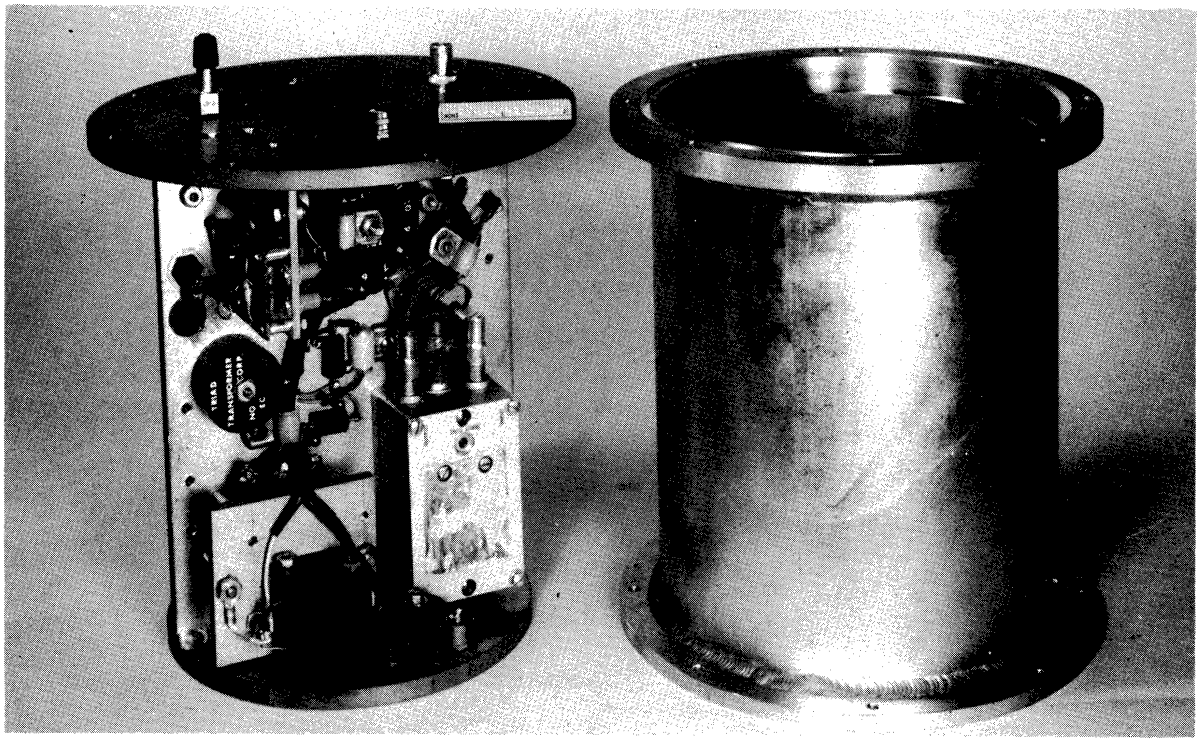

Figure 44. RF power amplifier.

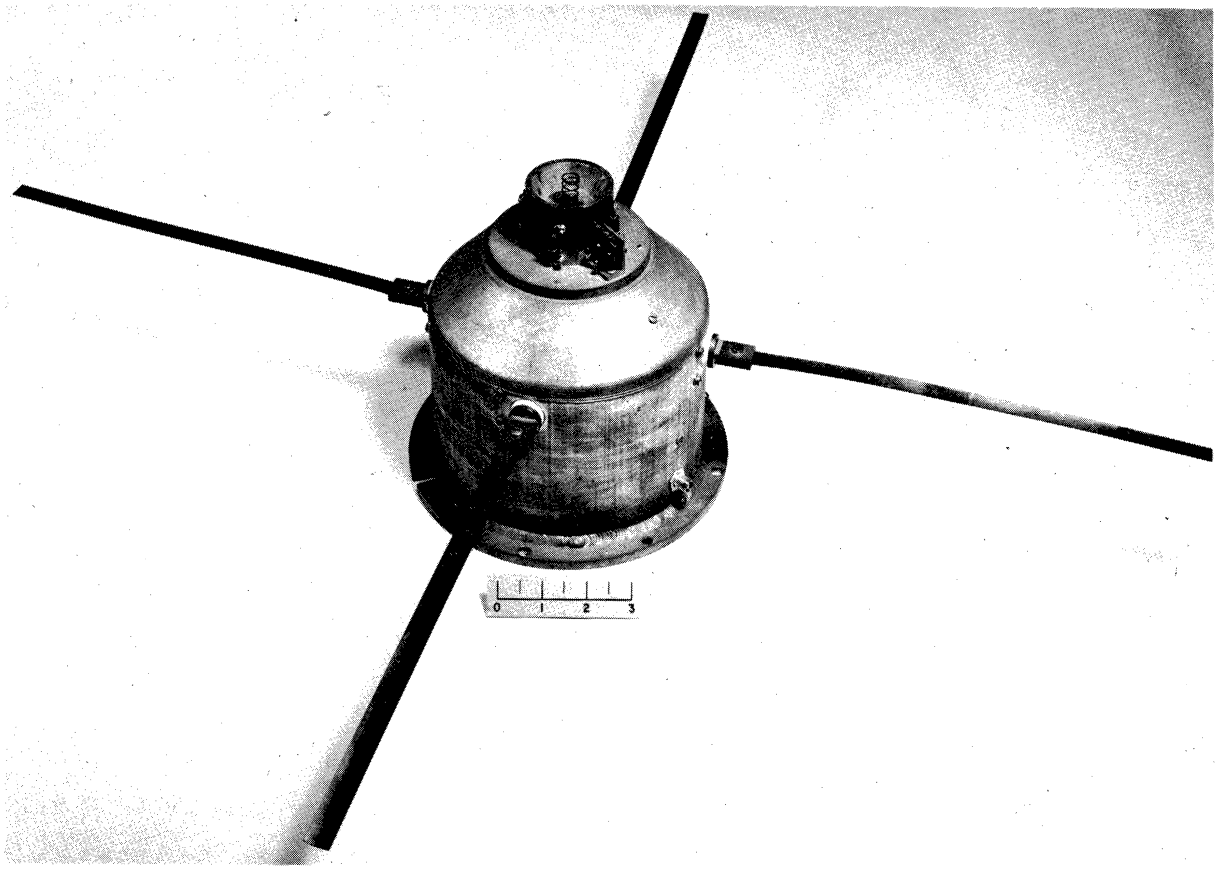


Figure 45. Turnstile antenna.

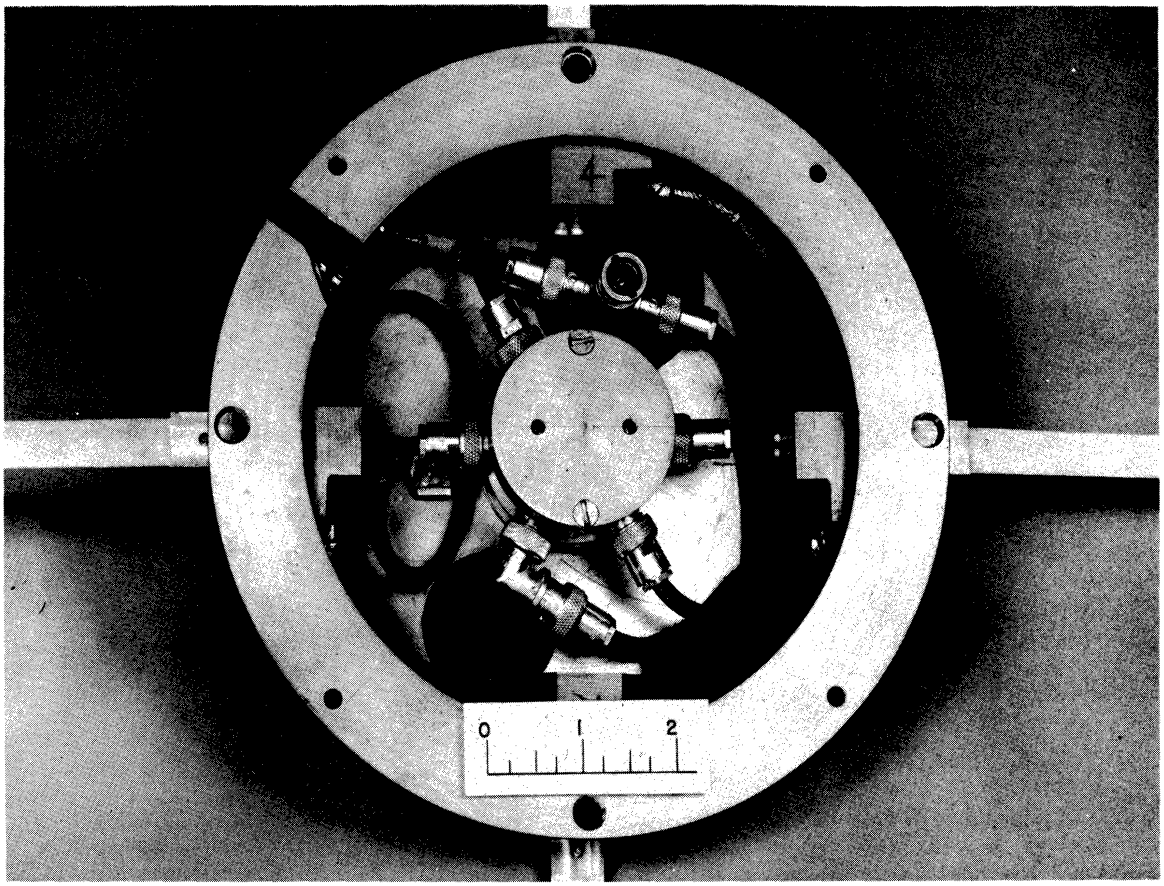


Figure 46. Turnstile antenna matching network.

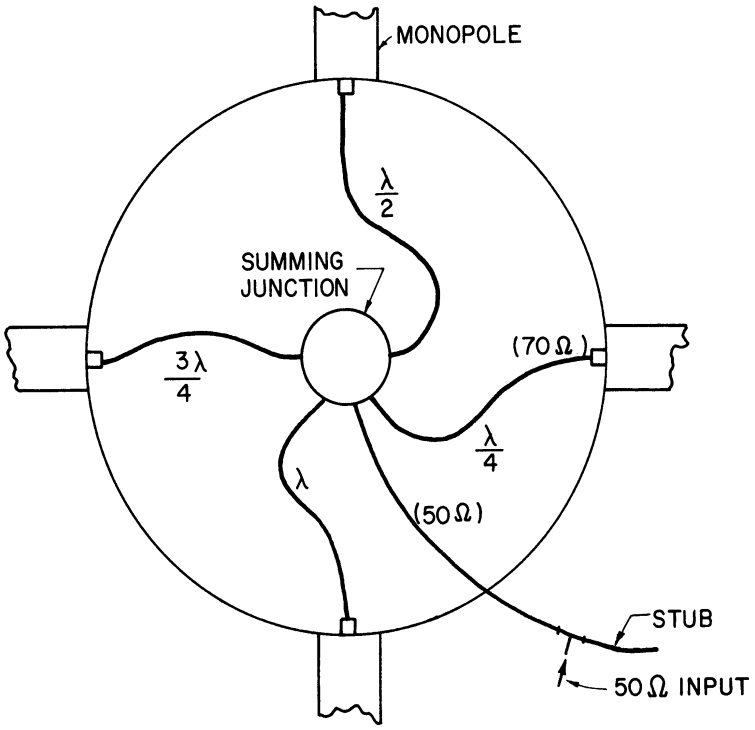


Figure 47. Turnstile antenna matching circuit.

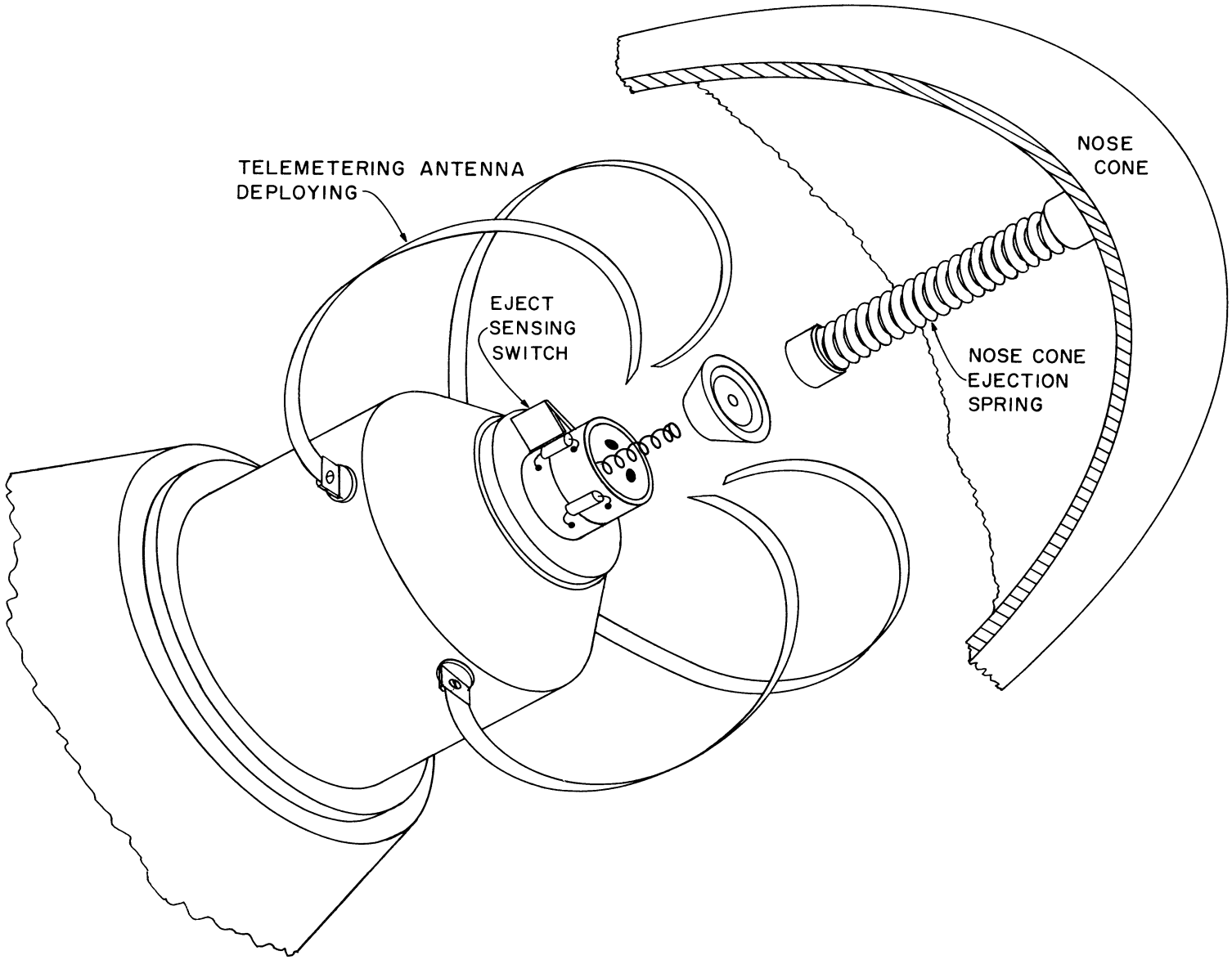


Figure 48. Turnstile deployment.

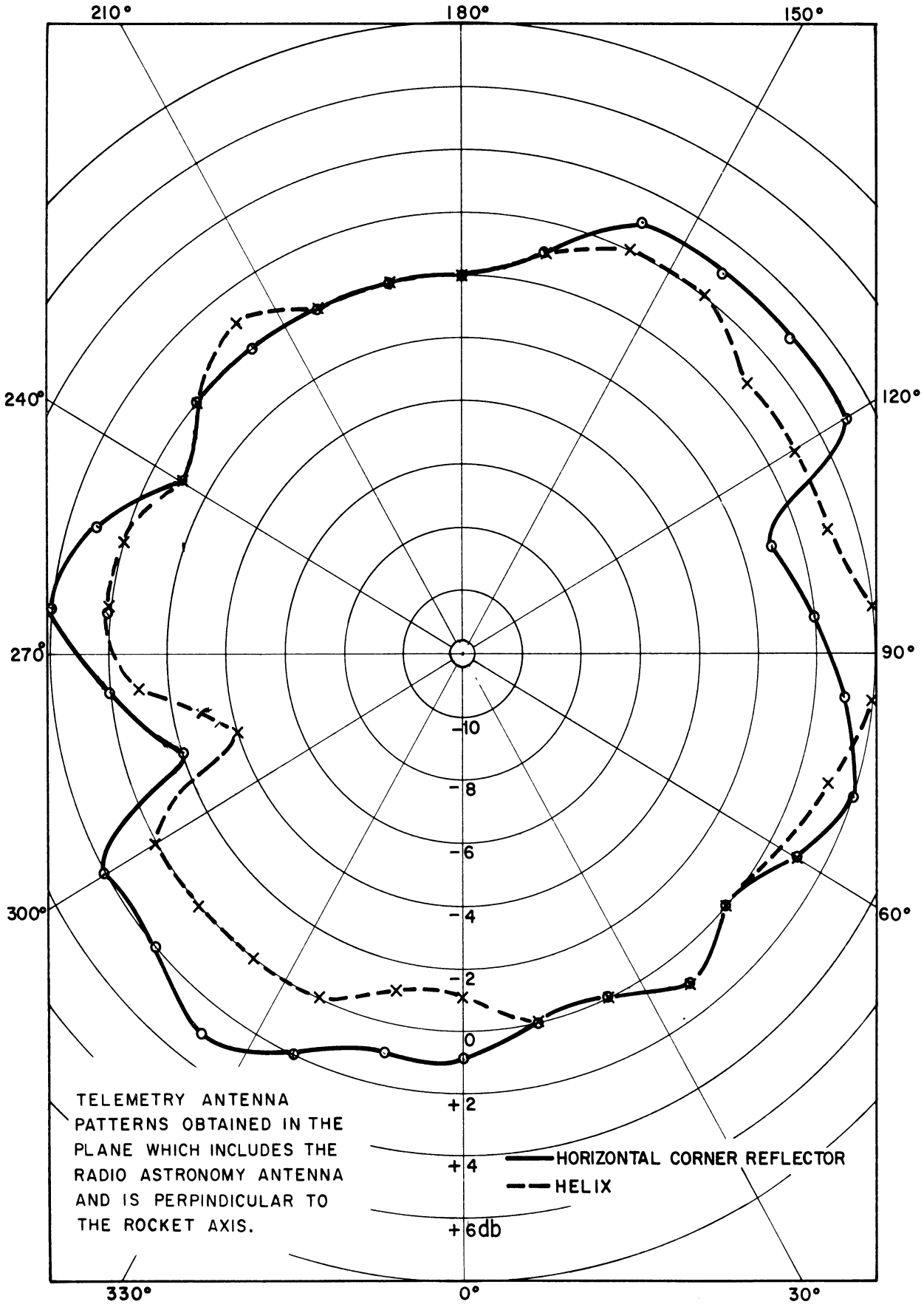


Figure 49. Turnstile antenna pattern.

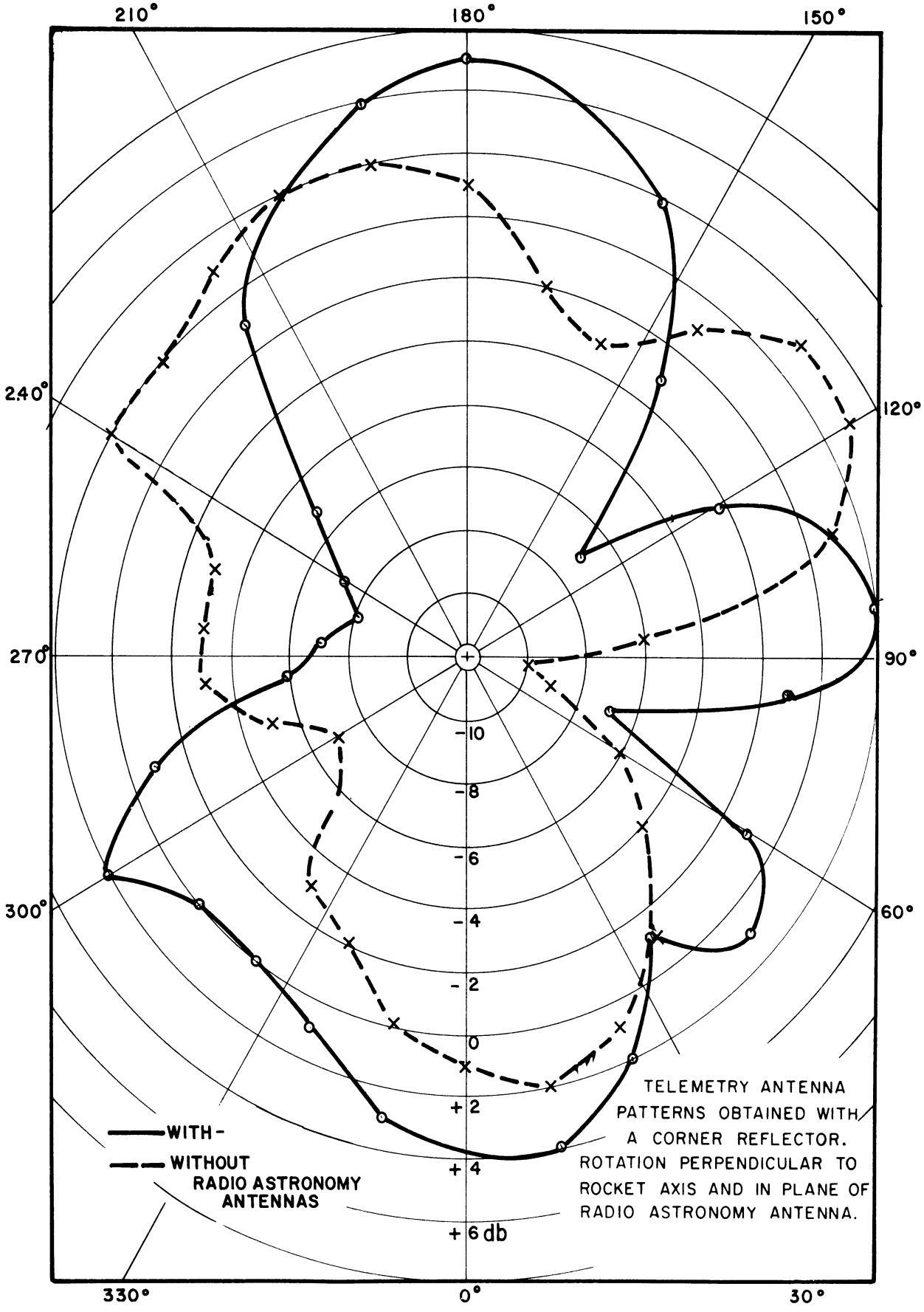


Figure 50. Turnstile antenna pattern.

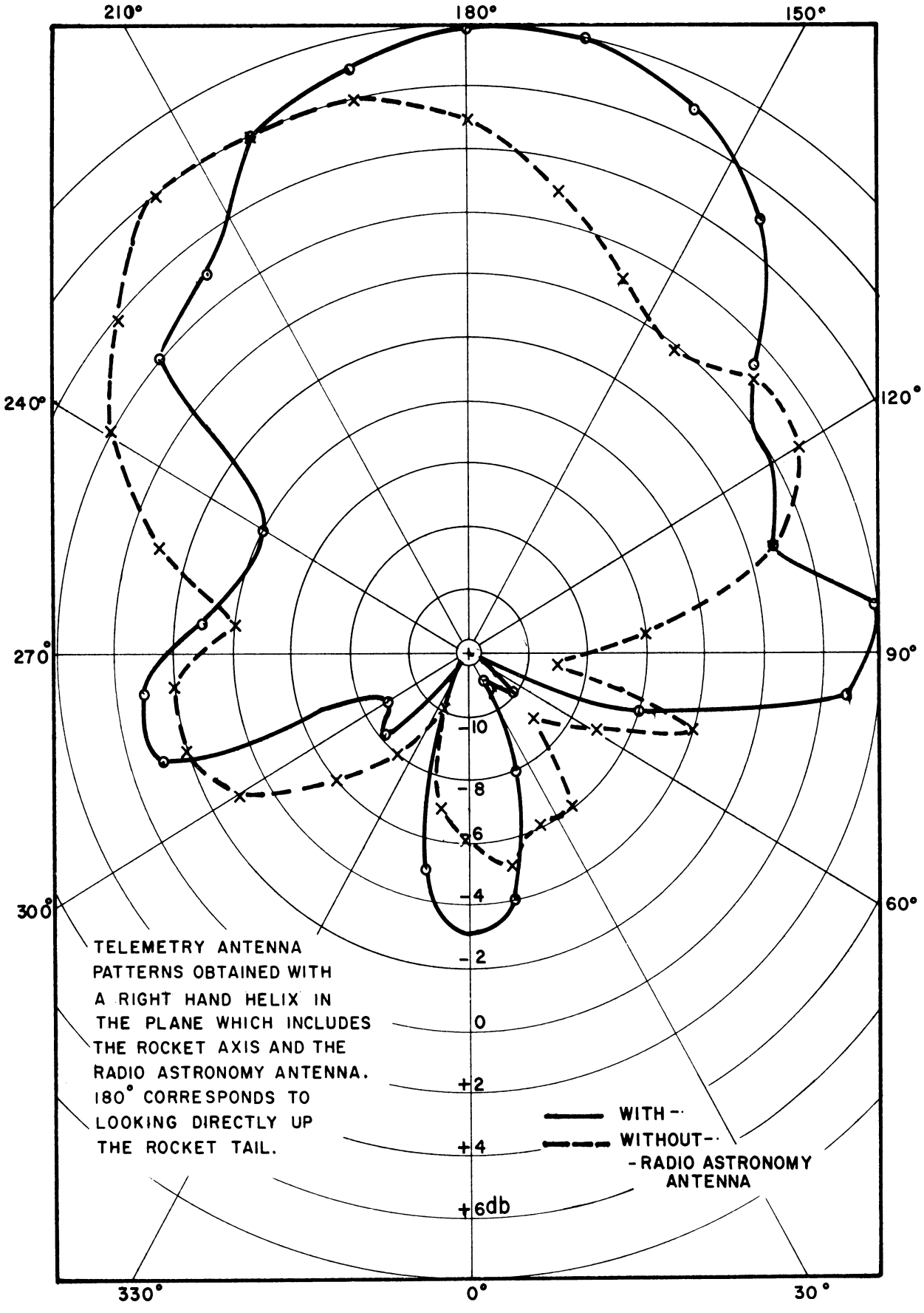


Figure 51. Turnstile antenna pattern.

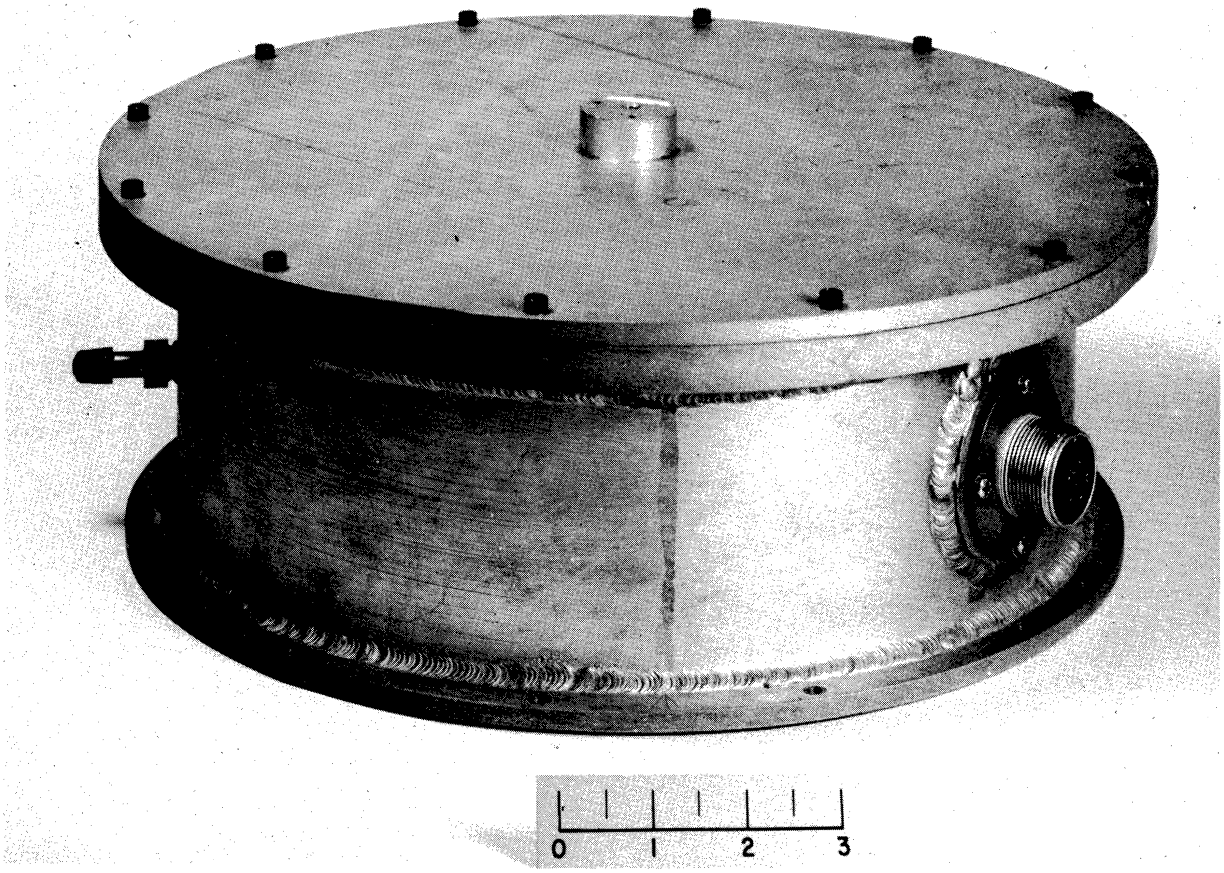


Figure 52. Battery container.

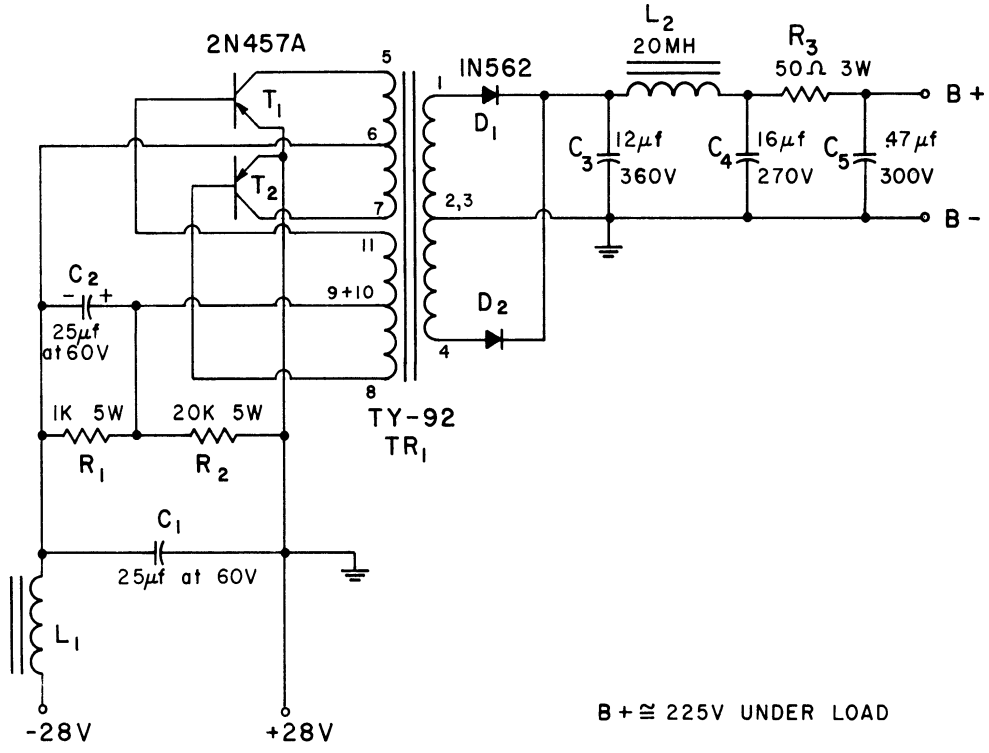


Figure 53. Radiometer DC-DC converter circuit.

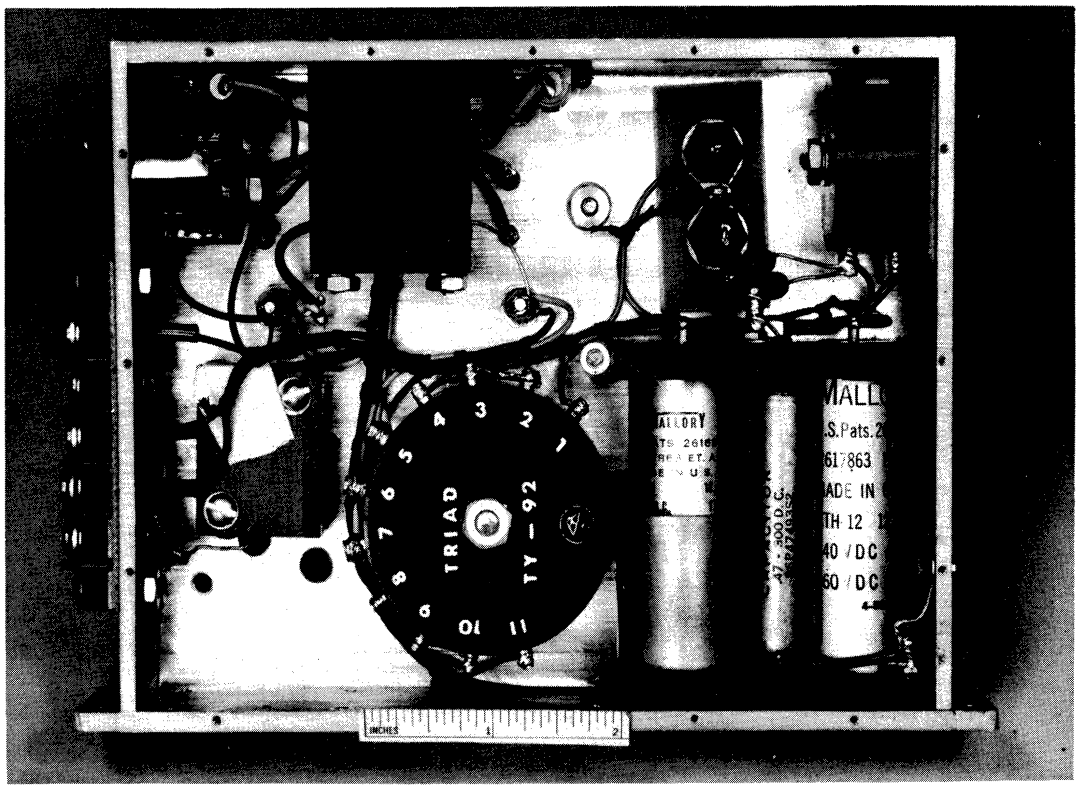


Figure 54. Radiometer DC-DC converter.

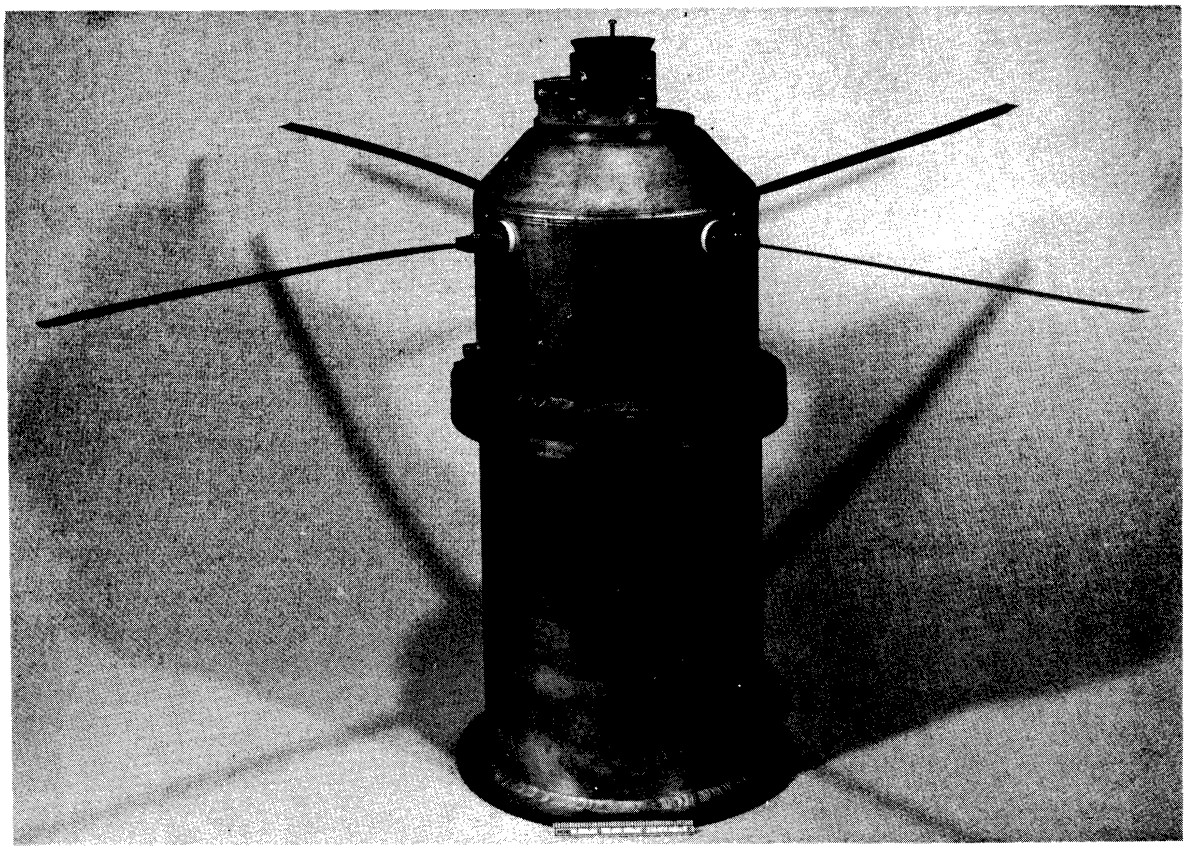

Figure 55. Telemetry pressurized can.

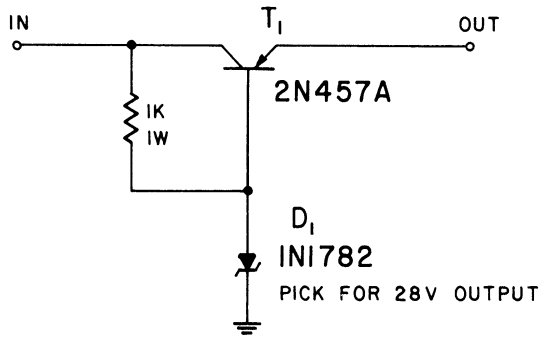


Figure 56. Telemetering filament pre-regulator circuit.

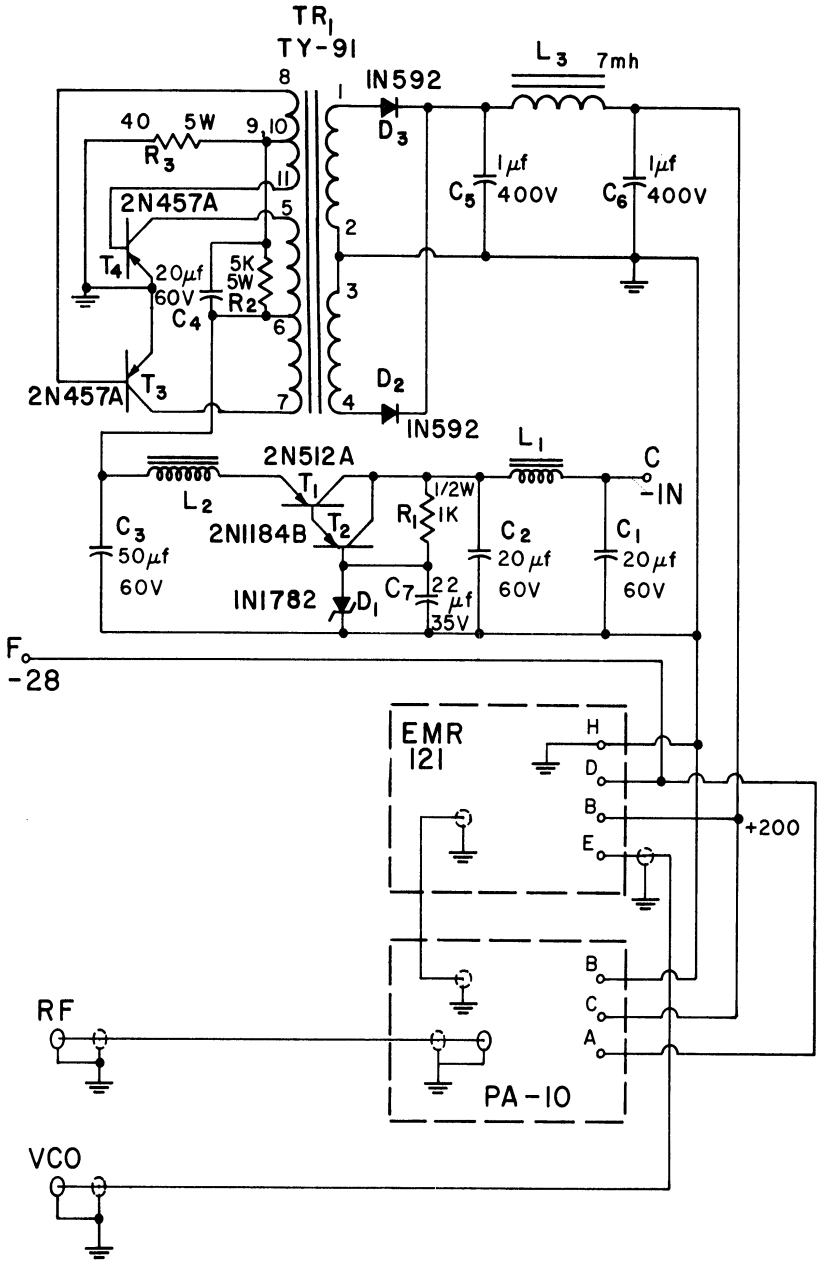


Figure 57. Telemetering DC-DC converter and pre-regulator circuit.

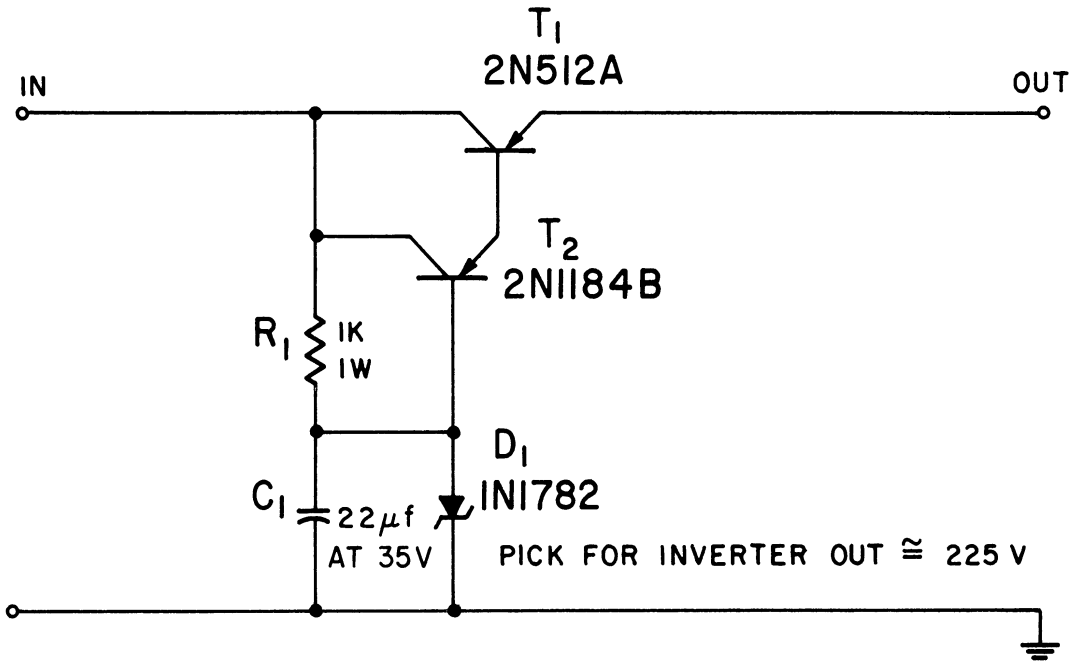


Figure 58. Radiometer DC-DC converter pre-regulator circuit.

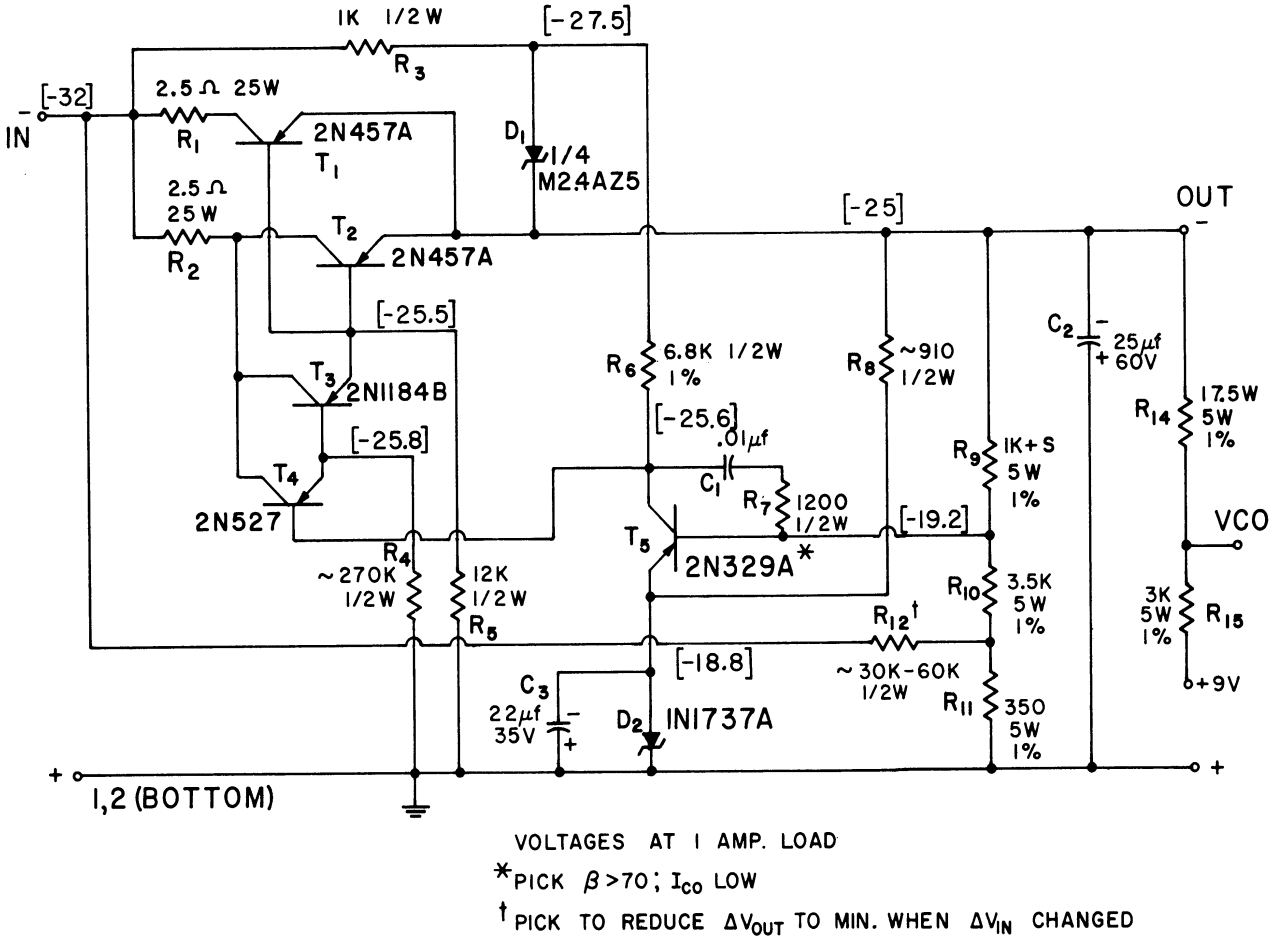


Figure 59. -25 v regulator circuit.

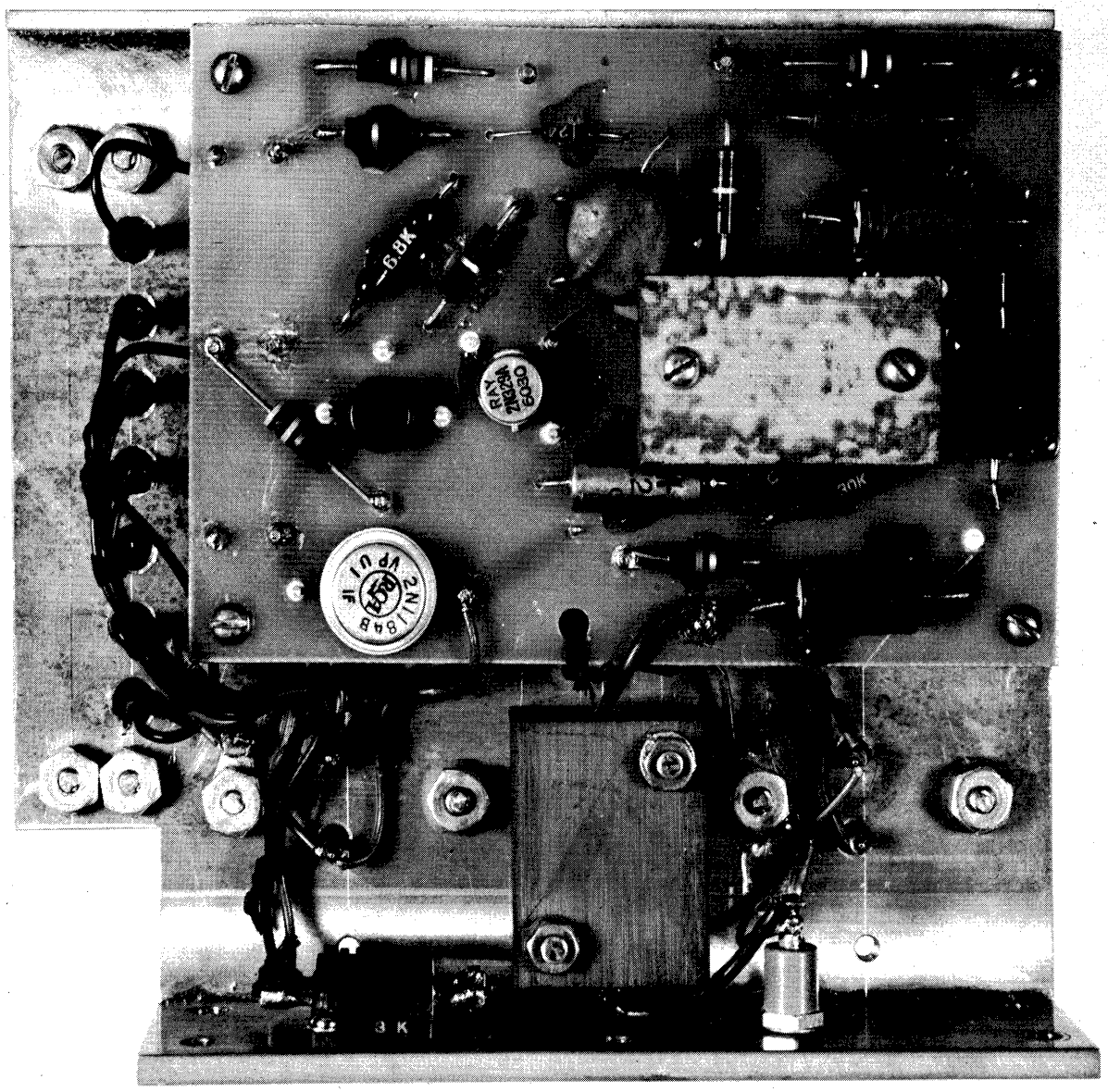


Figure 60. -25 v regulator.

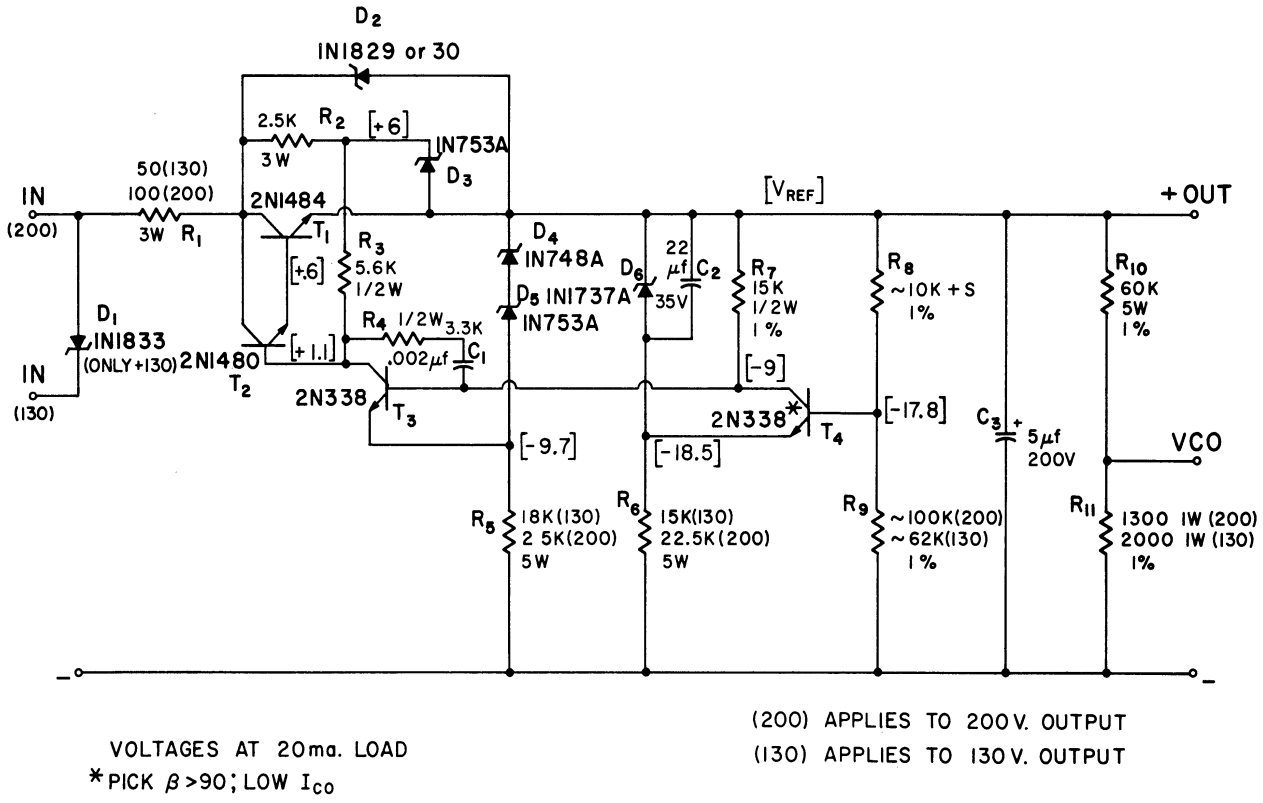


Figure 61. B+ regulator circuit.

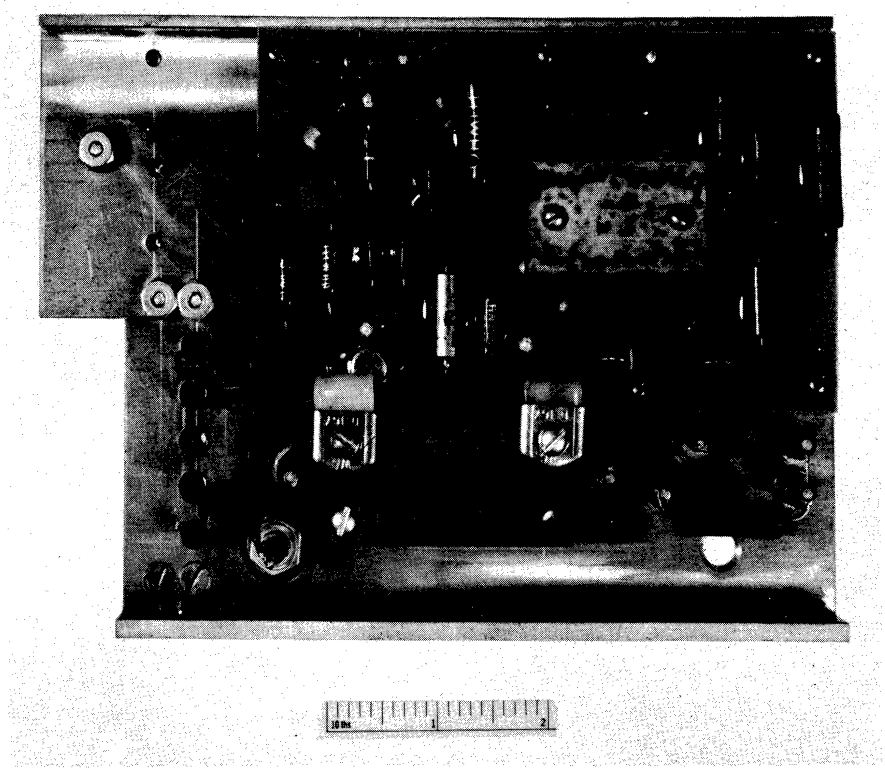

Figure 62. B+ regulator.

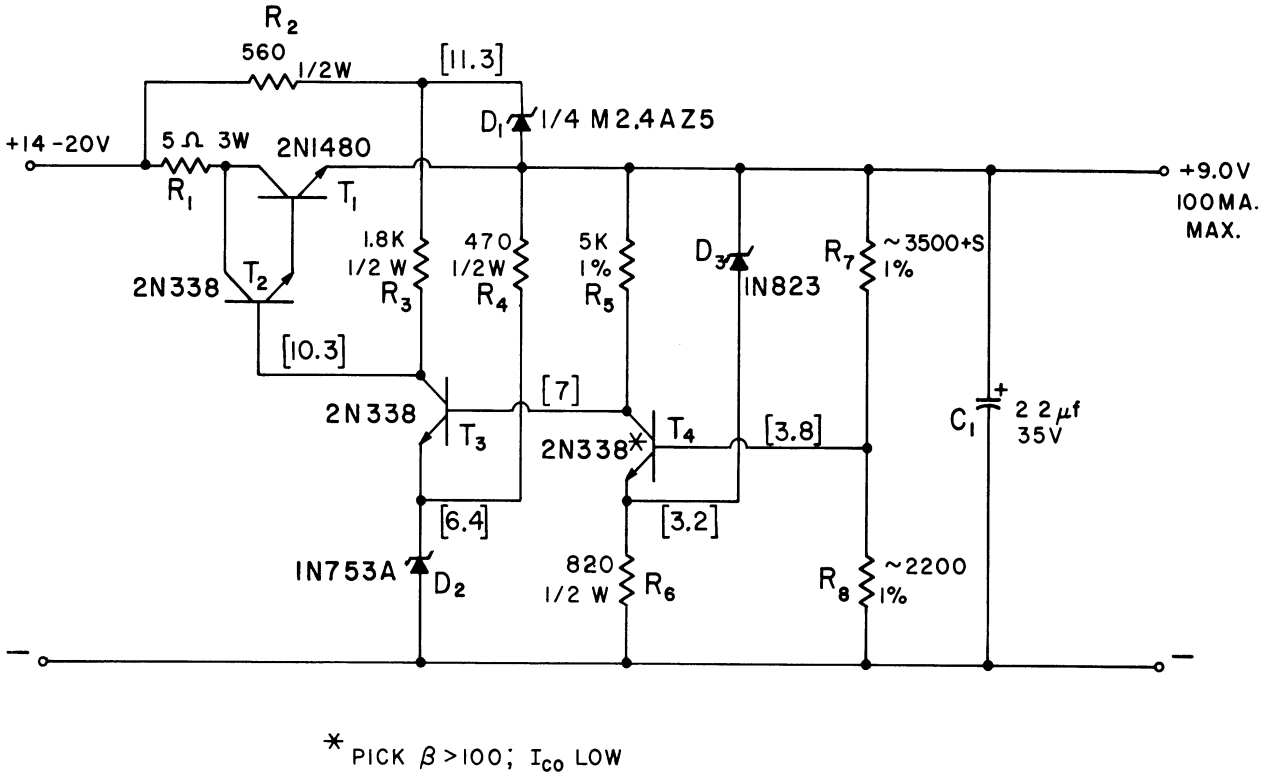


* PICK $\beta > 100$; $I_{CO}$ LOW

Figure 63. +9 v regulator circuit.

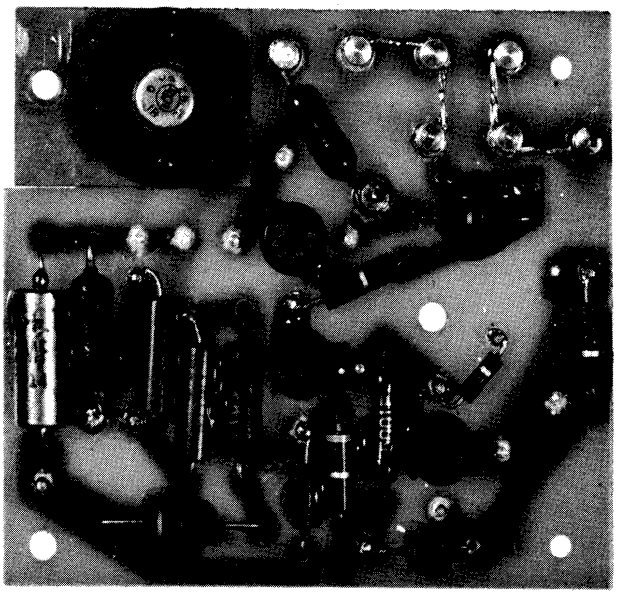

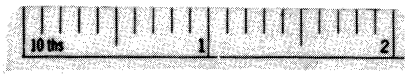


Figure 64. +9 v regulator.

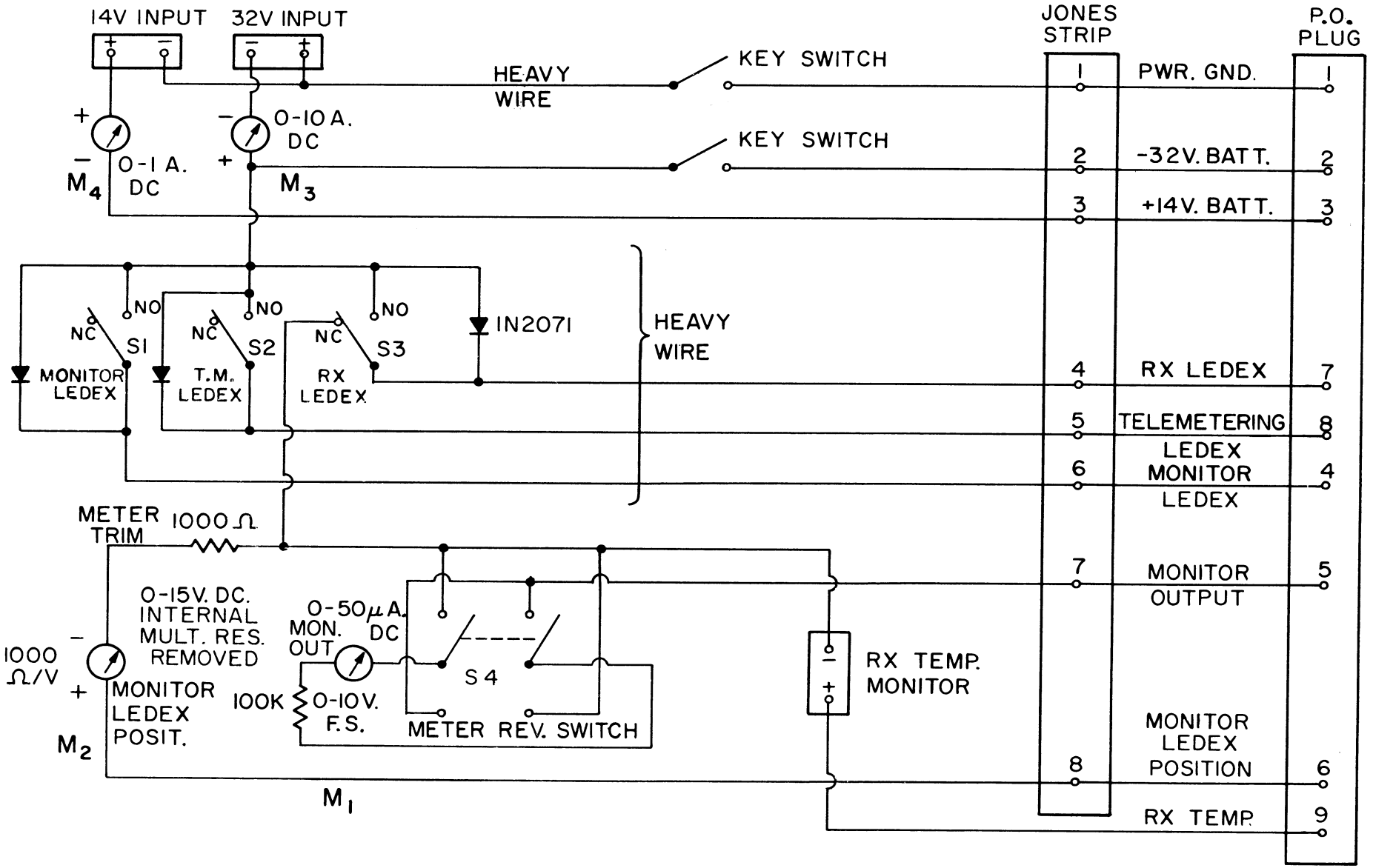


Figure 66. Remote control box circuit.

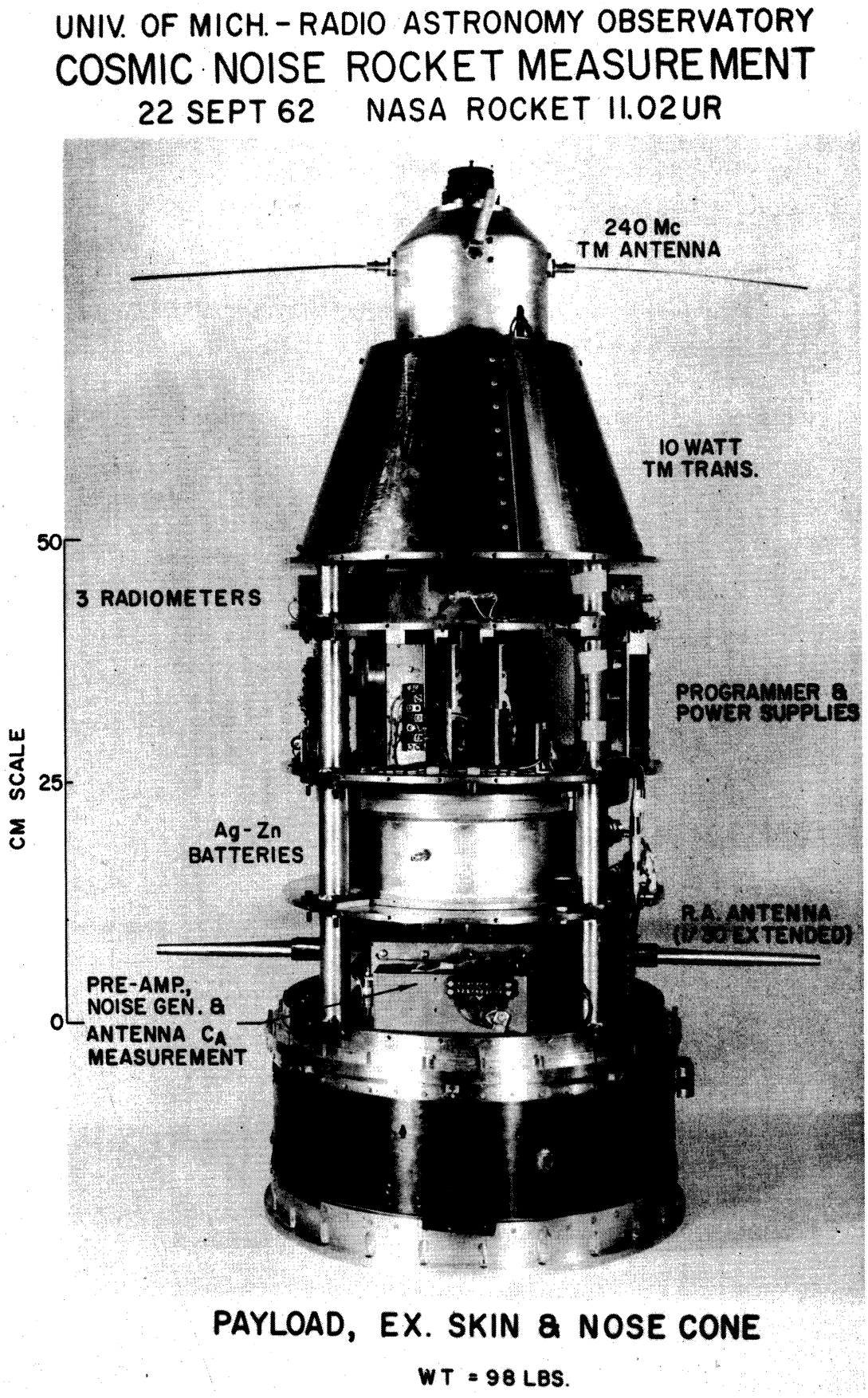


Figure 67. Closeup of payload.

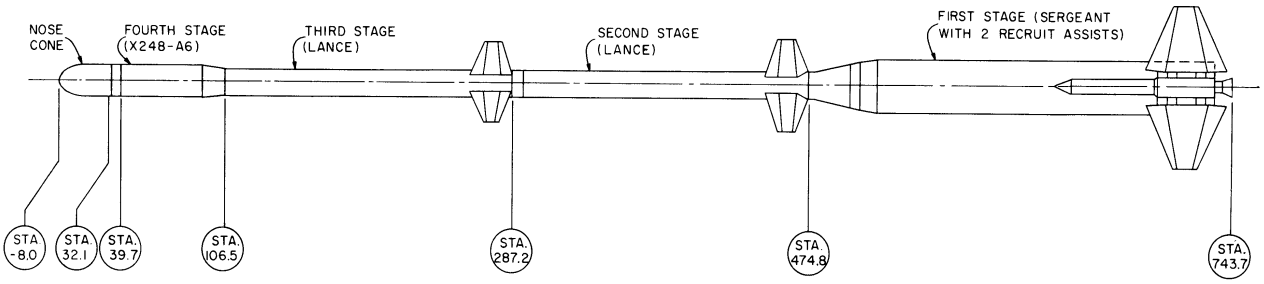


Figure 69. Argo D-8 rocket assembly.

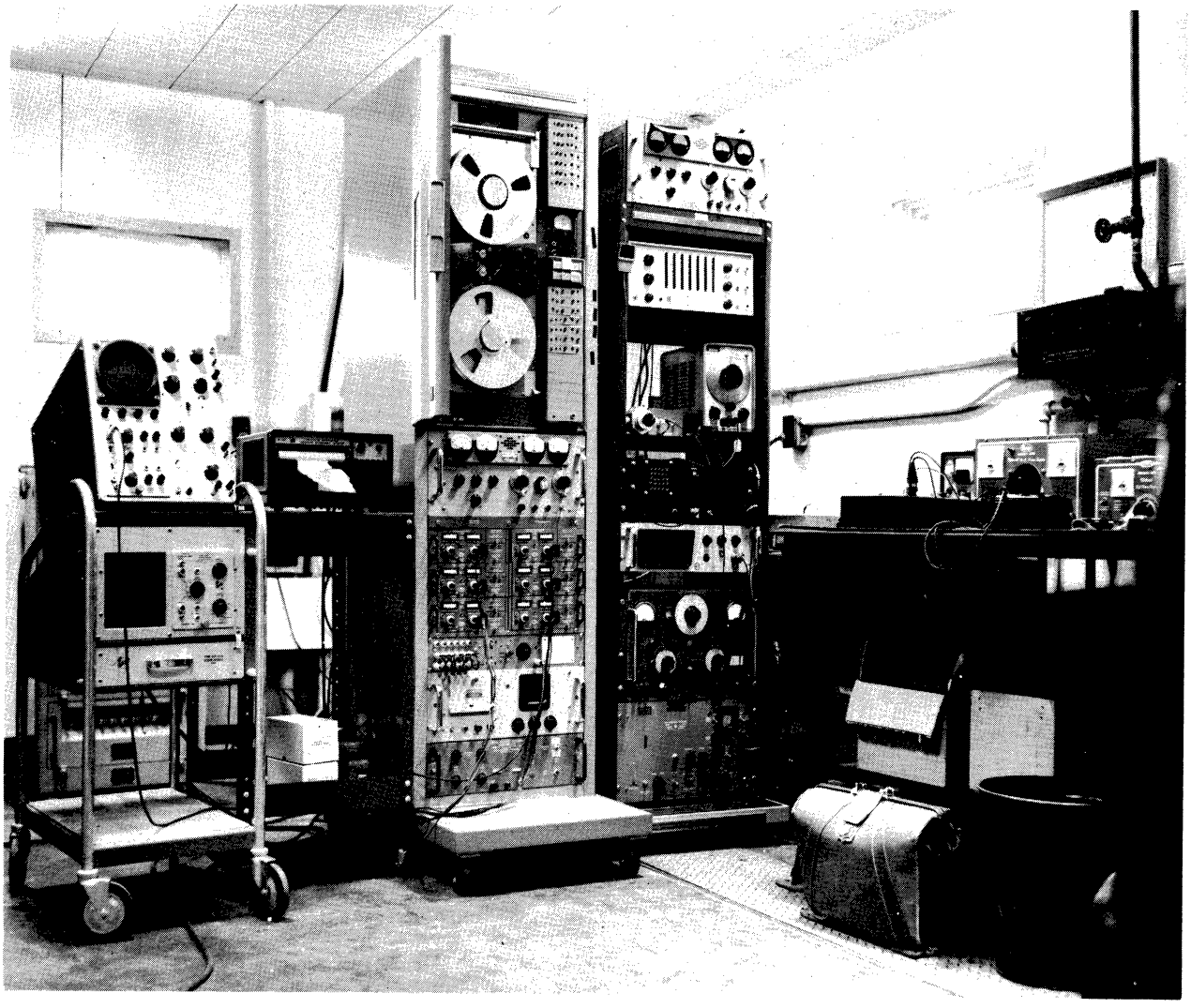

Figure 70. Telemetering ground station at Wallops Island.

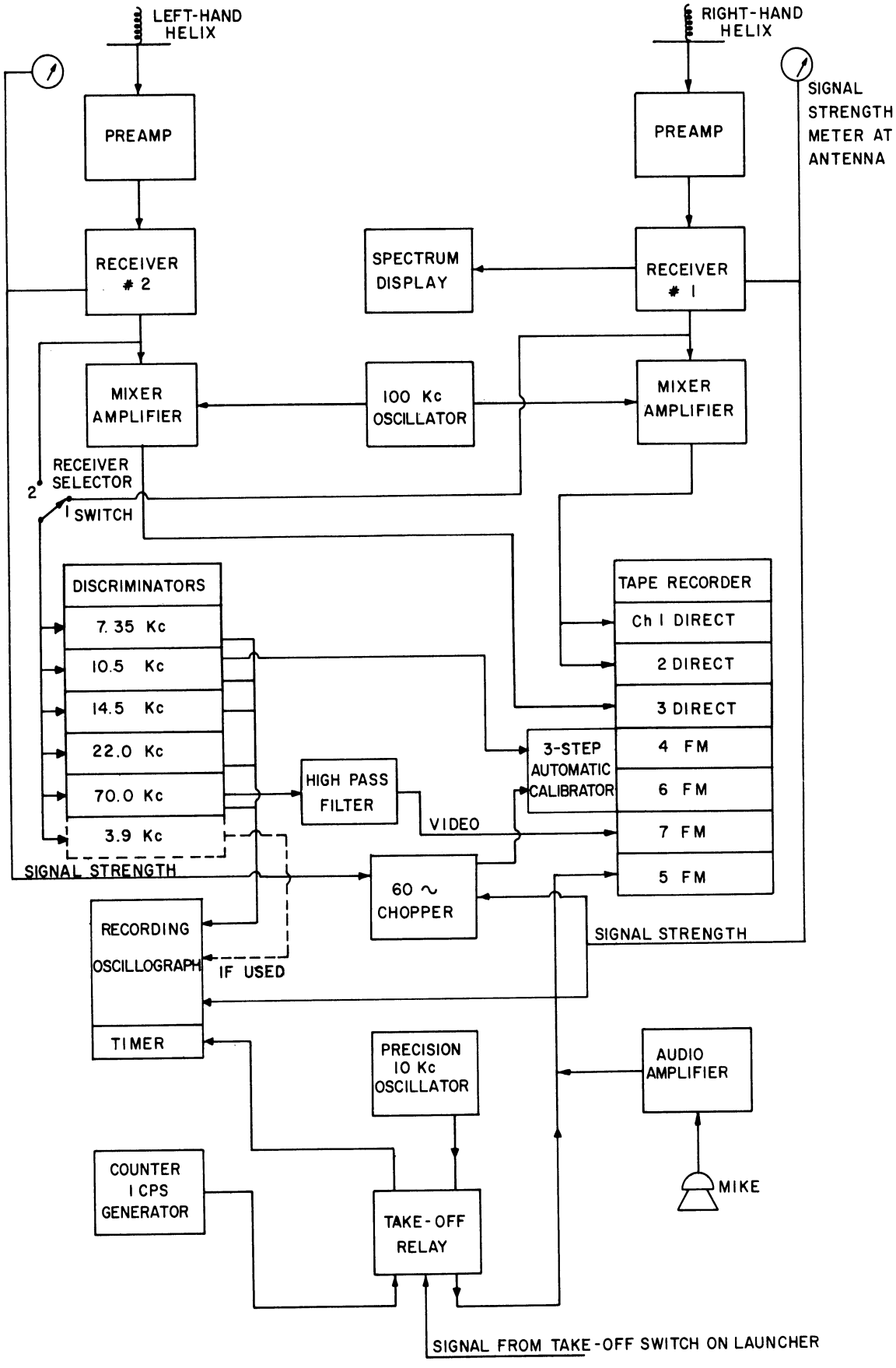


Figure 71. Ground station block diagram for recording.

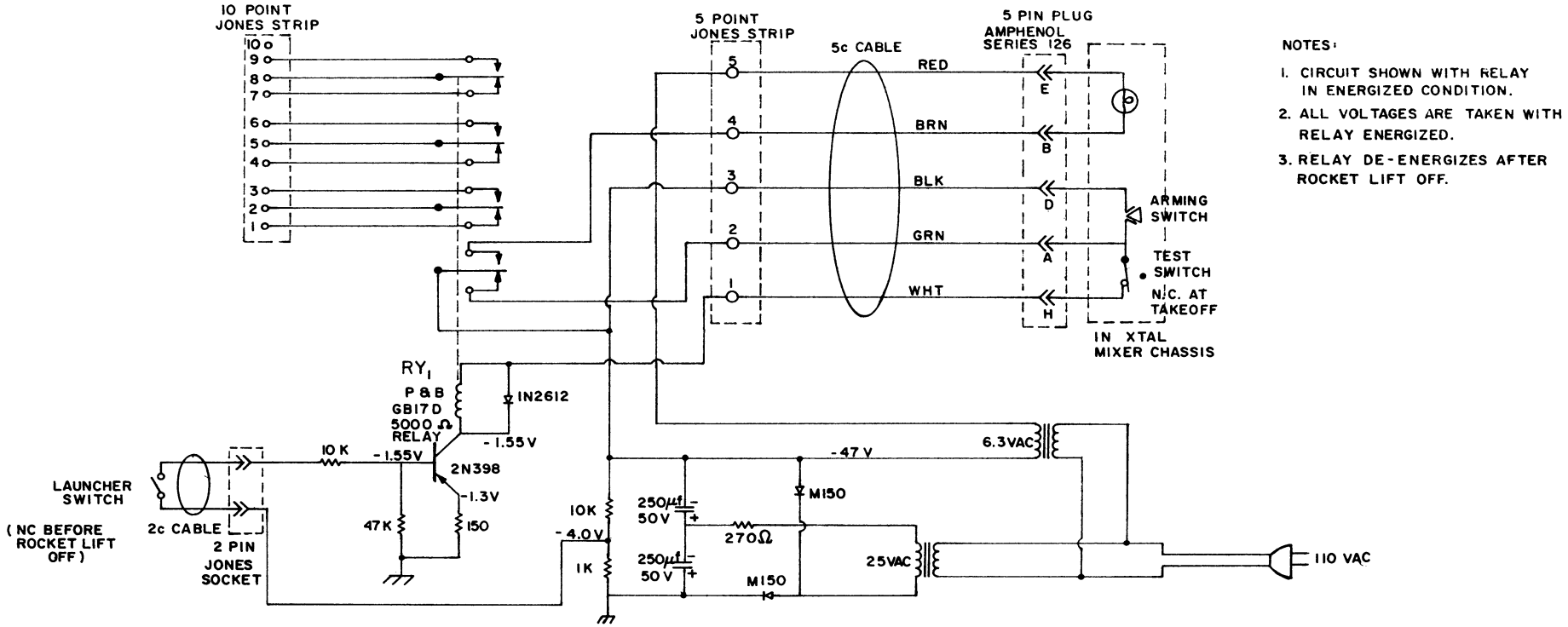


Figure 72. Take-off relay circuit.

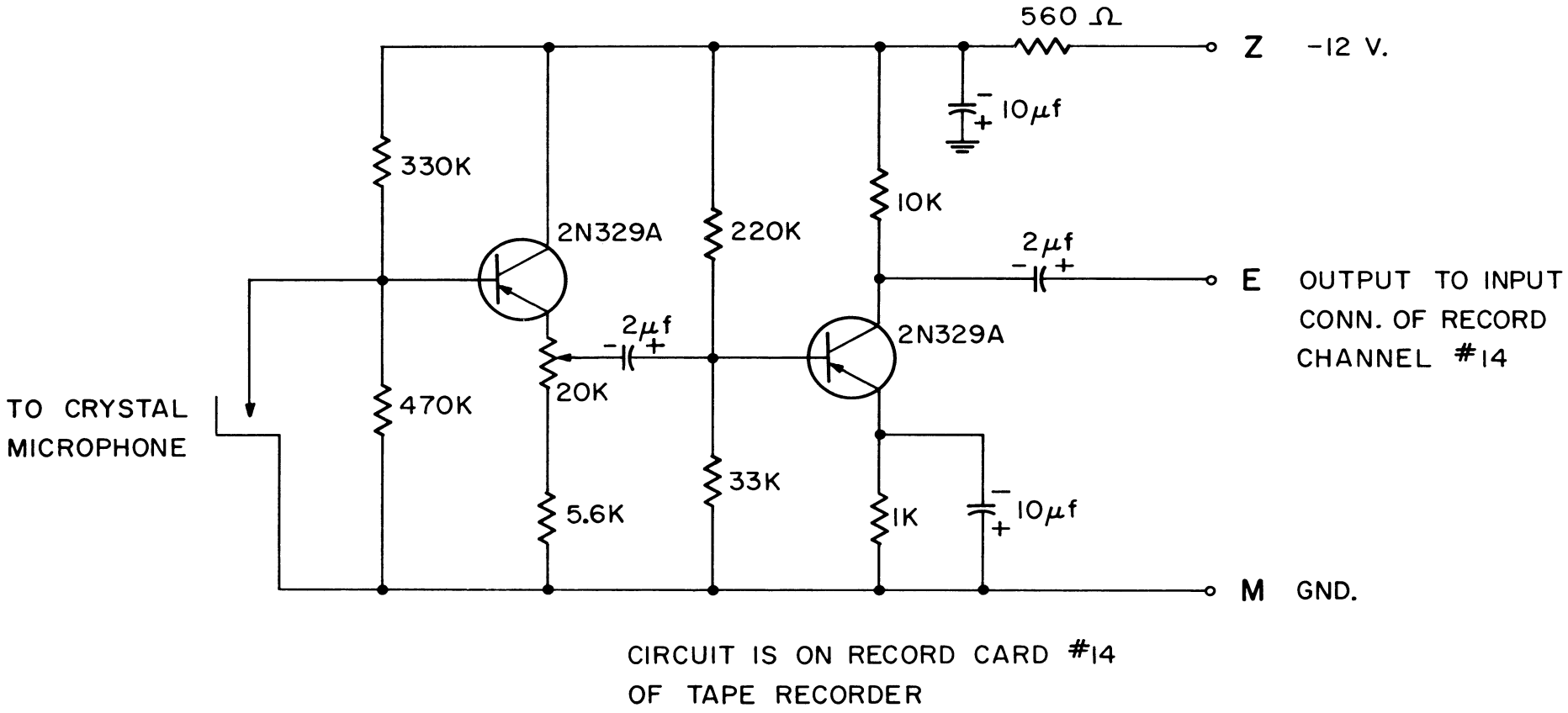


Figure 73. Ground station voice amplifier circuit.

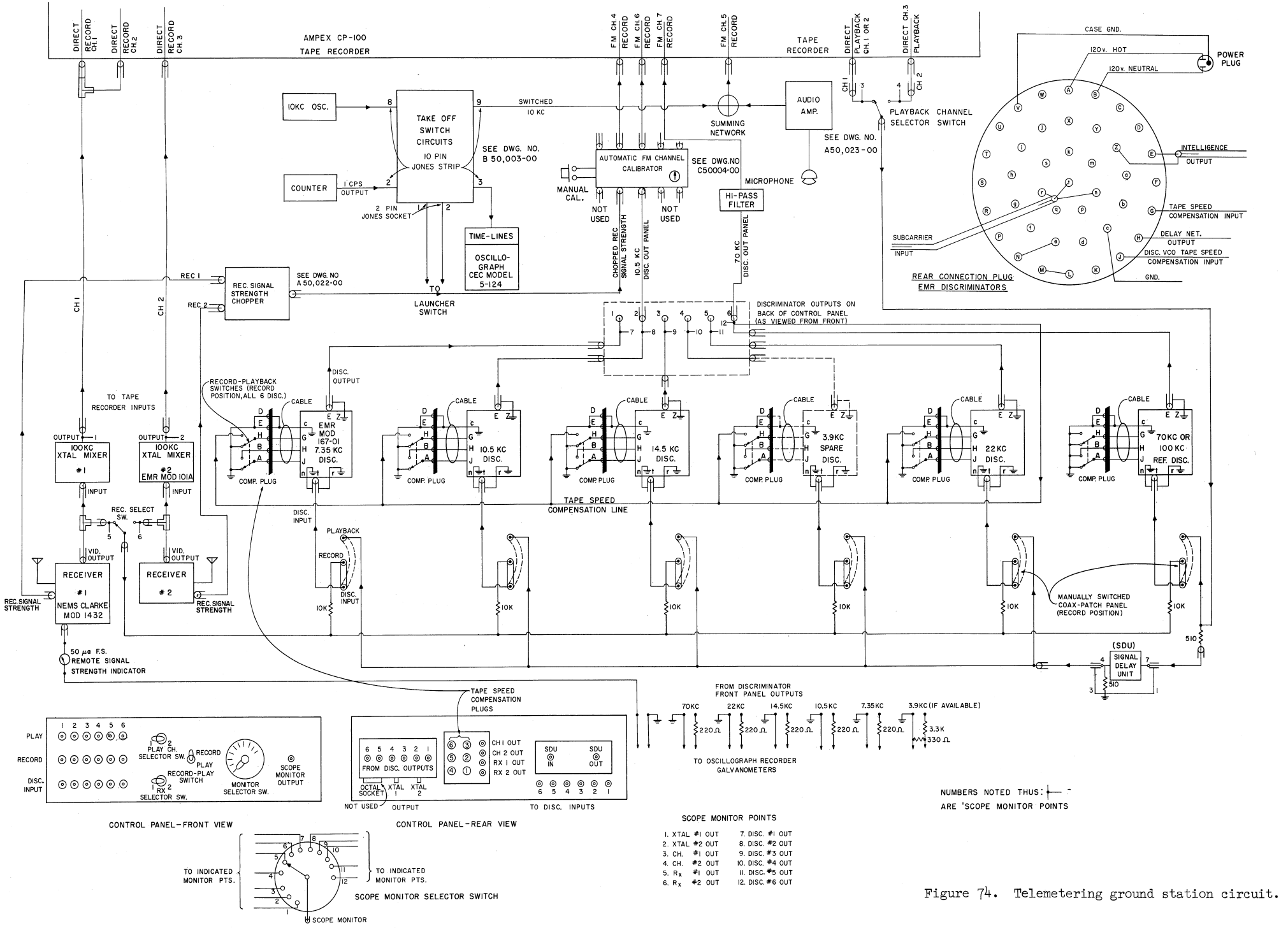


Figure 74. Telemetering ground station circuit.

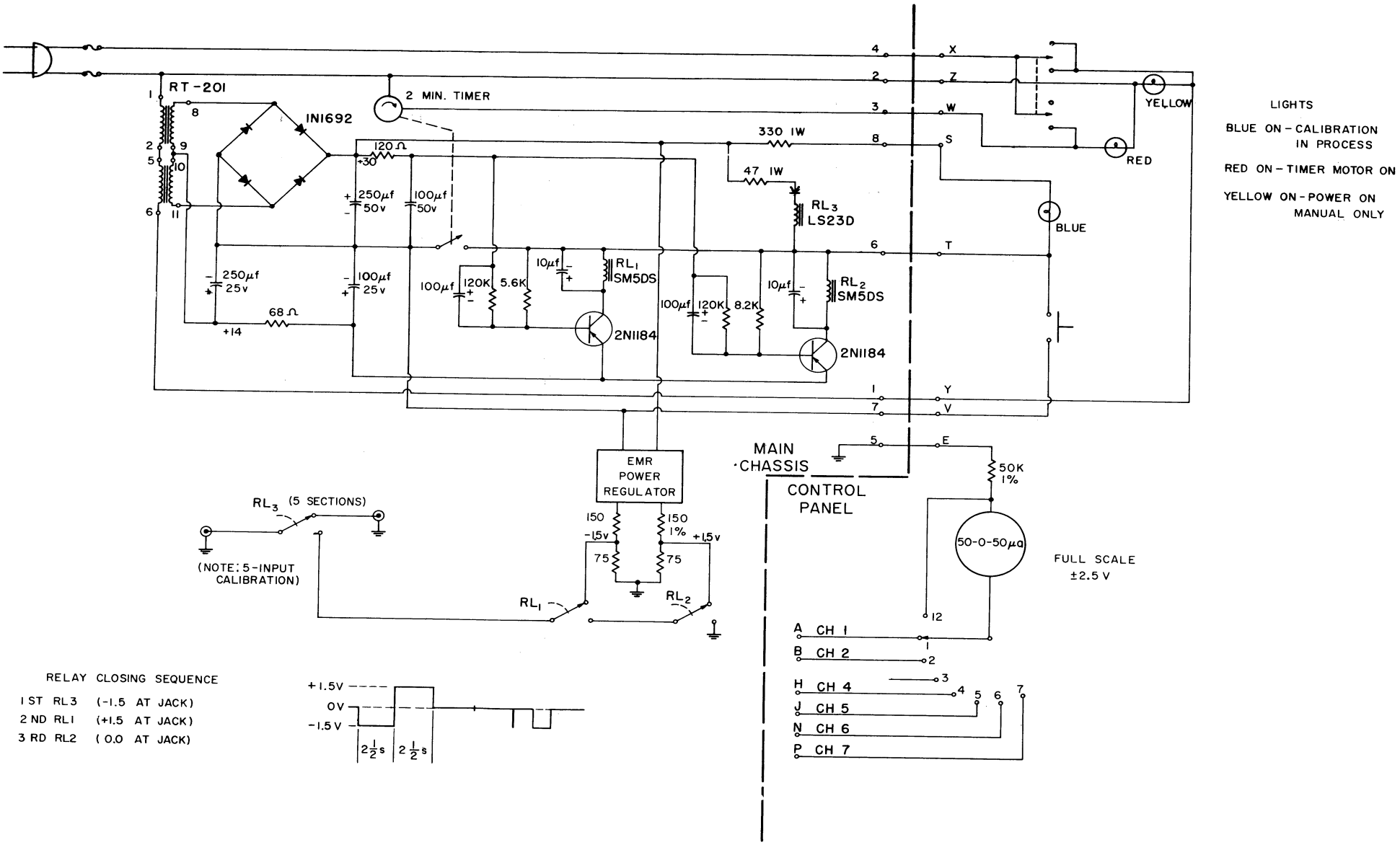


Figure 75. Tape recorder automatic FM channel calibrator.

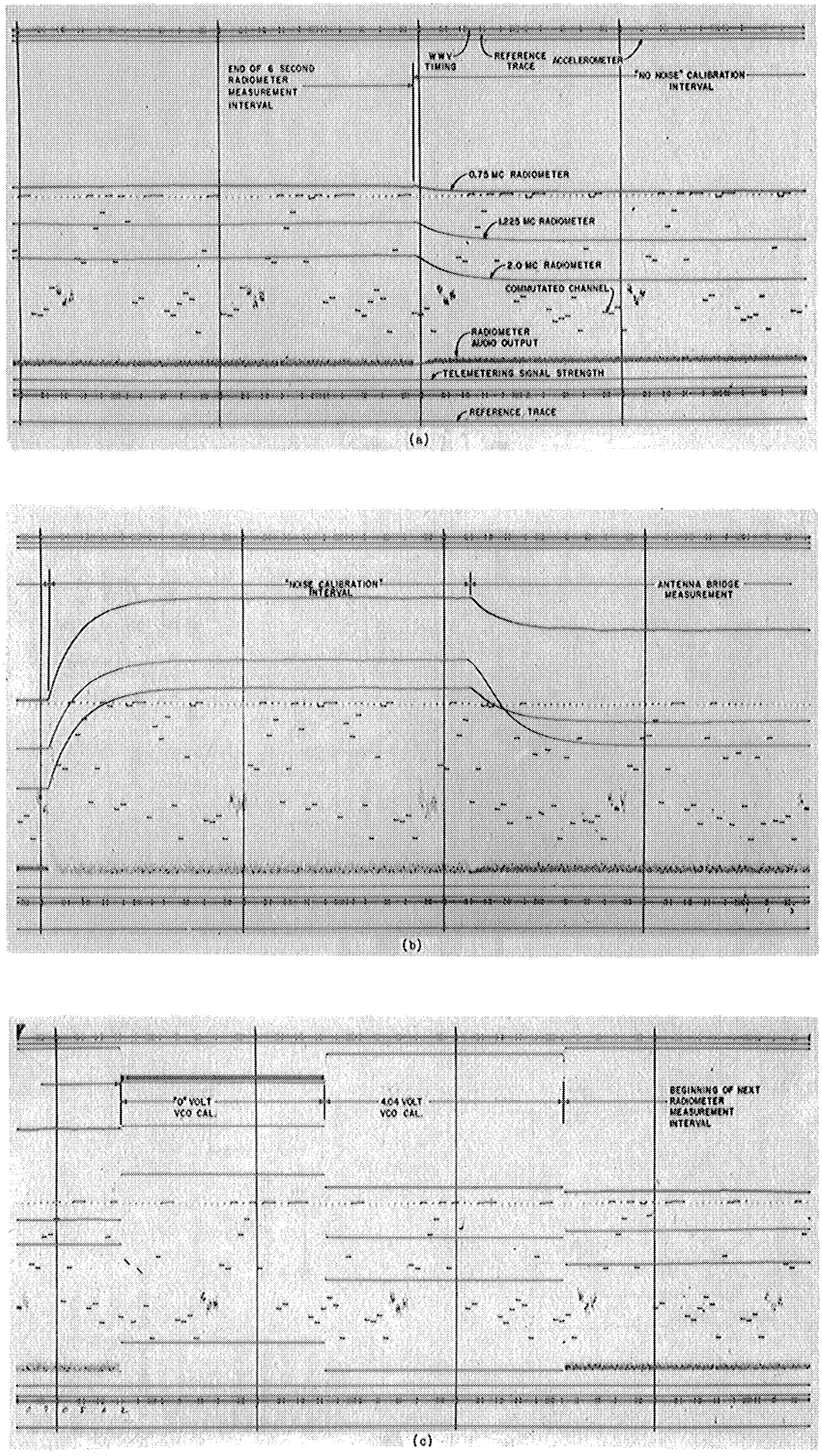


Figure 76. Typical telemetering record.

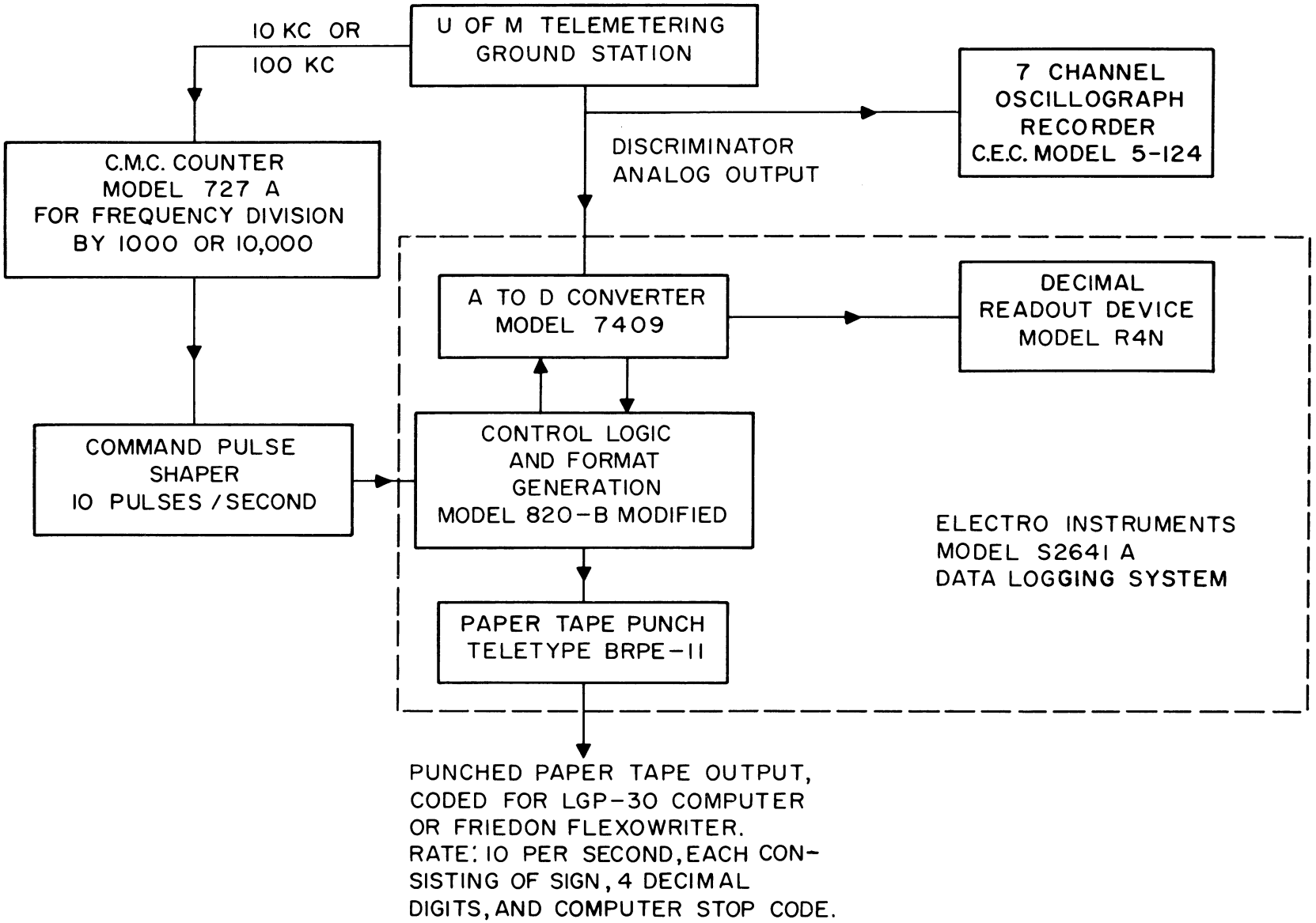


Figure 77. Analog to digital data logging system.